DEPARTMENT OF THE AIR FORCE

AIR UNIVERSITY

AIR FORCE INSTITUTE OF TECHNOLOGY

Wright-Patterson Air Force Base, Ohio

AFIT/GAE/AA/88D-29

FINITE ELEMENT ANALYSIS OF COMPOSITE PLATES INCLUDING SHEAR DEFORMATION

THESIS

Marc E. Owens
Captain, USAF

AFIT/GAE/AA/88D-29

Approved for public release; distribution unlimited

AFIT/GAE/AA/88D-29

FINITE ELEMENT ANALYSIS OF COMPOSITE PLATES INCLUDING SHEAR DEFORMATION

THESIS

Presented to the Faculty of the School of Engineering
of the Air Force Institute of Technology
Air University
In Partial Fulfillment of the
Requirements for the Degree of
Master of Science in Aeronautical Engineering

Marc E. Owens, B.S.
Captain, USAF

December 1988

Preface

This thesis is part of an overall research project on composite plates and shells sponsored by the Air Force Office of Scientific Research, Dr. Anthony Amos contract monitor, Dr. Anthony Palazotto AFIT/ENY, principal investigator.

Like most research, this effort would have been impossible to complete alone. I am deeply indebted to my faculty advisor, Dr. Anthony N. Palazotto, for his advice, patience, and explana tion of many difficult subjects. I would like to express my appreciation to Captain Scott Dennis, the author of the code, for his explana tions of its operation and suggestions of areas of investigation to clear up certain problems. I would like to thank Kris Larsen for her help with the AFIT computers and helping me learn my way around the system. Finally, I would like to thank my wife, [redacted] for her patience and support during those many nights when I was tucked away at my desk.

Contents

List of Figures

List of Tables

List of Symbols

σ_{ij}	stress tensor
a_{ijkl}	elasticity tensor
ε_{ij}	strain tensor
σ_i, ε_i	stress and strain in contracted notation
C_{ij}	elasticity tensor in contracted notation
E_i	elastic modulus
ν_{ij}	Poisons ratio
G_{ij}	shear modulus
Q_{ij}	reduced stiffnesses
$\bar{Q}_{ij}$	transformed reduced stiffnesses
u_i	displacement components
u_i°	displacement componment of datum surface
ζ	transverse coordinates
ψ_i	rotational displacement due to bending
θ_i, ϕ_i	unknown degrees of freedom
ξ_α	inplane coordinates
h	thickness of plate
e_{ij}	Green's strain tensor
ω_{ij}	rotational displacement
k	$-4/3h^3$
u	displacement in x-direction
v	displacement in y-direction
w	transverse displacement
ε_i°	strain on datum surface
$\varkappa_{ij}$	curvature
Π_p	potential energy
U, U_1, U_2	internal strain energy
V	work done by external forces
Ω	domain of datum surface
u_i	energy terms

A_{ij}-G_{ij}	elasticity arrays
K, N_1, N_2	stiffness arrays
q	nodal degrees of freedom vector
Δq	small increment of nodal displacement
K_T	tangential stiffness matrix
${}_iL_j$	linear strain definition arrays
${}_iH_j$	nonlinear strain definition arrays
d	displacement gradient vector
$\tilde{K}$, $\tilde{N}_1$, $\tilde{N}_2$	stiffness arrays
$\hat{K}$, $\hat{N}_1$, $\hat{N}_2$	stiffness arrays
${}_iS_j$	linear strain definition arrays
$\mathcal{N}_k$	linear Lagrangian shape functions
$\mathcal{H}_k$	Hermitian shape function arrays
$\mathcal{D}$	shape functions and their derivatives
ζ_k, η_k	natural coordinates
$\mathbb{N}_k$	array of Lagrangian shape functions and their derivatives
$\mathbb{H}_k$	array of Hermitian shape functions and their derivatives
J	Jacobian matrix
Γ	inverse of Jacobian matrix
a	dimensions of plate in x-direction
b	dimensions of plate in y-direction
R	applied nodal loading vector
F(q)	equilibrium equations
W_i	Gaussian weighting factors
q_o	applied incremental load
$\bar{w}$, $\bar{q}$	nondimensionalized deflection and load
S	thickness ratio
AR	aspect ratio

Abstract

The purpose of this research is to study the effects of material properties, thickness ratio, aspect ratio, boundary conditions, and ply layup on the reactions of a transversely loaded rectangular composite plate. Geometric nonlinearities, i.e. the von Karman nonlinear plate equations, and through the thickness shear effects were included. Both geometrically linear and nonlinear solutions were done. This research was done using an existing finite element code with a four-noded, 28 DOF rectangular element.

All plates were 48 plies thick to be representative of a "real world" application. The ply layups were chosen to be a representative sampling of layups used in the field and had at least 50% of the plies in the 0° direction.

Material properties had the largest effect when the plate was thick. The linear solution approaches the classical laminated plate theory solution as the plate gets thin. The nonlinear solution deflects much less than the linear solution because the higher order terms significantly stiffen the plate. For a clamped plate the linear and nonliear solutions are comparible until the plate is quite thin.

Aspect ratio has a large effect on the plate for an isotropic material. However, in the ply layups investigated, aspect ratio had much less effect because half the fibers were oriented in the direction of the short dimension of the plate.

Ply layup did not have a great effect on the deflections of the plate. This occured because all the layups chosen had at least half the plies oriented in the same direction.

I. INTRODUCTION

Advanced composite materials are being used increasingly in many engineering and civilian applications, from aerospace structural components to sports equipment. The high stiffness to weight ratio, coupled with the flexibility in the selection of the lamination scheme, which can be tailored to match the design requirements, make laminated composite plates ideal structural components for many applications. The increased use of laminated plates in various structures has created considerable interest in their analysis.

In many situations, simplifying assumptions can be made to help the analyst get timely and accurate results. For many structural components, only geometric nonlinearity may be important. For these cases, the structural components experience only small material strains under load but may fail catastrophically due to their geometric configuration. A large class of structural systems may be accurately represented based on nonlinear geometrical, small strain, and linear elastic material behavior.

Many of the nonlinear displacement terms may be considered negligable in a geometrically nonlinear analysis depending on the specific situation. An accurate load-displacement charactarization of a flat plate is based on the von Karman equations where many nonlinear rotational terms have been discarded as negligable. This characterization gives an accurate representaion for plate deflections that are many times the plate thickness. This formulation is valid for only moderate rotations and is called an intermediate nonlinearity approach.

Laminated plates also have an additional complication. Three dimensional effects can become very important because of potentially large directional variations of stiffness properties due to tailoring. Also, the problem of delamination consideration, which only now is considered due to low velocity impact, requires a higher order theory to capture the transverse shear stress terms. Whereas classical two dimensional assumptions may be valid for an identical plate structure consisting of isotropic materials, they may lead to large errors for orthotropic materials. Therefore, through the thickness effects should be considered when analyzing composite materials.

The general class of problems that include large displacements and intermediate rotations, small strains, linearly elastic material behavior, and parabolic transverse shear distribution is addressed in this thesis. Unfortunately, closed form solutions are very limited and cannot include all of the desired features. Therefore, the finite element numerical approach is chosen as the solution technique in this research.

Previous Work

Previous related work is presented from two areas. First, linear and nonlinear techniques for analyzing plate structures are discussed. Second, finite element numerical solution techniques are discused.

Plate Theories. The classical linear approach, known as Kirchhoff flat plate theory (41) is based on the following assumptions: 1) the plate is thin, 2) the displacements and rotations are small, 3) normals to the plate datum surface before deformation remain normal after deformation, and 4) transverse normal stress is negligable.

The third assumption effectively neglects transverse shear strains although the transverse shear stresses must be included in the equilibrium equations. Since the plate is thin, it is assumed to be in a state of plane stess, i.e. the transverse normal stress is assumed to be negligibly small. Also, because the plate is thin, the effects of the normal tranverse strains are often neglected compared to the effects of the inplane strains, i.e. the length of a normal to the datum surface is often assumed to remain constant throughout deformation. The normal transverse strain can be included in the analysis through the constitutive relations. In deriving the equilibrium equations, statically equivalent forces and moments acting on the datum surface are defined by integrating stresses through the thickness.

As mentioned previously, the Kirchhoff flat plate theory applies to a plate so thin that all transverse deformation effects, i.e. transverse stresses and strains, can be neglected. As the plate becomes thicker relative to its inplane dimensions, these transverse effects become more pronounced, especially the transverse shear deformations (10,12,13). The first theories that included the tranverse shear deformations relaxed the assumption on the deformed normals to the plate datum surface. Now, the normal is permitted to rotate so that plane sections perpendicular to the datum surface remain plane but not necessarily perpendicular. The plate strain displacement relations are derived from kinematics and the 3-D strain displacement relations. The transverse shear is obtained by including independent degrees of freedom in the kinematics. The plate is fully described by the behavior of the datum surface and therefore these approaches represent 2-D theories (32).

The shell kinematics developed by Bassett, as discussed

in (8), express the displacements as an infinite power series in the thickness parameter or coordinate. Hildebrand, Reissner, and Thompson (HRT) (8) introduced truncated Bassett kinematics to analyze thin elastic orthotropic plates and the importance of the transverse stresses and strains. HRT found that the effects of the second order displacement terms on the transverse shear deformation were negligible. Additionally, terms in the transverse displacement that resulted in nonzero transverse normal strains were found to be negligable. Reissner used these kinematics to analyze plates (39). Mindlin similarly included rotary inertia terms in the dynamic analysis of plates (15).

The Reissner-Mindlin (RM) kinematics do not satisfy the transverse shear boundary conditions on the top and bottom surfaces of the plate since a constant shear angle through the thickness is assumed, i.e. plane sections remain plane. Because of this, the theories based on these kinematics usually require shear correction factors to satisfy equilibrium.

Levinson (14), Murthy (16), and Reddy (32) have developed theories that include cubic terms in the inplane displacement kinematics which produce zero transverse shear stresses at the top and bottom surfaces of the plate. Satisfying zero transverse shear stresses on the top and bottom surfaces of the plate gives a parabolic shear strain distribution through the thickness, thus agreeing more closely with linear elasticity. The number of variables in the kinematics is equal to that in the RM theory, but shear correction factors are not needed.

The preceding discussion applied primarily to plates made of isotropic materials. HRT (8) were the first to

apply plate equaitions to an orthotropic material. Reddy (32) discusses anisotropic laminated plate structures including various transverse shear deformation treatments in his text.

The simpifying assumption of laminated anisotropy is often used to apply a 2-D theory to plates made of layers of composite materials (32), In this approach, the individual properties of the composite elements, the fibers and the matrix, are "smeared" and thus each lamina is treated as an orthotropic material. Also, laminated anisotropy assumes perfect bonding between layers, i.e. the interply adhesive has infinitesimal thickness but infinite stiffness. This approach leads to classical laminated plate theory (CLPT). The references by Jones (11) and Ashton and Whitney (2) are thorough presentations of CLPT. CLPT relies on the Kirchhoff assumptions on the datum surface normals; however both references point out that the transverse shear deformation is more significant in laminated anisotropic structures over similar isotropic constructions.

Yang, Norris, and Stavsky (48) generalized the RM theory to laminated anisotropic plates. Whitney and Pagano (47) were the first to apply it to composite plates. Thick composite plate closed form solutions were developed by Reddy and Chao (35).

Reddy (32,38) extended the cubic kinematical approach to analyze laminated anisotropic plates and he and Soldatos applied them to solve several linear static and buckling problems (26,33,38).

Pagano (20,21,22,23) and Srinivas and Rao (39) developed some exact solutions of 3-D elasticity equations governing composite plates that have been used to validate these theories. They conclude that CLPT gives fairly good

approximations for both the displacements and stresses if the plate is thin. Thinness, as defined for layered composite plates, not only considers length to thickness ratios but also the degree of anisotropy. Transverse stresses are calculated from the eqilibrium equations and the CLPT inplane stresses. Higher order shear theories do not give much better transverse stress results but displacements show a marked improvement over CLPT for the thicker plates. Transverse stresses are calculated best from equilibrium instead of from the constitutive relations (11).

Much of the previously mentioned research in the analysis of composite plates is limited to geometrically linear problems. Reddy (31) concludes this may have been due to the complexity of the nonlinear partial differential equation associated with the large deflection theory of composite plates. Approximate solutions to the large deflection theory (in von Karman's sense) of laminated composite plates were attempted by Whitney and Leissa (46), Bennett (4), Bert (5), Zaghloul and Kennedy (49), and Noor and Hartley (17). Zaghloul and Kennedy (49) used a finite difference successive iterative technique in their analysis. In all of these studies, with the exception of (17), the transverse shear effects were neglected. The finite element employed by Noor and Hartley (17) includes the effect of transverse shear strains; however, it is algebraically complex and involves a large degree of freedom per element and thus one can preclude the use of such elements in the nonlinear analysis of composite plates. The finite element developed by Reddy (30) was extended to nonlinear bending of composite plates (36,37).

Finite Element Plate Applications. General 3-D

elements could be used to model plate structures. Unfortunately, since the plate is thin, numerical ill conditioning results. Also, using 3-D elements would involve many degrees of freedom (DOF) that may not be necessary. Consequently, elements that are specifically designed for plate structures are developed.

The most popular approach is to degenerate the 3-D displacement relations to form the element. This first appeared in the form of the Ahmed element (1). In elements of this type, transverse displacements and rotations are treated independently and therefore, are well suited to Reissner-Mindlin shear deformation theories. Also, normal stress is assumed to be zero consistent with most plate theories. However, it develops serious shear "locking" problems as the plate becomes thinner. Consequently, this method is generally used with some means to remedy the locking phenomenon. Zienkiewicz, Taylor, and Too (50) introduced reduced or selective integration to alleviate these shear locking problems.

Application of material anisotropy in finite elements was done by Pryor and Barker (27) who developed a linear flat plate element based on laminated anisotropic plate theory including RM shear deformations. They suggest an approach where each layer of the laminate has rotational degrees of freedom which allows the satisfaction of transverse stress continuity at each laminate boundary.

This idea has been applied using linear theory and the Ahmad element by several investigators (9). Recently, Palazotto and Witt (25) extended the approach to a geometrically nonlinear shell formulation and applied it to flat plates. Hinrichsen and Palazotto (9) used a cubic spline function to represent the transverse displacements of

a flat plate and found that while giving a higher order approximation to displacements, the equations were simplified over the work of (25) which essentially used a quadratic spline.

Shear locking may be reduced in finite element formulations by using higher order kinematics to represent the displacements through the thickness. Putcha and Reddy (28) used cubic kinematics to formulate a mixed element for nonlinear anisotropic plate analysis. For many of the cases examined, the element did not lock as its thickness was decreased even using exact integration.

The simultaneous nonlinear equations that result from the finite element discretizations are typically solved using direct iteration or Newton-Raphson method. Thorough overviews of solution techniques can be found in Stricklin and Haisler (43), Bathe and Cimento (3), Riks (40), and Waszczszyn (45). The direct iteration is generally not used because it often diverges, and the Newton-Raphson, without modifications, is not used because it is inefficient and sometimes unreliable. A form of the Newton-Raphson method that is guaranteed to converge increments many small load steps instead of a single increment to reach a target load. One way to make this approach more efficient, is to not update the tangent stiffness matrix with each iteration. This form is called the modified Newton-Raphson method.

As can be seen, much work has been done in the analysis of composite flat plate structures. Unfortunaly, not as much attention has been placed on studying their nonlinear response. The research effort here will focus on geometrically nonlinear composite plate behavior including the very important influence of transverse shear deformation.

The research presented here used a finite element code developed by Dennis (7). This code was designed to analyze a fully nonlinear cylindrical shell. However, since a plate can be modeled as a cylindrical shell of infinite radius, this code can be used for flat plate analysis. The code includes through the thickness shear effects and the von Karman geometric nonlinearity equations as applied to composite materials.

II. THEORY

Reference (7) contains a very complete development of the equations for a finite element code for a fully nonlinear cylindrical shell. Within this code there is also the capability to analyze both the linear and the von Karman plate problems studied in this research. Both types of analysis include the through the thickness shear effects. This causes the linear solution to be different than the classical plate theory solution. This also causes the von Karman solution obtained to be different than the "classical" von Karman plate solution. The highlights of the derivation are repeated here and, whenever possible, the derivation is related to the von Karman plate problem. The linear plate problem is a simplification of the von Karman plate problem.

Constitutive Relationships

We begin by assuming a linear constitutive relationship between stresses, σ_{ij}, and strains, ε_{ij}, of the form

$$\sigma_{ij} = a_{ijkl}\,\varepsilon_{kl} \qquad i,j,k,l = 1,2,3 \tag{2.1}$$

where a_{ijkl} are constants of the elasticity tensor.

In this research, we deal with materials that are transversely isotropic with respect to planes parallel to the 2-3 plane. In this case Eqn (2.1) becomes

$$\begin{Bmatrix} \sigma_1 \\ \sigma_2 \\ \sigma_3 \\ \sigma_4 \\ \sigma_5 \\ \sigma_6 \end{Bmatrix} = \begin{bmatrix} C_{11} & C_{12} & C_{13} & 0 & 0 & 0 \\ C_{12} & C_{22} & C_{23} & 0 & 0 & 0 \\ C_{13} & C_{23} & C_{33} & 0 & 0 & 0 \\ 0 & 0 & 0 & C_{44} & 0 & 0 \\ 0 & 0 & 0 & 0 & C_{55} & 0 \\ 0 & 0 & 0 & 0 & 0 & C_{66} \end{bmatrix} \begin{Bmatrix} \varepsilon_1 \\ \varepsilon_2 \\ \varepsilon_3 \\ \varepsilon_4 \\ \varepsilon_5 \\ \varepsilon_6 \end{Bmatrix} \qquad (2.2)$$

where contracted notation is introduced

$$\sigma_1=\sigma_{11},\ \sigma_2=\sigma_{22},\ \sigma_3=\sigma_{33},\ \sigma_4=\sigma_{23},\ \sigma_5=\sigma_{13},\ \sigma_6=\sigma_{12} \qquad (2.3a)$$

$$\varepsilon_1=\varepsilon_{11},\ \varepsilon_2=\varepsilon_{22},\ \varepsilon_3=\varepsilon_{33},\ \varepsilon_4=2\varepsilon_{23},\ \varepsilon_5=2\varepsilon_{13},\ \varepsilon_6=2\varepsilon_{12} \qquad (2.3b)$$

Transverse isotropy assumes $E_2=E_3$ and $\nu_{12}=\nu_{13}$ and the C_{ij} written in terms of engineering constants become

$$C_{11} = E_1 \frac{1-\nu_{23}^2}{\Delta}, \quad C_{12} = C_{13} = E_1\nu_{21}\frac{1+\nu_{23}}{\Delta}$$

$$C_{33} = C_{22} = E_2 \frac{1+\nu_{12}\nu_{21}}{\Delta} \qquad (2.4)$$

$$C_{23} = E_2 \frac{\nu_{23}+\nu_{12}\nu_{21}}{\Delta}, \quad C_{44} = G_{23},\ C_{55} = G_{13},\ C_{66} = G_{12}$$

$$\Delta = 1 - 2\nu_{12}\nu_{21} - \nu_{23}^2 - 2\nu_{12}\nu_{21}\nu_{23}$$

By assuming an approximate case of plane stress, i.e. $\sigma_3=0$, Eqn (2.2) becomes

$$\begin{Bmatrix} \sigma_1 \\ \sigma_2 \\ \sigma_6 \\ \sigma_4 \\ \sigma_5 \end{Bmatrix} = \begin{bmatrix} Q_{11} & Q_{12} & 0 & 0 & 0 \\ Q_{12} & Q_{22} & 0 & 0 & 0 \\ 0 & 0 & Q_{66} & 0 & 0 \\ 0 & 0 & 0 & Q_{44} & 0 \\ 0 & 0 & 0 & 0 & Q_{55} \end{bmatrix} \begin{Bmatrix} \varepsilon_1 \\ \varepsilon_2 \\ \varepsilon_6 \\ \varepsilon_4 \\ \varepsilon_5 \end{Bmatrix} \qquad (2.5)$$

where $Q_{ij} = C_{ij} - \dfrac{C_{i3}C_{j3}}{C_{33}}$

For transverse isotropy it can be shown that

$$Q_{11} = E_1/\Delta,\ Q_{12} = \nu_{21}E_2/\Delta,\ Q_{22} = E_2/\Delta,$$

$$Q_{66} = G_{12},\ Q_{44} = G_{23},\ Q_{55} = G_{13}, \qquad (2.6)$$

$$\Delta = 1 - \nu_{12}\nu_{21}$$

For a plate constructed of layers of transversely orthotropic material, the fibers are generally oriented at some angle away from the geometric axis of the plate. Therefore, the constitutive relations of Eqn (2.5) must be transformed into the plate coordinates resulting in Eqns (2.7) and (2.8).

$$\begin{Bmatrix} \sigma_1 \\ \sigma_2 \\ \sigma_6 \end{Bmatrix}^k = \begin{bmatrix} \bar{Q}_{11} & \bar{Q}_{12} & \bar{Q}_{16} \\ \bar{Q}_{12} & \bar{Q}_{22} & \bar{Q}_{26} \\ \bar{Q}_{16} & \bar{Q}_{26} & \bar{Q}_{66} \end{bmatrix}^k \begin{Bmatrix} \varepsilon_1 \\ \varepsilon_2 \\ \varepsilon_6 \end{Bmatrix} \qquad (2.7)$$

$$\begin{Bmatrix} \sigma_4 \\ \sigma_5 \end{Bmatrix}^k = \begin{bmatrix} \bar{Q}_{44} & \bar{Q}_{45} \\ \bar{Q}_{45} & \bar{Q}_{55} \end{bmatrix}^k \begin{Bmatrix} \varepsilon_4 \\ \varepsilon_5 \end{Bmatrix} \tag{2.8}$$

Where the $\bar{Q}_{ij}$(i,j=1,2,6) and $\bar{Q}_{mn}$(m,n=4,5) are elements of symmetric arrays of transformed stiffnesses for the k^{th} ply.

Kinematic Relations

We begin the derivation of the kinematic relationships by assuming a truncated power series inplane displacement function. This will lead to the desired parabolic transverse shear strains. This displacement function was developed in (28) and is shown in Eqn (2.9) where u_i°, ψ_i, θ_i, and ϕ_i are functions of the inplane coordinates only:

$$u_i = u_i^\circ + \zeta\psi_i + \zeta^2\theta_i + \zeta^3\phi_i \tag{2.9}$$

where u_i (1 = 1,2) are total inplane displacements,

u_i° is the translation displacement of the datum surface,

ζ is the through the thickness coordinate,

ψ_i is rotational displacements due to bending, and

θ_i, ϕ_i are unknown DOF to be determined.

We then assume that the transverse shear strains, $\varepsilon_4=\varepsilon_5=0$ on the surface. For an orthotropic material, this implies that the transverse shear stresses, $\sigma_4=\sigma_5=0$ on the surface. For example, for a flat plate of thickness h with ξ_i(i=1,2) representing the inplane coordinates

$$\varepsilon_5\Big|_{\zeta=\pm h/2} = \frac{\partial u_1}{\partial \zeta} + \frac{\partial u_3}{\partial \zeta_1} \qquad (2.10)$$

$$= \Big[\ \psi_1 + 2\zeta\theta_1 + 3\zeta^2\phi_1 + u^\circ_{3,1} + \zeta\psi_{3,1} + \zeta^2\theta_{3,1}$$

$$+ \zeta^3\phi_{3,1}\ \Big]\Big|_{\zeta=\pm h/2} = 0$$

Where the subscript ,α represents partial differentiation of the variable with to respect to α. For Eqn (2.10) to hold true at the top and bottom of the plate, $\theta_1=\psi_3=\phi_3=0$. Also, based on (8) we neglect $\zeta^2\theta_3$ term in u_3 as small compared to u°_3. Now solve Eqn (2.10) for ϕ_1:

$$\left[\ \psi_1 + 3\zeta^2\phi_1 + u^\circ_{3,1}\ \right]\Big|_{\zeta=\pm h/2} = 0 \qquad (2.10a)$$

$$\psi_1 + 3(h/2)^2\phi_1 + u^\circ_{3,1} = 0$$

$$\phi_1 = -\frac{4}{3h^2}\left[\ u^\circ_{3,1} + \psi_1\ \right]$$

This leads to parabolic transverse shear strain shown in Eqn (2.11):

$$\varepsilon_5 = \left[\ 1 - \frac{4}{3h^2}\zeta^2\ \right]\left[\ \psi_1 + u^\circ_{3,1}\ \right] \qquad (2.11)$$

a similar approach can be used on ε_4. This leads to the kinematic equations used in this research as shown in Eqn (2.12):

$$u_1 = u + \zeta\psi_1 - \frac{4}{3h^2}\zeta^3\left[\psi_1 + w_{,1}\right] \qquad (2.12a)$$

$$u_2 = v + \zeta\psi_2 - \frac{4}{3h^2}\zeta^3\left[\psi_2 + w_{,2}\right] \qquad (2.12b)$$

$$u_3 = w \qquad (2.12c)$$

The von Karman plate strain displacement relations are given for the inplane strains by Eqn (2.13):

$$\begin{aligned} \varepsilon_1 &= u_{1,1} + \tfrac{1}{2} w^2_{,1} \\ \varepsilon_2 &= u_{2,2} + \tfrac{1}{2} w^1_{,2} \\ \varepsilon_6 &= u_{1,2} + u_{2,1} + w_{,1}w_{,2} \end{aligned} \qquad (2.13)$$

These come from the Green's strain tensor (24) shown in Egn (2.14):

$$2e_{ij} = 2\varepsilon_{ij} + (\varepsilon_{ki} + \omega_{ki})(\varepsilon_{kj} + \omega_{kj}) \qquad (2.14)$$

where,

e_{ij} = Greens strain tensor

$$2\varepsilon_{ij} = u_{i,j} + u_{j,i} \qquad (2.14a)$$

$$2\omega_{ij} = u_{i,j} - u_{j,i} \qquad (2.14b)$$

Then, assume the following: 1) strains are small, so $\varepsilon_{ki}\varepsilon_{kj}$ terms can be neglected, 2) rotations relative to the x and y axis are moderately small, this allows $\varepsilon_{ki}\omega_{kj}$ and $\omega_{ki}\varepsilon_{kj}$ terms to be neglected, and 3) rotations relative to ζ are negligable, this allows $\omega_{33}\omega_{33}$ term to be neglected. If one Substitutes Eqn (2.12) into Eqn (2.13) and sets $e_{ij}=\varepsilon_{ij}$, the following is obtained

$$\varepsilon_1 = u_{,1} + \zeta\psi_{1,1} + \zeta^3 k(w_{,11} + \psi_{1,1}) + \tfrac{1}{2}w^2_{,1}$$

$$\varepsilon_2 = v_{,2} + \zeta\psi_{2,2} + \zeta^3 k(w_{,22} + \psi_{2,2}) + \tfrac{1}{2}w^2_{,2} \qquad (2.15)$$

$$\varepsilon_6 = u_{,2} + v_{,1} + \zeta(\psi_{1,2} + \psi_{2,1}) + \zeta^3 k(2w_{,12} + \psi_{1,2} + \psi_{2,1}) + w_{,1}w_{,2}$$

where $k = -\dfrac{4}{3h^2}$

Notice that the nonlinear terms (i.e. $\frac{1}{2}w^2_{,1}$ $\frac{1}{2}w^2_{,2}$ and $w_{,1}w_{,2}$) are functions only of the inplane coordinate and not the transverse coordinate ζ.

If Eqn (2.15) is rewritten in a more convienent form for matrix manipulations to be conducted shortly, the following is obtained where p is handled using repeating subscript rule

$$\varepsilon_1 = \varepsilon_1^\circ + \zeta^p x_{1p} \qquad (2.16)$$

where

$$\varepsilon^\circ = u_{,1} + \tfrac{1}{2}w^2_{,1} \qquad (2.16a)$$

$$x_{11} = \psi_{1,1} \qquad (2.16b)$$

$$x_{13} = k(w_{,11} + \psi_{1,1}) \qquad (2.16c)$$

$$x_{1p}(p=2,4,5,6,7) = 0$$

$$\varepsilon_2 = \varepsilon_2^\circ + \zeta^p x_{2p} \qquad (2.17)$$

where

$$\varepsilon^\circ = v_{,2} + \tfrac{1}{2}w^2_{,2} \qquad (2.17a)$$

$$x_{21} = \psi_{2,2} \qquad (2.17b)$$

$$x_{23} = k(w_{,22} + \psi_{2,2}) \qquad (2.17c)$$

$$\varkappa_{2p}(p=2,4,5,6,7) = 0$$

$$\varepsilon_6 = \varepsilon_6^\circ + \zeta^p \varkappa_{6p} \tag{2.18}$$

where

$$\varepsilon_6^\circ = u_{,2} + v_{,1} + w_{,1} w_{,2} \tag{2.18a}$$

$$\varkappa_{61} = \psi_{1,2} + \psi_{2,1} \tag{2.18b}$$

$$\varkappa_{63} = k(2w_{,12} + \psi_{1,2} + \psi_{2,1}) \tag{2.18c}$$

$$\varkappa_{6p}(p=2,4,5,6,7) = 0$$

Also, it can be readily seen from Eqn (2.11) that

$$\varepsilon_5 = \varepsilon_5^\circ + \zeta^p \varkappa_{5p} \tag{2.19}$$

where

$$\varepsilon_5^\circ = w_{,1} + \psi_1 \tag{2.19a}$$

$$\varkappa_{52} = 3k(w_{,1} + \psi_1) \tag{2.19b}$$

$$\varkappa_{5p}(p=1,3,4,5,6,7) = 0$$

and

$$\varepsilon_4 = \varepsilon_4^\circ + \zeta^p \varkappa_{4p} \tag{2.20}$$

where

$$\varepsilon_4^\circ = w_{,2} + \psi_2 \tag{2.20a}$$

$$\varkappa_{42} = 3k(w_{,2} + \psi_2) \tag{2.20b}$$

$$\varkappa_{4p}(p=1,3,4,5,6,7) = 0$$

Plate Potential Energy

The strain energy terms are given by

$$\Pi_p = U - V \tag{2.21}$$

where

U = internal strain energy
V = work done by external forces

we divide the internal strain energy into two parts (i.e. $U=U_1+U_2$) where U_1 represents the inplane terms and U_2 represents the through the thickness terms. Eqns (2.7), (2.8), (2.16), (2.17), (2.18), (2.19), (2.20), and (2.21) give the internal strain energy of the plate

$$U_1 = \frac{1}{2}\int_\Omega \int_h \Big[\bar{Q}_{11}(\varepsilon_1^\circ + \zeta^p \varkappa_{1p})^2 + \bar{Q}_{22}(\varepsilon_2^\circ + \zeta^p \varkappa_{2p})^2 + 2\,\bar{Q}_{12}(\varepsilon_1^\circ + \zeta^p \varkappa_{1p})(\varepsilon_2^\circ + \zeta^r \varkappa_{2r}) + \bar{Q}_{66}(\varepsilon_6^\circ + \zeta^p \varkappa_{6p})^2 + 2\,\bar{Q}_{16}(\varepsilon_1^\circ + \zeta^p \varkappa_{1p})(\varepsilon_6^\circ + \zeta^r \varkappa_{6r}) + 2\,\bar{Q}_{26}(\varepsilon_2^\circ + \zeta^p \varkappa_{2p})(\varepsilon_6^\circ + \zeta^r \varkappa_{6r}) \Big] d\zeta d\Omega \qquad (2.22a)$$

$$U_2 = \frac{1}{2}\int_\Omega \int_h \Big[\bar{Q}_{44}(\varepsilon_4^\circ + \zeta^2 \varkappa_{42})^2 + \bar{Q}_{55}(\varepsilon_5^\circ + \zeta^2 \varkappa_{52})^2 + 2\,\bar{Q}_{45}(\varepsilon_4^\circ + \zeta^2 \varkappa_{42})(\varepsilon_5^\circ + \zeta^2 \varkappa_{52}) \Big] d\zeta d\Omega \qquad (2.22b)$$

where,

$p,r = 1,2,3$

$\bar{Q}_{ij}$ generally vary as a function of ζ since a laminate is constructed of plies with different fiber orientations, and

Ω represents the plate middle, or datum, surface area.

Also, if one combines Eqns (2.16), (2.17), and (2.18), the following is obtained

$$\varepsilon = \varepsilon^{\circ} + \kappa\, z \tag{2.23a}$$

where

$$\varepsilon = \begin{Bmatrix} \varepsilon_1 \\ \varepsilon_2 \\ \varepsilon_6 \end{Bmatrix},\ \varepsilon^{\circ} = \begin{Bmatrix} \varepsilon_1^{\circ} \\ \varepsilon_2^{\circ} \\ \varepsilon_6^{\circ} \end{Bmatrix},\ \kappa = \begin{bmatrix} \kappa_{11} & \kappa_{123} \\ \kappa_{21} & \kappa_{223} \\ \kappa_{61} & \kappa_{623} \end{bmatrix},\ z \begin{Bmatrix} \zeta \\ \zeta^2 \\ \zeta^3 \end{Bmatrix} \tag{2.23b}$$

and

$$Q = \begin{bmatrix} \bar{Q}_{11} & \bar{Q}_{12} & \bar{Q}_{16} \\ & \bar{Q}_{22} & \bar{Q}_{26} \\ & & \bar{Q}_{66} \end{bmatrix}$$

We can now represent the first part of the internal strain energy more convieniently thus

$$U_1 = \tfrac{1}{2} \int_{\Omega} \int_{h} (Q\varepsilon)^{T} \varepsilon \; d\zeta d\Omega \tag{2.24}$$

Eqn (2.24) can be rewritten in terms of the plate mid surface where the ζ dependence has been integrated out by defining a series of elasticity arrays

$$U_1 = \tfrac{1}{2} \int_{\Omega} (u_1 + u_2 + u_3)\; d\Omega \tag{2.25}$$

where,

$$u_1 = \int_h \varepsilon^{\circ T}\, Q\, \varepsilon^{\circ}\; d\zeta = \int_h \varepsilon_j^{\circ}\; \varepsilon_i^{\circ}\; \bar{Q}_{ij}\; d\zeta = \varepsilon_j^{\circ}\; \varepsilon_i^{\circ}\; A_{ij} \tag{2.25a}$$

$$u_2 = \int_h 2\; \varepsilon^{\circ T}\, Q\, \kappa\, z\; d\zeta = \int 2\; \varepsilon_j^{\circ}\; \bar{Q}_{ij}\; \kappa_{ip}\; \zeta^{p}\; d\zeta$$

$$= 2\; \varepsilon_j^{\circ}\; (\kappa_{i1} B_{ij} + \kappa_{i2} D_{ij} + \kappa_{i3} E_{ij}) \tag{2.25b}$$

$$u_3 = \int_h Z^T (K\ Q\ K)\ Z\ d\zeta = \int_h \varkappa_{jp}\ \varkappa_{ir}\ \bar{Q}_{ij}\ \zeta^{p+r}\ d\zeta$$

$$= \varkappa_{j1}\varkappa_{i1}D_{ij} + 2\varkappa_{j1}\varkappa_{i2}E_{ij} + (2\varkappa_{j1}\varkappa_{i3} + \varkappa_{j2}\varkappa_{i2})F_{ij}$$

$$+ 2\varkappa_{j2}\varkappa_{i3}G_{ij} \qquad (2.25c)$$

where i,j = 1,2,6 and p,r = 1,2,3 (repeating subscript rule again applies) and

$$[A_{ij},B_{ij},D_{ij},E_{ij},F_{ij},G_{ij}] = \int_h \bar{Q}_{ij}\ [1,\zeta,\zeta^2,\zeta^3,\zeta^4,\zeta^5]\ d\zeta \qquad (2.25d)$$

Substituting Eqns (2.16), (2.17), and (2.18) into Eqns (2.25a), (2.25b), and (2.25c) results in the following:

$$u_1 = \varepsilon^\circ_j\ \varepsilon^\circ_i\ A_{ij} \qquad (2.26)$$

$$u_2 = 2\ \varepsilon^\circ_j\ (\varkappa_{i1}B_{ij} + \varkappa_{i3}E_{ij}) \qquad (2.27)$$

$$u_3 = \varkappa_{j1}\varkappa_{i1}D_{ij} + 2\varkappa_{j1}\varkappa_{i3}F_{ij} \qquad (2.28)$$

The von Karman plate relations only retain the nonlinear displacement terms in the transverse displacement, w. Note that only cubic and quartic terms will result in nonlinear terms in the equilibrium equations ($\delta\Pi_p$=0). The only cubic and quartic terms in w come from (2.26) and (2.27). Also, for symmetrically arranged laminates (i.e. the case in this research) $B_{ij} = E_{ij} = 0$ for all i,j. Therefore,

$$U_1 = \tfrac{1}{2} \int_\Omega \varepsilon^\circ_j\ \varepsilon^\circ_i\ A_{ij}\ d\Omega \qquad (2.29)$$

and with a similar treatment as U_1, U_2 becomes

$$U_2 = \frac{1}{2}\int_\Omega (\varepsilon^\circ_m \varepsilon^\circ_n A_{mn} + \varepsilon^\circ_n \varkappa_{m2} D_{mn} + \varkappa_{n2}\varkappa_{m2} F_{mn})\, d\Omega \qquad (2.30)$$

where

$$[A_{mn},\ D_{mn},\ F_{mn}] = \int_h [1,\ \zeta^2,\ \zeta^4]\ Q_{mn}\, d\zeta \qquad m,n = 4,5$$

Now we have all the pieces in place for the "modified" von Karman approach. Modified in that it includes the through the thickness shear terms.

Finite Element Solution

The first part of the derivation is independent of the particular element chosen. The second part concerns the specific element used in this research. We begin the element independent portion of the derivation by developing an expression for the strain energy of the form

$$\Pi_p = \frac{q^T}{2}\left[K + \frac{N_1}{3} + \frac{N_2}{6} \right] q - q^T R \qquad (2.31)$$

where,

q is a column array of nodal displacements,

R is a column array of nodal loads,

K is an array of constant stiffness coefficients,

N_1 is an array of stiffness coefficients that are linear in displacement, and

N_2 is an array of stiffness coefficients that are quadratic in displacement.

Taking the first variation if Eqn (2.31) gives

$$\delta\Pi_p = \delta q^T \left[\left\{ K + \frac{N_1}{2} + \frac{N_2}{3} \right\} q - R \right] = 0 \qquad (2.32)$$

$$= \delta q^T F(q) = 0$$

F(q) represents the equilibrium equations For an arbitrary and independent δq

$$F(q) = 0 \tag{2.33}$$

$$F(q) = \left\{ K + \frac{N_1}{2} + \frac{N_2}{3} \right\} q - R = 0 \tag{2.34}$$

Eqn (2.33) can be expanded in a Taylor series giving

$$F(q + \Delta q) = F(q) + \frac{\partial F}{\partial q} \Delta q + \cdots = 0 \tag{2.35}$$

Now neglect higher order terms because Δq is small and rearranging gives

$$\frac{\partial F}{\partial q} \Delta q = -F(q) \tag{2.36}$$

$$[\ K + N_1 + N_2\ ]\ \Delta q = -F(q)$$

$$K_T\ \Delta q = -F(q) \tag{2.37}$$

where, K_T = tangent stiffness matrix

$$K_T = K + N_1 + N_2 \tag{2.38}$$

Eqn (2.37) is solved in an iterative manner by a Newton-Raphson technique. The current values of q are inserted in $N_1$and N_2 on both sides of Eqn (2.37) and the ensuing linear equations are solved for Δq. Δq is then added to q and the new q is inserted into $N_1$and N_2again and so on. This is continued until the RHS becomes arbitraily small.

The preceeding derivation assumed a definition of K, N_1, and N_2 such that these terms repeated themselves in the first variation (i.e. Eqn (2.31) to Eqn (2.32)) and aqain in the Taylor series expansion (i.e. Eqn (2.33) to Eqn (2.35)).

Rajasekaran and Murray (29) and Dennis (7) have developed a procedure which insures this repetition. The overall technique is shown here for a "modified" von Karman flat plate. For a more detailed development see the references listed above.

We begin by dividing each strain component of Eqns (2.16), (2.17), and (2.18) into linear and nonlinear parts:

$$\varepsilon_i^\circ = {}_\circ L_i^T \, d + \tfrac{1}{2} \, d^T \, {}_\circ H_i \, d$$

$$\varkappa_{ip} = {}_p L_i^T \, d + \tfrac{1}{2} \, d^T \, {}_p H_i \, d \qquad (2.39)$$

where ${}_j L_i (j = 0,1,2,3,4,5,6,7)$ are column arrays,
${}_j H_i$ are symmetric arrays,
$i = 1,2,6$ and $p = 1$ to 7, and
d^T is the displacement gradient vector.

$$d^T = \{ u \; u_{,1} \; u_{,2} \; v \; v_{,1} \; v_{,2} \; w \; w_{,1} \; w_{,2} \; w_{,11}$$

$$w_{,22} \; w_{,12} \; \psi_1 \; \psi_{1,1} \; \psi_{1,2} \; \psi_2 \; \psi_{2,1} \; \psi_{2,2} \} \qquad (2.40)$$

Each ${}_j L_i$ are 18x1 column arrays and each ${}_j H_i$ is an 18x18 array. From Eqns (2.16), (2.17), and (2.18) it can be seen that

$$\begin{aligned}
&{}_\circ L_1(2) = 1 \\
&{}_\circ L_2(6) = 1 \\
&{}_\circ L_6(3) = {}_\circ L_6(5) = 1 \\
&{}_1 L_1(14) = 1 \\
&{}_1 L_2(18) = 1 \\
&{}_1 L_6(15) = {}_1 L_6(17) = 1
\end{aligned} \qquad (2.41a)$$

$$
\begin{aligned}
&{}_3L_1(10) = {}_3L_1(14) = k \\
&{}_3L_2(11) = {}_3L_2(18) = k \\
&{}_3L_6(12) = 2k,\ {}_3L_6(15) = {}_3L_6(17) = k \\
&\\
&{}_oH_1:\ (8,8) = 1 \\
&{}_oH_2:\ (9,9) = 1 \\
&{}_oH_6:\ (8,9) = 2
\end{aligned}
\qquad (2.41b)
$$

where the number in the parenthesis denotes the position of the given value in the particular array. All other positions are zero.

Now substituting Eqn (2.39) into Eqn (2.29), which is repeated here, one obtains (recall these expressions are for inplane strain energy using strain at the datum surface)

$$U_1 = \tfrac{1}{2} \int_\Omega \varepsilon^\circ_j \, \varepsilon^\circ_i \, A_{ij} \, d\Omega \qquad (2.29)$$

gives

$$U_1 = \tfrac{1}{2} \int_\Omega d^T \left[\hat{K} + \hat{N}_1 + \tfrac{1}{4}\hat{N}_2 \right] d \, d\Omega \qquad (2.42)$$

where

$$\hat{K} = A_{ij} \, {}_oL_i \, {}_oL_j^T \qquad (2.43a)$$

$$\hat{N}_1 = A_{ij} \, {}_oL_i \, d^T \, {}_oH_j \qquad (2.43b)$$

$$\hat{N}_2 = A_{ij} \, {}_oH_i \, d \, d^T \, {}_oH_j \qquad (2.43c)$$

and the repeating subcript rule again applies.

Unfortunately, not all these terms show the required repetition when the variation and derivative are taken. That is, new terms will result. In order to get required repititions, the following substitutions are made:

In Eqn (2.43b) let

$$ {}_oL_i \; d^T \, {}_oH_j = \tfrac{1}{3} \left[{}_oL_i \; d^T \, {}_oH_j + d^T \, {}_oL_i \; {}_oH_j + {}_oH_i \; d \; {}_oL_j \right] \qquad (2.44) $$

and in Eqn (2.43c) let

$$ {}_oH_i \; d \; d^T \, {}_oH_j = \tfrac{1}{3} \left[{}_oH_i \; d \; d^T \, {}_oH_j + \tfrac{1}{2} \, d^T \, {}_oH_i \; d \; {}_oH_j + {}_oH_i \; d \; d^T \, {}_oH_j + \tfrac{1}{2} \, d^T \, {}_oH_i \; d \; {}_oH_j \right] \qquad (2.45) $$

With these substitutions, Eqn (2.42) can be rewritten

$$ U_1 = \tfrac{1}{2} \int_\Omega d^T \left[\hat{K} + \frac{\hat{N}_1}{3} + \frac{\hat{N}_2}{6} \right] d \; d\Omega \qquad (2.46) $$

The tranverse shear energy terms are handled in a similar manner. These are much simpler because the tranverse shear terms are linear in displacement and therefore all ${}_jH_m$ terms are zero. Therefore, let

$$ \begin{aligned} \varepsilon_m^\circ &= {}_oS_m^T \, d \\ \gamma_{2m} &= {}_2S_m^T \, d \end{aligned} \qquad m = 4,5 \qquad (2.47) $$

From Eqns (2.19) and (2.20) it can be seen that

$$ \begin{aligned} {}_oS_4(9) &= {}_oS_4(16) = 1 \\ {}_oS_5(8) &= {}_oS_5(13) = 1 \\ {}_2S_4(9) &= {}_2S_4(16) = 3k \\ {}_2S_5(8) &= {}_2S_5(13) = 3k \end{aligned} \qquad (2.48) $$

Because these strains are assumed to be linear, strain energy terms brought about by through the thickness shears are only given for $\tilde{K}$. $\tilde{N}_1$ and $\tilde{N}_2$ are zero. Thus, by

substituting Eqn (2.47) into Eqn (2.30) one obtains the U_2 internal energy function

$$U_2=\frac{1}{2}\int_{\Omega} d^T\left[A_{mn}\ {}_0S_m\ {}_0S_n^T+2D_{mn}\ {}_0S_m\ {}_2S_n^T+F_{mn}\ {}_2S_m\ {}_2S_n^T\right]d\ d\Omega \tag{2.49}$$

The repeating forms for the first variation and Taylor Series expansion which are added to $\hat{K}$ are formed by making the substitution below:

$${}_pS_m\ {}_rS_n^T = \frac{1}{2}\left[{}_pS_i\ {}_rS_j^T + {}_rS_i\ {}_pS_j^T\right] \qquad p,r = 0,2 \tag{2.50}$$

The last step in the element independent portion of the derivation is the discretation of the domain. This is done by approximating the continuum displacements by interpolation, or shape functions. So let

$$u = N\ q \tag{2.51}$$

where,

u = vector of continuum displacements

N = array of shape functions

q = nodal values of displacements

Then, the displacement qradient vector d is approximated from Eqn (2.51) by

$$d = \mathcal{D}\ q \tag{2.52}$$

where $\mathcal{D}$ is the array of shape functions and their derivatives. $\mathcal{D}$ is defined for a specific element and will be derived subsequently. Substituting Eqn (2.43) into Eqn (2.46) and including the tranverse shear terms of Eqn (2.49) in $\hat{K}$, the following potential energy function is obtained

$$\Pi_p = \frac{q^T}{2}\left[K + \frac{N_1}{3} + \frac{N_2}{6} \right] q - q^T R \qquad (2.53)$$

In Eqn (2.53)

$$K = \int_\Omega \mathcal{D}^T \hat{K} \mathcal{D}\, d\Omega$$

$$N_1 = \int_\Omega \mathcal{D}^T \hat{N}_1 \mathcal{D}\, d\Omega \qquad (2.54)$$

$$N_2 = \int_\Omega \mathcal{D}^T \hat{N}_2 \mathcal{D}\, d\Omega$$

Derivation of $\mathcal{D}$ for a 28 DOF element

Now we begin the second portion of the finite element derivation. This part is element dependent. The continuum displacements are approximated by the nodal displacements and shape functions. These shape functions are chosen such that the following requirements are met;

(1) continuous displacements within an element,

(2) the element must be able to represent constant strain,

(3) rigid body modes are present in the assumed displacements,

(4) compatibility exists between elements, and

(5) the element should not have a preferred direction, this is desired, not required.

From our displacement function, Eqn (2.12), it can be seen that seven degrees of freedom (DOF) are present at each node. These are u, v, w, $w_{,1}$, $w_{,2}$, ψ_1, and ψ_2. Continuity of displacement only is required for u, v, ψ_1, and ψ_2. Therefore, Lagrangian shape functions may be used since they gaurantee C°continuity. Continuity of displacement and their derivatives is required for w (i.e. w, $w_{,1}$, $w_{,2}$) and

Hermitian shape functions can be constucted that will provide C^1 continuity.

Dennis (7) begins the element definition by assuming the following 12 term quartic for the transverse displacement w, of a plate with four corner nodes. See figure 2.1.

$$w(x,y) = a_1 + a_2x + a_3y + a_4x^2 + a_5xy + a_6y^2 + a_7x^3 + a_8x^2y + a_9xy^2 + a_{10}y^3 + a_{11}x^3y + a_{12}xy^3 \qquad (2.55)$$

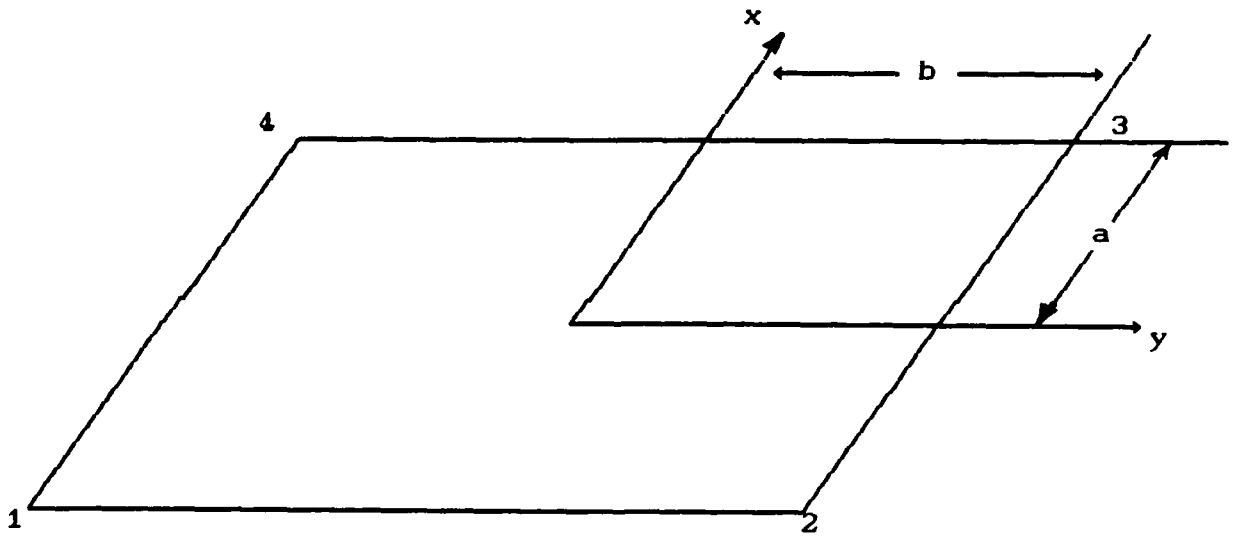

FIGURE 2.1. Rectangular Plate Element with Four Nodes

Now, Eqn (2.55) can be rewritten in the form of Eqn (2.51)

for an element as shown below.

$$w(x,y) = \underset{1\times 12}{\left[\begin{array}{cccc} \hat{\mathcal{H}}_1 & \mathcal{H}_2 & \mathcal{H}_3 & \mathcal{H}_4 \end{array}\right]}^{1\times 3} \underset{12\times 1}{\left\{\begin{array}{c} \hat{q}_1 \\ q_2 \\ q_3 \\ q_4 \end{array}\right\}}^{1\times 3} \qquad (2.56)$$

(note: (n x m) is the matrix order indicator)

where, for the k^{th} node,

$$q_k^T = \{\, w \;\; w,_1 \;\; w,_2 \,\}_k \qquad (2.56a)$$

$\mathcal{H}_k$ = Hermitian shape functions shown below

$$\mathcal{H}_k^T = \left\{\begin{array}{c} \mathcal{H}_{k1} \\ \mathcal{H}_{k2} \\ \mathcal{H}_{k3} \end{array}\right\} = \left\{\begin{array}{l} \frac{1}{8}(1+\zeta_k\zeta)(1+\eta_k\eta)(2+\zeta_k\zeta+\eta_k\eta-\zeta^2-\eta^2) \\ \frac{a}{8}\zeta_k(1+\zeta_k\zeta)^2(\zeta_k\zeta-1)(1+\eta_k\eta) \\ \frac{b}{8}\eta_k(1+\zeta_k\zeta)(\eta_k\eta-1)(1+\eta_k\eta)^2 \end{array}\right\} \qquad (2.56b)$$

where the k^{th} node has the natural coordinates (ζ_k, η_k) and $\zeta = x/a$ and $\eta = y/b$. See figure 2.2.

For the remaining nodal DOF u, v, ψ_1, and ψ_2 only C° continuity is required so we will use Lagrangian shape functions. For these DOF, we approximate Eqn (2.51) in the form shown below:

$$\underset{4\times 1}{\left\{\begin{array}{c} u \\ v \\ \psi_1 \\ \psi_2 \end{array}\right\}} = \underset{4\times 16}{\left[\begin{array}{cccc|c|cccc} N_1 & 0 & 0 & 0 & \cdots & N_4 & 0 & 0 & 0 \\ 0 & N_1 & 0 & 0 & \cdots & 0 & N_4 & 0 & 0 \\ 0 & 0 & N_1 & 0 & \cdots & 0 & 0 & N_4 & 0 \\ 0 & 0 & 0 & N_1 & \cdots & 0 & 0 & 0 & N_4 \end{array}\right]} \underset{16\times 1}{\left\{\begin{array}{c} q_1 \\ q_2 \\ q_3 \\ q_4 \end{array}\right\}} \qquad (2.57)$$

where for the k^{th} node,

$$q_k^T = \{\, u \;\; v \;\; \psi_1 \;\; \psi_2 \,\}_k \qquad (2.57a)$$

N_k are Lagrangian shape functions

$$N_k = \tfrac{1}{4}(1+\zeta_k\zeta)(1+\eta_k\eta) \qquad (2.57b)$$

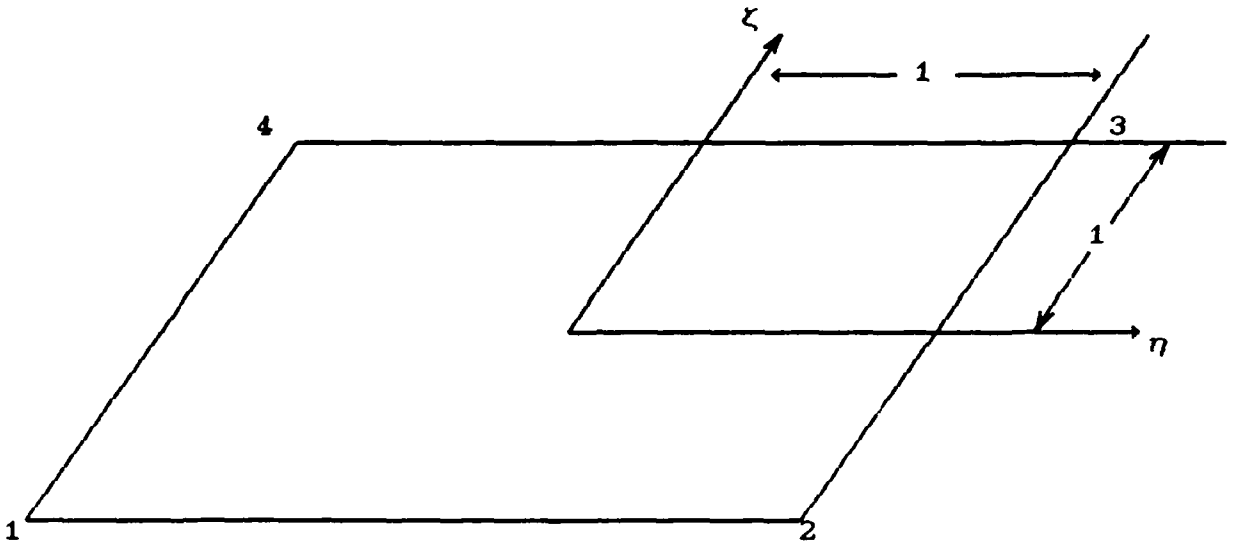

FIGURE 2.2. Rectangular plate element of Figure 2.1 in natural coordinates, $\zeta=x/a$ and $\eta=y/b$. This is the only element used.

Combining Eqn (2.56) and Eqn (2.57), the displacement gradient vector, Eqn (2.40), may be expressed as in Eqn (2.58) below:

$$\underset{18\times 1}{d(\zeta,\eta)} = Dq = \underset{18\times 28}{\begin{bmatrix} N_1 & 0 & 0 & \cdots & N_4 & 0 & 0 \\ 0 & H_1 & 0 & \cdots & 0 & H_4 & 0 \\ 0 & 0 & N_1 & \cdots & 0 & 0 & N_4 \end{bmatrix}} \underset{28\times 1}{\begin{Bmatrix} q_1 \\ \vdots \\ q_4 \end{Bmatrix}} \qquad (2.58)$$

where for the k^{th} node,

$$q_k^T = \{\, u \;\; v \;\; w \;\; w_{,1} \;\; w_{,2} \;\; \psi_1 \;\; \psi_2 \,\}_k \qquad (2.58a)$$

and

$$\mathbb{N}_k = \begin{bmatrix} N_k & 0 \\ N_{k,\zeta} & 0 \\ N_{k,\eta} & 0 \\ 0 & N_k \\ 0 & N_{k,\zeta} \\ 0 & N_{k,\eta} \end{bmatrix}_{6\times 2} \qquad \mathbb{H}_k = \begin{bmatrix} \mathcal{H}_{k1} & \mathcal{H}_{k2} & \mathcal{H}_{k3} \\ \mathcal{H}_{k1,\zeta} & \mathcal{H}_{k2,\zeta} & \mathcal{H}_{k3,\zeta} \\ \mathcal{H}_{k1,\eta} & \mathcal{H}_{k2,\eta} & \mathcal{H}_{k3,\eta} \\ \mathcal{H}_{k1,\zeta\zeta} & \mathcal{H}_{k2,\zeta\zeta} & \mathcal{H}_{k3,\zeta\zeta} \\ \mathcal{H}_{k1,\eta\eta} & \mathcal{H}_{k2,\eta\eta} & \mathcal{H}_{k3,\eta\eta} \\ \mathcal{H}_{k1,\eta\zeta} & \mathcal{H}_{k2,\eta\zeta} & \mathcal{H}_{k3,\eta\zeta} \end{bmatrix}_{6\times 3} \tag{2.58b}$$

The displacement gradient vector in terms of elemental coordinates (x,y) of Figure 1 is related to the element in natural coordinates (ζ,η) (i.e. Eqn (2.58) and Figure 2) by the Jacobian matrix, J. A general derivation of the Jacobian follows. Assume a function f(x,y) that represents the elements of d in Eqn (2.40) where x,y are functions of the natural coordinates ζ,η. Taking the partial derivatives of f gives

$$\begin{aligned} f_{,\zeta} &= f_{,x}\, x_{,\zeta} + f_{,y}\, y_{,\zeta} \\ f_{,\eta} &= f_{,x}\, x_{,\eta} + f_{,y}\, y_{,\eta} \end{aligned} \tag{2.59}$$

then,

$$\begin{Bmatrix} f_{,x} \\ f_{,y} \end{Bmatrix} = \begin{bmatrix} x_{,\zeta} & y_{,\zeta} \\ x_{,\eta} & y_{,\eta} \end{bmatrix}^{-1} \begin{Bmatrix} f_{,\zeta} \\ f_{,\eta} \end{Bmatrix} = \begin{bmatrix} \Gamma_{11} & \Gamma_{12} \\ \Gamma_{21} & \Gamma_{22} \end{bmatrix} \begin{Bmatrix} f_{,\zeta} \\ f_{,\eta} \end{Bmatrix} \tag{2.60}$$

In addition, second derivatives are required of the w DOF, for example, from Eqn (2.59)

$$\begin{aligned} f_{,\zeta\zeta} &= (f_{,x}\, x_{,\zeta})_{,\zeta} + (f_{,x}\, y_{,\zeta})_{,\zeta} \\ &= (f_{,xx}\, x_{,\zeta} + f_{,xy}\, y_{,\zeta})x_{,\zeta} + f_{,x}\, x_{,\zeta\zeta} \\ &\quad + (f_{,yy}\, y_{,\zeta} + f_{,xy}\, x_{,\zeta})y_{,\zeta} + f_{,y}\, y_{,\zeta\zeta} \end{aligned} \tag{2.61}$$

Using similar expressions for $f_{,\zeta\eta}$ $f_{,\eta\eta}$ we get

$$\begin{Bmatrix} f_{,xx} \\ f_{,yy} \\ f_{,xy} \end{Bmatrix} = \begin{bmatrix} x_{,\zeta}^2 & y_{,\zeta}^2 & 2y_{,\zeta}x_{,\zeta} \\ x_{,\eta}^2 & y_{,\eta}^2 & 2y_{,\eta}x_{,\eta} \\ x_{,\zeta}x_{,\eta} & y_{,\zeta}y_{,\eta} & (y_{,\zeta}x_{,\eta}+x_{,\zeta}y_{,\eta}) \end{bmatrix}^{-1} \left[\begin{Bmatrix} f_{,\zeta\zeta} \\ f_{,\eta\eta} \\ f_{,\zeta\eta} \end{Bmatrix} - \begin{bmatrix} x_{,\zeta\zeta} & y_{,\zeta\zeta} \\ x_{,\eta\eta} & y_{,\eta\eta} \\ x_{,\zeta\eta} & y_{,\zeta\eta} \end{bmatrix} \begin{bmatrix} \Gamma_{11} & \Gamma_{12} \\ \Gamma_{21} & \Gamma_{22} \end{bmatrix} \begin{Bmatrix} f_{,\zeta} \\ f_{,\eta} \end{Bmatrix} \right] \qquad (2.62)$$

Rearranging Eqn (2.62) and combining terms into a 3x5 matrix, Λ, gives

$$\begin{Bmatrix} f_{,xx} \\ f_{,yy} \\ f_{,xy} \end{Bmatrix} = [\Lambda] \begin{Bmatrix} f_{,\zeta} \\ f_{,\eta} \\ f_{,\zeta\zeta} \\ f_{,\eta\eta} \\ f_{,\zeta\eta} \end{Bmatrix} \qquad (2.63)$$

Combining Eqn (2.60) and (2.63) gives the inverse of the Jacobian matrix and relates the coordinate systems if Figures 1 and 2 by the following

$$d(x,y) = \Gamma\, d(\zeta,\eta) \qquad (2.64)$$

where,

$$\Gamma = \underset{18x18}{\begin{bmatrix} \Gamma_1 & 0 & 0 \\ 0 & \Gamma_2 & 0 \\ 0 & 0 & \Gamma_2 \end{bmatrix}} \qquad (2.64a)$$

and

$$\Gamma_1 = \begin{bmatrix} 1 & 0 & 0 & 0 & 0 & 0 \\ 0 & \Gamma_{11} & \Gamma_{12} & 0 & 0 & 0 \\ 0 & \Gamma_{21} & \Gamma_{22} & 0 & 0 & 0 \\ 0 & 0 & 0 & 1 & 0 & 0 \\ 0 & 0 & 0 & 0 & \Gamma_{11} & \Gamma_{12} \\ 0 & 0 & 0 & 0 & \Gamma_{21} & \Gamma_{22} \end{bmatrix}_{6\times6} \qquad (2.64b)$$

$$\Gamma_2 = \begin{bmatrix} 1 & 0 & 0 & 0 & 0 & 0 \\ 0 & \Gamma_{11} & \Gamma_{12} & 0 & 0 & 0 \\ 0 & \Gamma_{21} & \Gamma_{22} & 0 & 0 & 0 \\ 0 & \Lambda_{11} & \Lambda_{12} & \Lambda_{13} & \Lambda_{14} & \Lambda_{15} \\ 0 & \Lambda_{21} & \Lambda_{22} & \Lambda_{23} & \Lambda_{24} & \Lambda_{25} \\ 0 & \Lambda_{31} & \Lambda_{32} & \Lambda_{33} & \Lambda_{34} & \Lambda_{35} \end{bmatrix}_{6\times6} \qquad (2.64c)$$

For the rectangular element assumed here, many terms are zero. What we are left with is $\Gamma_{11}=1/a$, $\Gamma_{22}=1/b$, $\Lambda_{13}=1/a^2$, $\Lambda_{24}=1/b^2$, and $\Lambda_{35}=1/ab$. Where a and b are the dimensions of the plate in the x and y direction, respectively. The remaining Γ's and Λ's are zero.

The 28 DOF element shown in figure 2.3 is now completely defined and is summarized below.

$$d = \Gamma D q \qquad (2.65)$$
$$= \mathcal{D} q$$

where the order of the appropriate matrix can be stated as

d = 18 x 1 (Eqn (2.40))

Γ = 18 x 18 (Eqn (2.64a))

D = 18 x 28 (Eqn (2.58)

q = 28 x 1 (Eqn (2.58a)

$\mathcal{D}$ is the matrix that is used in Eqn (2.54) to calculate the components of the tangential stiffness matrix.

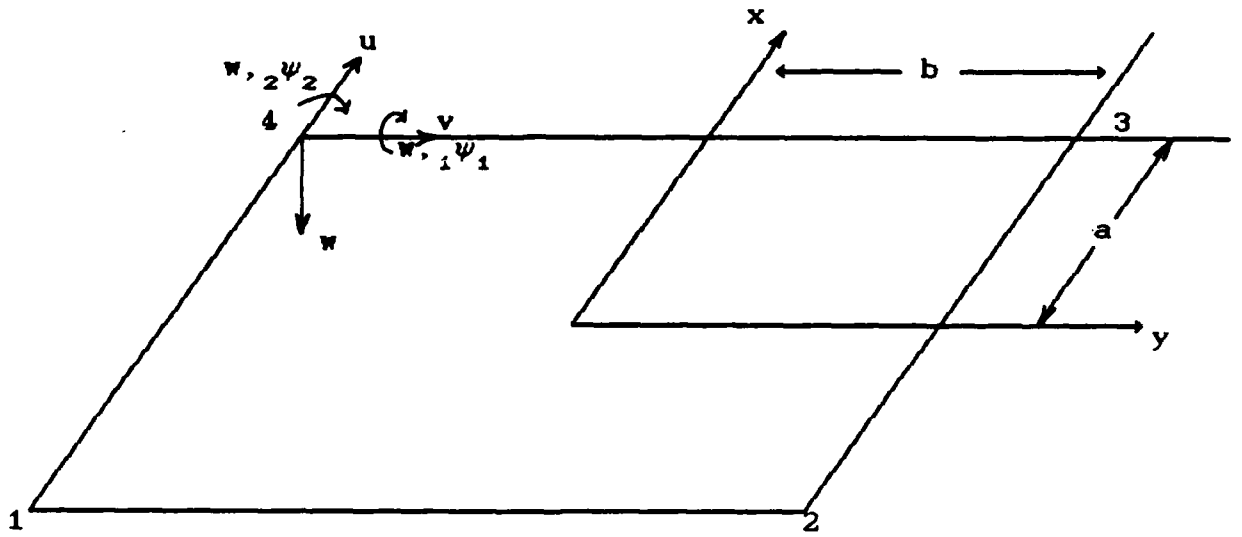

FIGURE 2.3. 28 DOF Rectangular Plate Element.

Solution Algorithms

Now that all quantities have been defined, the solution algorithm is presented. The integrals inherent in Eqn (2.37) are calculated for an individual element. Each element's contribution is added to the global stiffness array according to the element's connectivity. Therefore, Eqn (2.37) is represented below for the entire plate.

$$\sum_{k=1}^{n} \left[\int_{\Omega_e} \mathcal{D}^T \left[\hat{K} + \hat{N}_1 + \hat{N}_2 \right] \mathcal{D} \, d\Omega_e \right]_k \Delta q =$$

$$- \sum_{k=1}^{n} \left[\int_{\Omega_e} \mathcal{D}^T \left[\hat{K} + \frac{\hat{N}_1}{2} + \frac{\hat{N}_2}{3} \right] \mathcal{D} \, d\Omega_e \right]_k q + R \qquad (2.66)$$

where,

Ω_e = 2-D domain of the element

n = number of elements in mesh

$\Delta q, q$ = global column arrays of displacement assembled from element Δq and q.

R = applied load array, of same dimension as global q.

R can be found using the same shape functions as used for element displacements and can be calculated an an elemental (and then assembled) or global basis. A dicussion of both methods can be found in Cook (6). Solutions to Eqn (2.66) are found iteratively where the RHS becomes small, i.e. equilibrium is satisfied. The integrations are carried out using Gaussian quadriture in natural coordinates ζ and η. As an example, look at the first term in the summation of Eqn (2.66):

$$\int_{\Omega_e} \mathcal{D}^T \left[\hat{K} + \hat{N}_1 + \hat{N}_2 \right] \mathcal{D} \, d\Omega_e =$$

$$= \int_{-1}^{1} \int_{-1}^{1} \mathcal{D}^T \left[\hat{K} + \hat{N}_1 + \hat{N}_2 \right] \mathcal{D} \, |J| \, d\zeta d\eta \qquad (2.67)$$

$$= \sum_{i=1}^{m} \sum_{i=1}^{m} W_i \, W_j \, \mathcal{D}^T \left[\hat{K} + \hat{N}_1 + \hat{N}_2 \right] \mathcal{D} \, |J|$$

where,

$|J|$ = determinant of the Jacobian matrix,

$\mathcal{D}$, $\hat{K}$, $\hat{N}_1$, $\hat{N}_2$, $|J|$ are evaluated at Gauss integration points (ζ_i, η_j),

W_i, W_j = weighting factors, and

m = order of the numerical integration.

In a linear analysis, displacements and rotations are assumed to be small, and therefore $\hat{N}_1$ and $\hat{N}_2$ are eliminated.

Also, since the relationships are linear, Eqn (2.34) is solved directly for q, i.e. iterative solutions are not necessary. So, Eqn (2.66) may be rewritten

$$\sum_{k=1}^{n} \left[\int_{-1}^{1} \int_{-1}^{1} \mathcal{D}^T \left[\hat{K} + \hat{N}_1 + \hat{N}_2 \right] \mathcal{D} \, |J| \, d\zeta d\eta \right]_k q = R \qquad (2.68)$$

The solution of Eqn (2.68) is accomplished by Gaussain elimination. The resulting displacements can be used to find the strains and then stresses at the Gauss points via previously derived relationships.

For a nonlinear analysis, the linearized incremental/iterative equations are solved by a Newton-Raphson technigue. For this research 5x5 integration was used rather than the 7x7 called for in the exact solution for the nonlinear cases and 4x4 integrations for the linear cases. Dennis (7) determined that this gave adequate accuracy and accelerated computer run times considerably. In the first iteration of the first increment, the displacement gradient vector is calculated by the linear technique described in the preceeding paragraph. N_1 and N_2 are then calculated and iteration continues until convergence is achieved. A global displacement convergence criterion is used (19) as shown below:

$$\frac{\sqrt{\sum_i (q_i^r)^2} - \sqrt{\sum_i (q_i^{r-1})^2}}{\sqrt{\sum_i (q_i^1)^2}} \times 100 \leq TOL \qquad (2.69)$$

where,

q_i^r, q_i^{r-1}, q_i^1 are the elements of q for the r^{th},

$(r-1)^{th}$, and first iterations of a given increment, and

TOL is a user defined convergence tolerance percentage and 1% was used in this research.

III. NUMERICAL DEVELOPMENT

In this section the results of this research effort are presented. The results are presented in four major areas. First, the results of the code verification, second, the specific parameters of the cases studied, third, the generation of the finite element mesh, and finally, some considerations reguarding symmetry of the mesh.

Code Verification

The finite element code used in this research was developed by Dennis (7) for a fully nonlinear cylindrical shell. It can also be used for the plate under consideration in this thesis. The code was verified as to its accuracy by Dennis (7). The verification presented here is not only to retest the accuracy of the code, but also to assure that the input decks of the program were formulated properly. Two verification cases were studied: a geometrically linear analysis and a geometrically nonlinear analysis.

For the geometrically linear case the orthotropic material studied was aragonite crystals with the following properties given in million psi:

$$E_1 = 20.83, \quad E_2 = 10.94, \quad G_{12} = 6.10,$$
$$G_{13} = 3.71, \quad G_{23} = 6.19, \quad \nu_{12} = 0.44, \quad \nu_{21} = 0.23 \tag{3.1}$$

The plate was rectangular in dimension a x b with a uniformly distributed transverse load. The transverse deflection w in table 3.1 is taken at the center of the plate, h is the thickness of the plate, and q_o is the load

per unit area of the plate. The values for comparison come from the exact solutions of Srinivas and Rao (42) as presented by Reddy (32).

Table 3.1. Verification of geometrically linear analysis.

a/b	a/h	$c_{11}^{a} w/hq_o$	
		Exact[b]	Present
0.5	7.142	387.23	387.90
	10.0	1408.5	1410.0
	20.0	21542	21552
1.0	7.142	191.07	191.71
	10.0	688.75	689.83
	20.0	10443	10447
2.0	7.142	39.790	40.240
	10.0	139.08	139.90
	20.0	2048.7	2051.8

[a] $c_{11} = 23.2 \times 10^6$ psi

[b] Srinivas and Rao

As can be seen, there is excellent agreement between the exact and the present finite element solution.

For the geometrically nonlinear case a test done by Dennis (7) was repeated. Dennis, in turn, was verifying the results of Putcha and Reddy (28). In this case the plate was 16 inches square, 1.6 inches thick, and subject to a uniform pressure q_o. The ply layup was $[0/\pm45/90]_s$ with the following material properties (where the modulii are expressed in million psi):

$$E_1=60,\ E_2=1.5,\ G_{12}=G_{13}=.9,\ G_{23}=.75,\ \nu_{12}=.25 \qquad (3.2)$$

Both simple and clamped supports with the boundary conditions as shown in Eqn (3.3), were investigated:

$$\begin{array}{lll} & \text{Simple} & \text{Clamped} \\ @x=\pm a/2: & v=w=\psi_2=0 & u=w=w_{,1}=\psi_1=0 \\ @y=\pm a/2: & u=w=\psi_1=0 & v=w=w_{,2}=\psi_2=0 \end{array} \qquad (3.3)$$

The pressure and center displacement were nondimensionalized as in Eqn (3.4):

$$\bar{q} = \frac{q_o a^4}{E_2 h^4}, \qquad \bar{w} = \frac{w(0,0)}{h} \qquad (3.4)$$

The plate was modeled using quarter plate symmetry with a 4x4 mesh for the simple case and 8x8 mesh for the clamped case. Results are shown in Table 3.3.

Table3.2. Verification of geometrically nonlinear analysis

$\bar{q}$	Dennis		Present	
	$\bar{w}$ (Simple)	$\bar{w}$ (Clamped)	$\bar{w}$ (Simple)	$\bar{w}$ (Clamped)
50	.2759	.1395	.2759	.1395
100	.4873	.2595	.4873	.2595
150	.6473	.3573	.6473	.3573
200	.7753	.4377	.7753	.4377
250	.8825	.5055	.8827	.5055

As can be seen from table 3.2 the results match extremely well. Also, the comparison of these results with Pucha and Reddy can be seen in figure 3.1. Again, agreement is excellent.

Parameters Studied

In this research two types of material were studied,

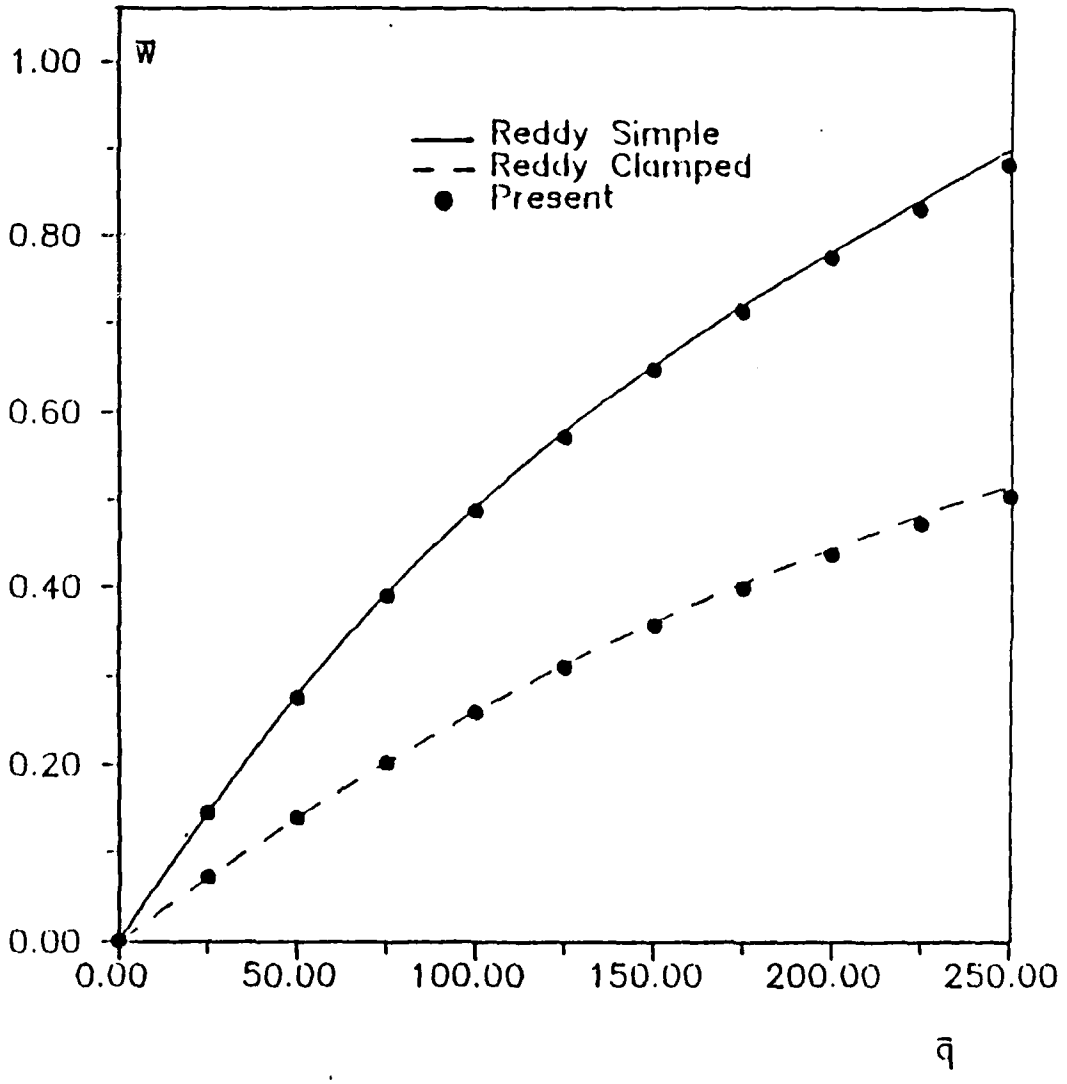

FIGURE 3.1. $\bar{w}$ vs $\bar{q}$ for [0/±45/90]$_s$ Laminated Plate.

along with two types of analysis, six thickness ratios, three aspect ratios, two boundary conditions, and four ply layups. All possible combinations of these six parameters were analyzed for a total of 576 test cases.

Materials. The two types of materials were chosen to have a large difference in their ratio of E_1 to G_{13}. This ratio is of interest because it is one of the driving parameters in determining how much effect the transverse shear stresses have on the response of the structure. The specifics of each material type are shown in Eqn (3.5):

Material A:

$$\frac{E_1}{E_2} = 40, \quad \frac{G_{13}}{E_2} = 0.5, \quad \frac{G_{23}}{E_2} = 0.2, \quad \nu_{12} = \nu_{13} = 0.25 \qquad (3.5a)$$

Material B:

$$\frac{E_1}{E_2} = 15, \quad \frac{G_{13}}{E_2} = 0.6, \quad \frac{G_{23}}{E_2} = 0.3, \quad \nu_{12} = \nu_{13} = 0.28 \qquad (3.5b)$$

For both materials $G_{12}=G_{13}$ and the ply thickness was set at 0.005 inches. For each material $E_1=20\text{x}10^6$ psi.

Analysis. The two types of analysis conducted were geometrically linear and geometrically nonlinear. Both types of analysis were discussed in the previous chapter. In early verification tests, it was seen that loads greater than 500 psi would cause large enough rotations so as to violate the von Karman limitations of moderate rotation, the criterion being that the rotations could not be greater than 17°. Therefore, for both types of analysis a maximum load of 500 psi was applied to the plate. In the linear cases the load was applied in one increment. In the nonlinear cases the load was applied in five equal increments of 100

psi. The nonlinear computer run times were roughly 20 times greater than the linear computer run times.

Thickness Ratio. Thickness ratio, S, is defined as the length of the plate in the x-direction, a, divided by the thickness. Six thickness ratios were studied. They were 10, 20, 30, 40, 50, and 60.

Aspect ratio. Aspect ratio, AR, is defined as the length of the plate in the x-direction, a, divided by the length of the plate in the y-direction, b. Three aspect ratios were investigated: 0.5, 1, and 2.

Boundary conditions. The two boundary conditions considered were simple and clamped. The boundary conditions were chosen so as not to restrict the inplane deflections at the boundary. This was done to eliminate as much of the inplane membrane stresses as possible so the effects of the transverse shear stresses would be more pronounced. The boundary conditions are shown in figure 3.2 where subscript t denotes tangential direction and subcript n denotes normal direction. In both cases displacements in and out of the plane of the page are allowed.

Ply layups. The four ply layups chosen were: $[0_{16}/90_8]_s$, $[0_{12}/60_6/-60_6]_s$, $[0_{12}/45_6/-45_6]_s$, and $[0_{12}/45_4/-45_4/90_4]_s$, where the numerical subcript denotes the number of plies in a given orientation and the subscript s denotes that the ply layup is symmetric about the midsurface. These layups represent several of the more common types of ply layups used today. The ply layups were all 48 plies thick, which is of the same order as the number of plies used in aircraft structures such as wing, tail, and stabilizer skins. Additionally, it was desired to have at least 50% of the plies in the 0° or x-direction.

Simple

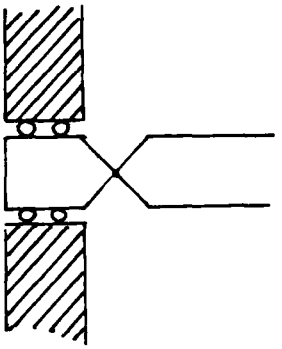

$w = \psi_t = 0$

Clamped

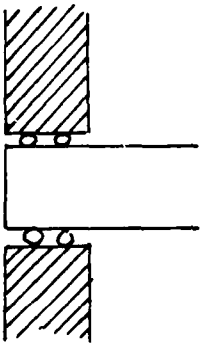

$w = w_{,t} = \psi_t = \psi_n = 0$

Figure 3.2. Boundary conditions.

Finite Element Mesh Generation

Because the number of plies was held constant and the ply thickness was the same for both materials, the thickness of the plate was constant for all cases studied. All plates were 0.24 inches thick. Consequently, the thickness

determined the inplane dimensions of the plate through the thickness ratio and aspect ratio of interest. The dimension in the x-direction, a, was set by the thickness ratio desired. For example, if a thickness ratio of 30 was needed, then the a dimension would be 7.2 inches. The dimension in the y-direction, b, was then set by the aspect ratio. Continuing the above example, if a was 7.2 inches and an aspect ratio of 2 was desired, then b would be 3.6 inches. The values of a and b for all thickness and aspect ratios is shown in table 3.3.

Table 3.3. Dimensions of plate for all thickness and aspect ratios.

S	a	b(AR=.5)	b(AR=1)	b(AR=2)
10	2.4	4.8	2.4	1.2
20	4.8	9.6	4.8	2.4
30	7.2	14.4	7.2	6.6
40	9.6	19.2	9.6	4.8
50	12.0	24.0	12.0	6.0
60	14.4	28.8	14.4	7.2

To illustrate the dimensions of the plate for any given value of S, the relative sizes of the plate for the different aspect ratios are shown in figure 3.3.

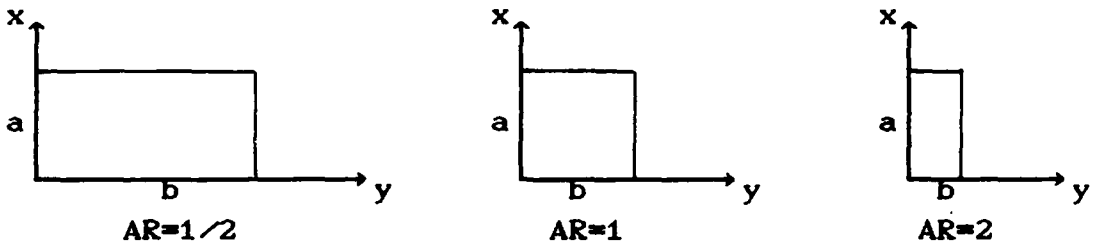

FIGURE 3.3. Relative plate planforms for any value of S.

For all cases studied, an 8x8 uniform mesh was used. Dennis (7) showed that this gives good accuracy with efficient computer run times. Also, quarter plate symmetry was used in all cases. Quarter plate symmetry allows for a finer mesh over a smaller portion of the plate and thus increases accuracy while decreasing computer run time. Dennis (7) also ran a convergence test which verified the accuracy of the 8x8 quarter plate mesh.

Quarter Plate Symmetry Considerations

Early in the research effort the question arose as to whether quarter plate symmetry was a valid assumption. In this section we will attempt to address that question. Several authors (18), (34) address the issue and conclude that for a symmetrically stacked ply layup, as in this research, quarter plate symmetry can be used because the coupling stiffness terms, B_{ij}, are all zero. While this is true, the bending stiffness terms, D_{ij}, are not all zero. And while the D_{ij} terms are not included computationally due to the numerical approach in the present formulation, they serve as a good baramoter of the degree to which coupling between bending and twisting will occur. The terms that generate the problems with reguards to symmetry

considerations are D_{16} and D_{26}. In order to study this, the worst case, i.e. largest, ratio of D_{16} and D_{26} to D_{11} was identified and a full and quarter plate model for both a linear and nonlinear analysis were tested. Values of both A_{ij} and D_{ij} are shown in tables 3.4 and 3.5 for both materials and all ply layups.

Table 3.4. Extensional stiffesses[a]

Mat.	Ply	A_{11}	A_{12}	A_{22}	A_{66}	A_{16}	A_{26}
A	$[0/90]_s$[b]	3.2451	.0300	1.6826	.0600	0.0	0.0
A	$[0/\pm60]_s$[c]	2.6159	.4639	1.4441	.4938	0.0	0.0
A	$[0/\pm45]_s$[d]	3.0572	.6085	.7136	.6385	0.0	0.0
A	$[0/\pm45/90]_s$[e]	2.8594	.4157	1.2970	.4456	0.0	0.0
B	$[0/90]_s$	3.3240	.0901	1.8229	.1920	0.0	0.0
B	$[0/\pm60]_s$	2.7428	.4837	1.6169	.5856	0.0	0.0
B	$[0/\pm45]_s$	3.1745	.6149	.9227	.7168	0.0	0.0
B	$[0/\pm45/90]_s$	2.9741	.4400	1.4730	.5419	0.0	0.0

[a] all values are 10^6
[b] actual ply layup $[0_{16}/90_8]_s$
[c] actual ply layup $[0_{12}/60_6/-60_6]_s$
[d] actual ply layup $[0_{12}/45_6/-45_6]_s$
[e] actual ply layup $[0_{12}/45_4/-45_4/90_4]_s$

Table 3.5. Bending stiffnesses[a]

Mat.	Ply	D_{11}	D_{12}	D_{22}	D_{66}	D_{16}	D_{26}
A	$[0/90]_s^a$	22243	144	1410	288	0	0
A	$[0/\pm60]_s^b$	20446	665	2166	809	231	682
A	$[0/\pm45]_s^c$	20976	838	1289	982	527	527
A	$[0/\pm45/90]_s^d$	20949	813	1367	956	312	312
B	$[0/90]_s$	22361	432	2345	922	0	0
B	$[0/\pm60]_s$	20662	905	3098	1394	234	643
B	$[0/\pm45]_s$	21180	1062	2265	1551	507	507
B	$[0/\pm45/90]_s$	21154	1039	2339	1528	300	300

[a]actual ply layup $[0_{16}/90_8]$
[b]actual ply layup $[0_{12}/60_6/-60_6]_s$
[c]actual ply layup $[0_{12}/45_6/-45_6]_s$
[d]actual ply layup $[0_{12}/45_4/-45_4/90]_s$

As can be seen from table 3.5, the worst case was chosen as material A with a $[0_{12}/60_6/-60_6]_s$ ply layup. In the test case, the plate was simply supported, with an S=30, and an aspect ratio of one. The full plate was modeled with an 8x8 mesh and the 1/4 plate was modeled with a 4x4 mesh. Both linear and nonlinear analysis were conducted and nondimensionalized center transverse deflections were compared. The deflections were nondimensionalized according to Eqn (3.6) where w_c represents the deflection at the center of the plate. Results are shown in Table 3.6.

$$\overline{w} = \frac{w_c h^3 E_2}{q_o a^4} \times 100 \qquad (3.6)$$

Table 3.6. Center deflection results of quarter plate symmetry verification tests.

	$\bar{w}$ (linear)	$\bar{w}$ (nonlinear)
Full Plate	.4573	.2275
1/4 Plate	.4856	.2334
% Difference	5.82	2.55

As can be seen from Table 3.6, there is good agreement between the the full and quarter plate. The author feels that quarter plate symmetry is an accurate way to model the plate based on the following factors: all comparisions of results will be made within this thesis and not to other published sources (primarily because there aren't any other published cases for the parameters studied), and, the primary emphasis in this thesis is on trends in the results and not absolute numbers.

IV. RESULTS/DISCUSSION

In this chapter the main results of the thesis are presented. The effects of material properties, aspect ratio, and ply layup are discussed in separate subsections. The effects of the type of analysis used, plate thickness, and boundary conditions lend themselves to being discussed as they come into play with respect to the parameter being analyzed. Most of the results in this thesis are presented in the form of graphs of the nondimensionalized center deflection, $\bar{w}$, versus thickness ratio, S. The center deflection $\bar{w}$ is nondimensionalized according to Eqn (4.1):

$$\bar{w} = \frac{w_c h^3 E_1}{q_o a^4} \times 10 \qquad (4.1)$$

There are three types of forces that characterize the response of the plate; membrane or inplane, bending, and shear. In a linear analysis the response is characterized by only bending and shear. This is because the membrane forces are a function of the membrane strains which are neglected in a linear analysis due to the transverse loading. In the nonlinear analysis all three types of forces are present. However, a thick plate is charaterized primarily by bending and shear because there is very little displacement in the inplane directions, making the membrane forces small compared to bending and shear. This makes it similar to the linear analysis. A thin plate is characterized primarily by membrane and bending forces.

Effects of Material Properties.

The graphs discussed here are representative of all the cases studied. For a complete set of graphs for $\bar{w}$ versus S considering all ply layups and aspect ratios that show the difference between the two materials see Appendix A. Only one case is discussed here for each boundary condition because the volume of data would be overwhelming and not convey much more information as one representative graph.

Simply supported plate. Figure 4.1 is a plot of $\bar{w}$ versus S for a simply supported plate with a $[0_{12}/45_4/-45_4/90_4]_s$ ply layup and an aspect ratio of 1/2. Linear and nonlinear results for both materials A and B are presented. The linear solution, i.e. solid line, asymptotically approaches the classical laminated plate theory (CLPT) solution, which, as will be shown later, is constant for all values of S, as the plate gets thinner. This is due to the fact that, as the plate gets thinner, the bending moments begin to dominate the response of the structure and the solution degenerates to a CLPT problem. Material A approaches the CLPT solution at approximately S=40, while material B approaches the CLPT solution at approximately S=25. As can be observed, as the plate gets thicker, the nondimensionalized center deflection increases for both materials from the CLPT solution because the transverse shear effects are coming more and more into play. Therefore, the main difference between the linear solution and the CLPT solution is that the effects of the transverse shear strains have been included. Note that for any given value of S, material A has a greater deflection than material B. This is because B has a higher transverse shear strength, i.e. lower E_1/G_{13} ratio, than A. Consequently,

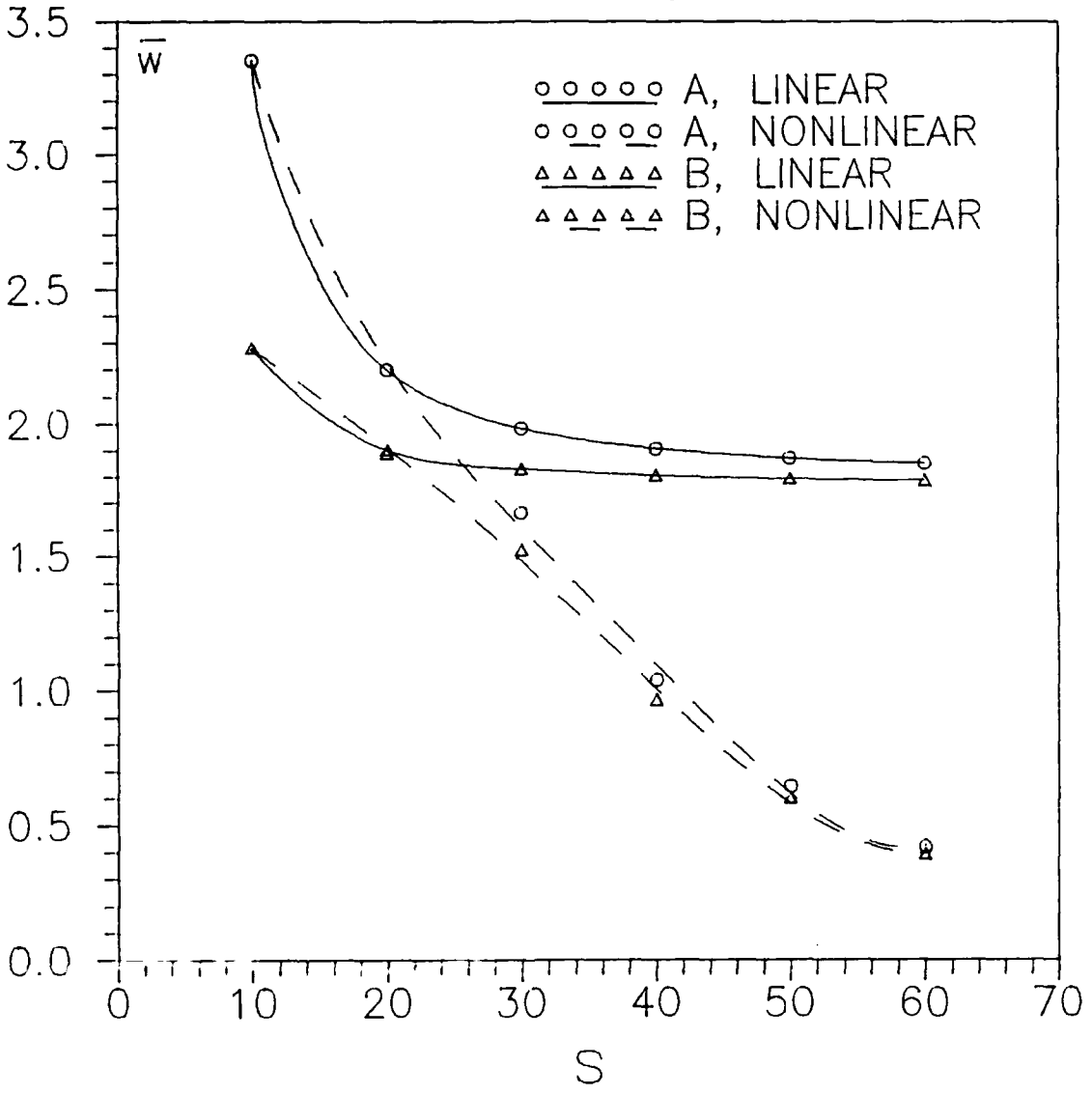

FIGURE 4.1. $\bar{w}$ vs s for a simply supported $[0_{12}/45_6/-45_6]_s$ plate with an aspect ratio of 1/2.

when the transverse shear has a major impact on the response of the plate, the ratio difference between the two materials becomes more important. Note also that as the plate gets thinner, the two linear solutions approach the same value. Again, this is because the bending forces become dominant and the major difference between the two materials, the E_1/G_{13} ratio, becomes less important as the magnitude of the transverse shear forces decrease relative to the membrane forces. However, there is always some difference between the solutions because there are differences in the smaller values of D_{ij}, as can be seen in table 3.4.

The nonlinear solutions, i.e. dashed lines, also asymptotically approach a constant value, but, this constant value is not reached until the plate is quite thin, i.e. S is greater than 60. This occurs when the higher order inplane strains are transformed into axial forces. The reason the deflections in the nonlinear solution are so much less than the linear solutions is because the higher order terms present in the inplane deflections translate into increased membrane stiffness which plays a greater role as the plate gets thinner and the inplane stresses begin to dominate the structural response. Note however, that for values of S between 10 and 20, there is virtually no difference between the linear and nonlinear solution. This is because in this range, the transverse shear strains, which are linear for both geometrically linear and nonlinear solutions (see Eqn (2.10)), dominate the response of the structure. From the plot of the curve in this range, the nonlinear solution would appear to have a greater deflection than the linear solution. This is not actually the case however, and this is a result of the functions that had to be used to plot the various curves. If the actual data

points are compared, it can be seen that for small values of S, the deflections of the nonlinear case are equal to that of the linear case and for larger values of S, the nonlinear is less than the linear. All simply supported plates investigated exhibited similar behavior.

Clamped Plate. Figure 4.2 is a plot of $\bar{w}$ versus S for a clamped plate with a $[0_{12}/60_6/-60_6]_s$ ply layup and an aspect ratio of one. Many of the same things can be said about fig 4.2 that were said about fig 4.1, i.e. assymptotically approaching the CLPT solution, effect of transverse shear, etc. Here it can be seen that in the linear solutions, material A is close to the CLPT solution for values of S greater than 50 and material B for values of S greater than 40. In the nonlinear case, the clamped plate is similar to the simply supported plate, in that the solution does not approach a constant value until the plate is quite thin, i.e. for values of S greater than 60. However, the most striking thing about this graph is the relative closeness of the linear and nonlinear solution as compared to the simply supported case of fig 4.1. This closeness is due to the significant stiffening which the clamped boundary condition imparts to the plate. Consequently, the higher order terms do not play as large a role in the deflections and ensuing strains and stresses.

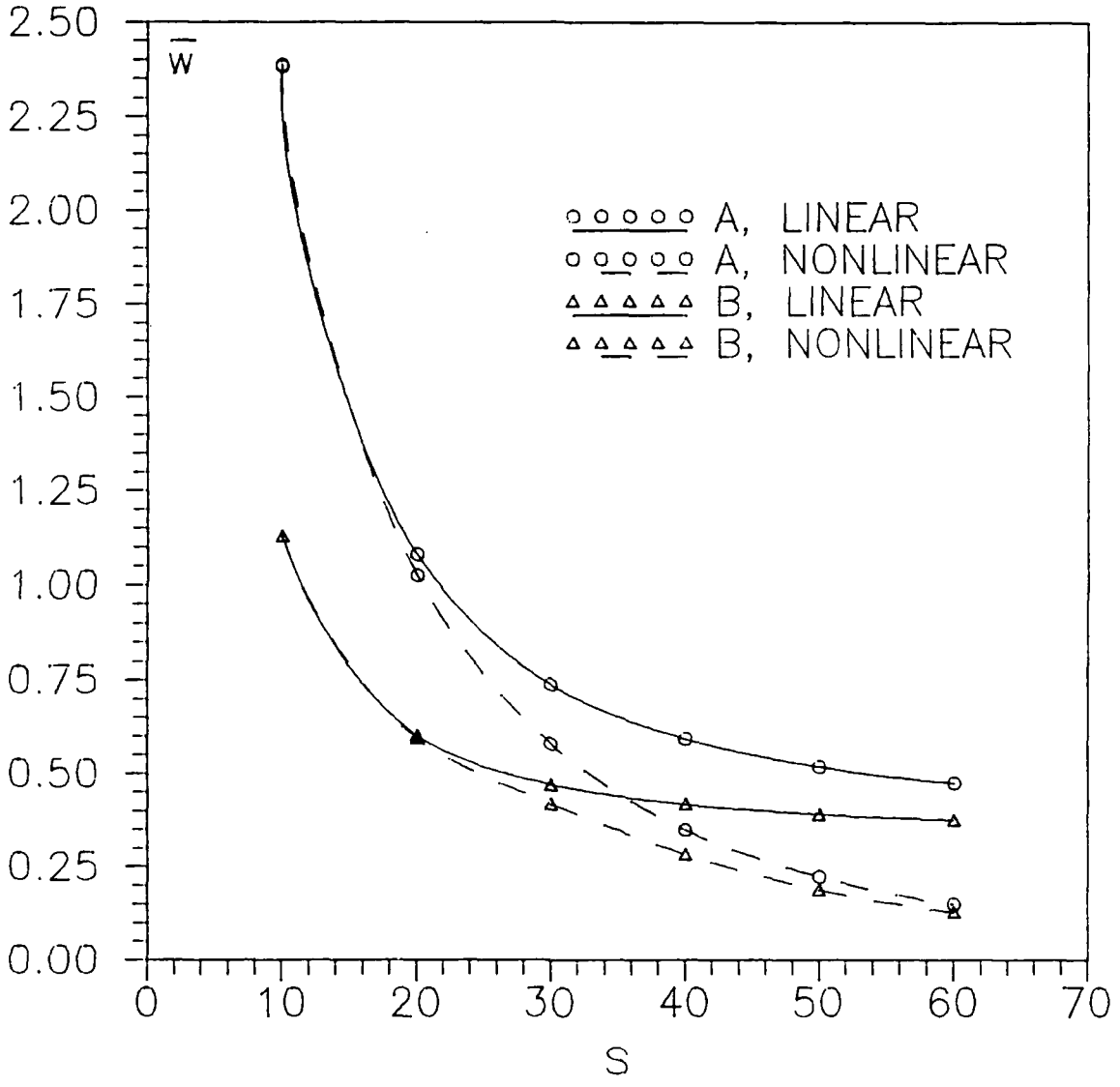

FIGURE 4.2. $\bar{w}$ vs s for a clamped $[0_{12}/60_6/-60_6]_s$ plate with an aspect ratio of one.

Figure 4.3 is a plot of $\bar{w}$ versus $\bar{q}$ for a simply supported plate with a $[0_{12}/45_4/-45_4/90_4]_s$ ply layup and and aspect ratio of one. The nondimensionalized incremental load, $\bar{q}$, is calculated by Eqn (4.2) where q_o represents the load in any given increment:

$$\bar{q} = \frac{q_o}{E_1} \times 10^6 \qquad (4.2)$$

For a complete set of w vs q graphs, see Appendix B. The results presented come from the nonlinear solution because it is incremental in nature. Solving Eqn (4.1) for w_c in terms of $\bar{w}$, one obtains

$$w_c = \frac{a^4}{10h^3E_1} \bar{w}\, q_o \qquad (4.3)$$

As can be seen from Eqn (4.3), the value of $\bar{w}$ represents the slope of the actual load versus displacement curve because E_1 and h are constant and a is constant for a given value of S. Based on fig 4.4, which shows the actual load-displacement curve for the same plate, it can be seen that as the slope of the curve gets more nonlinear and flatter, the plate gets thinner. This occurs because the higher order terms in the assumed displacement function are coming more into play as the membrane forces begin to dominate the solution. Again, considering figure 4.3 for a thick plate, i.e. S=10, $\bar{w}$ is nearly constant. This implies that w_c, (figure 4.4) the actual displacement, increases linearly with the incremental load, q_o. This is because for thick plates the linear and nonlinear solutions are identical which can be seen in figures 4.1 and 4.2. Note that as the plate becomes thinner, the difference in the curves for different material properties is reduced. This

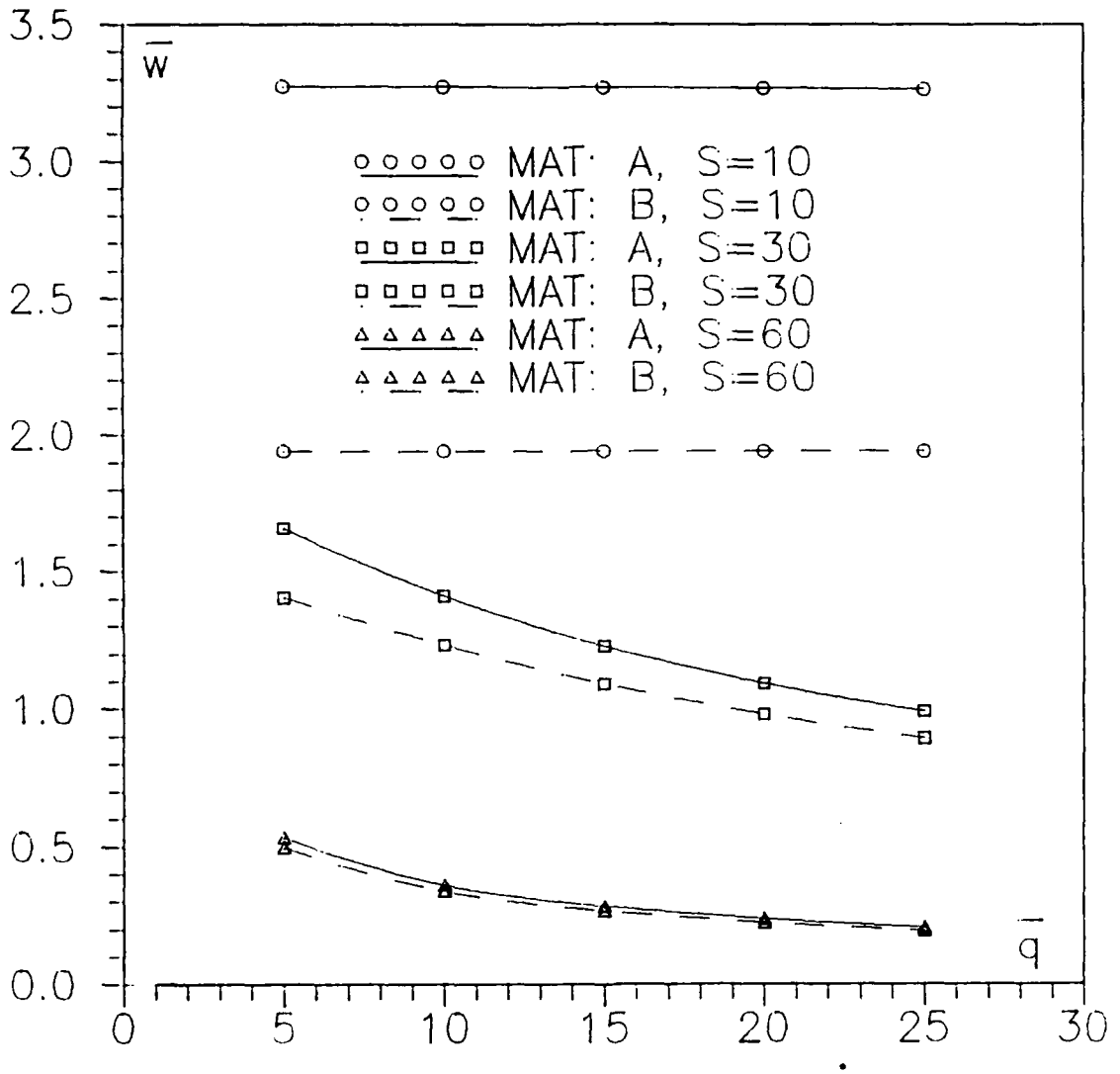

FIGURE 4.3. $\bar{w}$ vs $\bar{q}$ for a simply supported $[0_{12}/45_4/-45_4/90_4]_s$ plate with an aspect ratio of one.

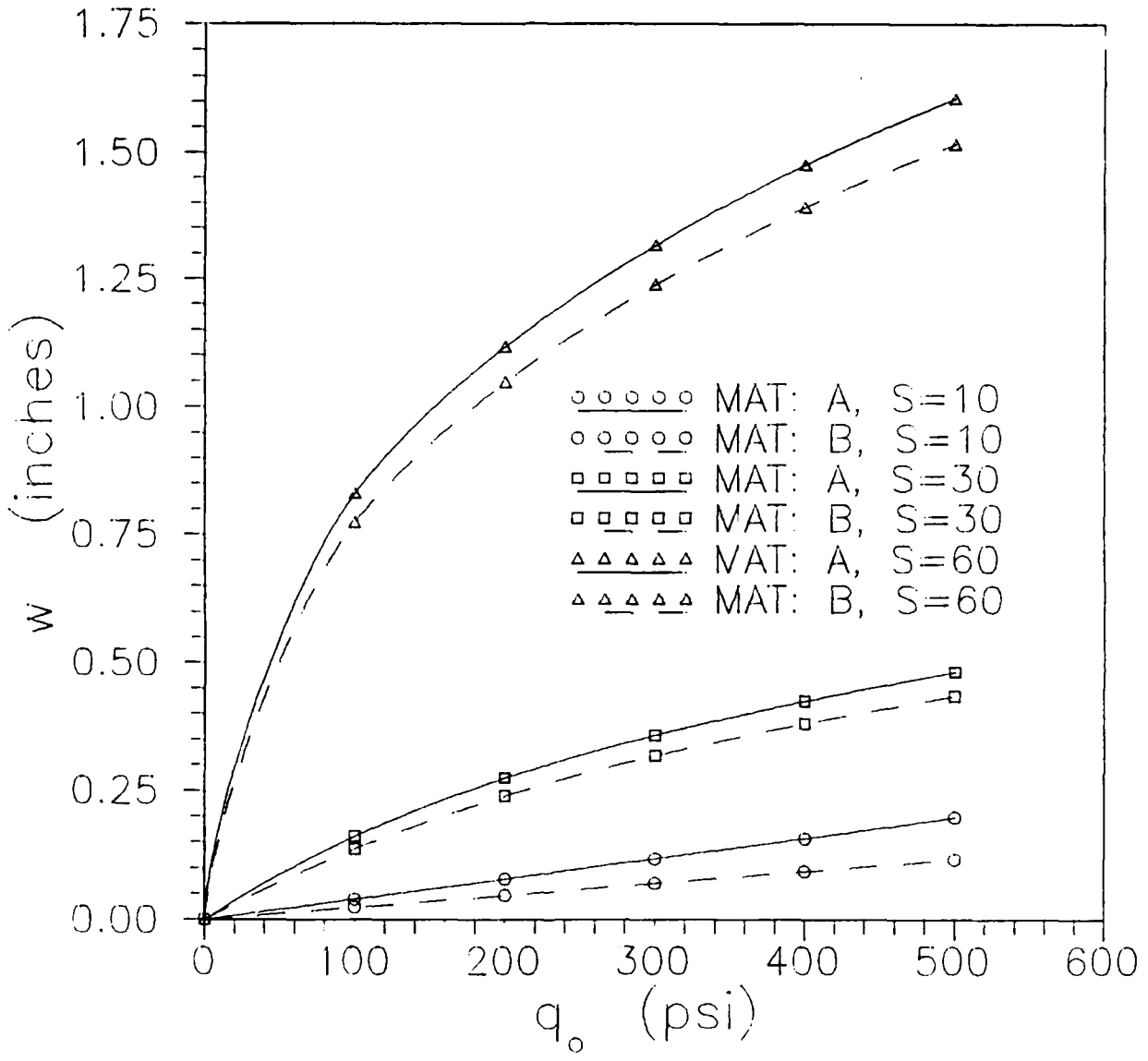

FIGURE 4.4. w vs q for a simply supported $[0_{12}/45_4/-45_4/90_4]_s$ plate with an aspect ratio of one.

is because as the plate gets thinner the membrane forces have more effect than the transverse shear forces on the deflections of the plate and therefore, the major difference between the materials, the E_1/G_{13} ratio, has less effect.

Effect of Aspect Ratio.

Next, we look at the effect of aspect ratio on the response of the plate. To serve as a relative basis of comparison between the various aspect ratios, a classical plate theory solution was conducted for a simply supported isotropic plate. Deflections were calculated using Navier's solution by double trigonometric series, shown in Eqn (4.4), as presented in Szilard (44):

$$w(x,y) = \frac{1}{D\pi^4} \sum_{\substack{m=1 \\ odd}}^{\infty} \sum_{\substack{n=1 \\ odd}}^{\infty} \frac{P_{mn}}{mn \left\{ \frac{m^2}{a^2} + \frac{n^2}{b^2} \right\}^2} \sin \frac{m\pi x}{a} \sin \frac{n\pi y}{b} \tag{4.4}$$

where m,n = 1,3,5,...,101 and

$$D = \frac{Eh^3}{12(1-\nu^2)} \tag{4.4a}$$

and for a uniform load,

$$P_{mn} = \frac{16q_o}{\pi^2 mn} \tag{4.4b}$$

The material properties chosen are shown in Eqn (4.5):

$$E = 20 \times 10^6 \text{ psi}, \quad h = .24 \text{ in}, \qquad \nu = .25, \quad q_o = 500 \text{ psi} \tag{4.5}$$

the nondimensionalized deflection was calculated by Eqn

(4.1) and is shown in table 4.1.

Table 4.1. Nondimensionalized center deflection[a] (classical solution) of a simply supported isotropic plate for various aspect and thickness ratios

S	$\bar{w}$(AR=.5)	$\bar{w}$(AR=1)	$\bar{w}$(AR=2)
10	.7851	.2968	.0491
20	.7851	.2968	.0491
30	.7851	.2968	.0491
40	.7851	.2968	.0491
50	.7851	.2968	.0491
60	.7851	.2968	.0491

[a]all $\bar{w}$ values are times 10^3

As can be seen in table 4.1, as the aspect ratio increases, $\bar{w}$ decreases but, as mentioned before, it is the same for all thickness ratios. The value of $\bar{w}$ for an aspect ratio of 1/2 is roughly three times of that for an aspect ratio of 1.0. In addition, $\bar{w}$ for an aspect ratio of two is roughly 1/5 of that for an aspect ratio of one. Thus, one can see the significant differences aspect ratio makes for an isotropic plate of the dimensions given in table 3.3.

The aspect ratio affect reported on next is observed for both materials and all ply layups. A complete set of plots for both materials and all aspect ratios can be seen in Appendix C. A representative graph for both simply supported and clamped boundary conditions are discussed next.

Simple Supports. Figure 4.5 shows $\bar{w}$ versus S for a simply supported plate with a $[0_{16}/90_8]_s$ ply layup made of material B. The curves for both the linear and nonlinear solutions for all three aspect ratios are shown. Like figure 4.1, the linear and nonlinear solutions are very close for S values less than 15 to 20. However, the most striking thing about this plot is the proximity of the

solutions for aspect ratios of one half and one using linear theory when compared to the relative magnitudes of $\bar{w}$ for an isotropic plate as shown in table 4.1. It can be seen for S=40, the value of $\bar{w}$ for an aspect ratio of 1/2 is 109% of $\bar{w}$ for an aspect ratio of one, and $\bar{w}$ for an aspect ratio of two is 38% of $\bar{w}$ for an aspect ratio of one. This similarity of results between the AR=1/2 and AR=1 cases occurs because, for these two aspect ratios, there are a greater number of fibers in the direction of the short dimension of the plate. Referring to the discussion of ply layups, at least half of the fibers in all ply layups is in the x-direction, and referring to table 3.3, the x-direction is the shorter dimension for an aspect one half and is the longer dimension for an aspect ratio of two. The short dimension of the plate has a greater influence on the response of the plate and so, when the short dimension of an orthotropic plate with an aspect ratio of one half is equal to the dimensions of a square, i.e. AR=1, orthotropic plate of the same ply layup, one would expect their response to be very similar. The nonlinear solutions converge to values of $\bar{w}$ that result in ratios that are somewhat closer to the isotropic case than the linear solution. Here, $\bar{w}$ for AR=1/2 is 164% of $\bar{w}$ for AR=1, and $\bar{w}$ for AR=2 is 62% of $\bar{w}$ for AR=1. Again, this occurs because the higher order terms in the inplane displacement function significantly stiffen the plate and transverse shear deflection effect is reduced. Like the isotropic case, as aspect ratio increases, $\bar{w}$ decreases. All simply supported plates exhibit similar behavior.

Clamped Supports. Figure 4.6 shows $\bar{w}$ versus S for a clamped plate with a $[0_{12}/45_4/-45_4/90_4]_s$ ply layup made of material B. The curves for both the linear and nonlinear solutions for all three aspect ratios is shown. Again

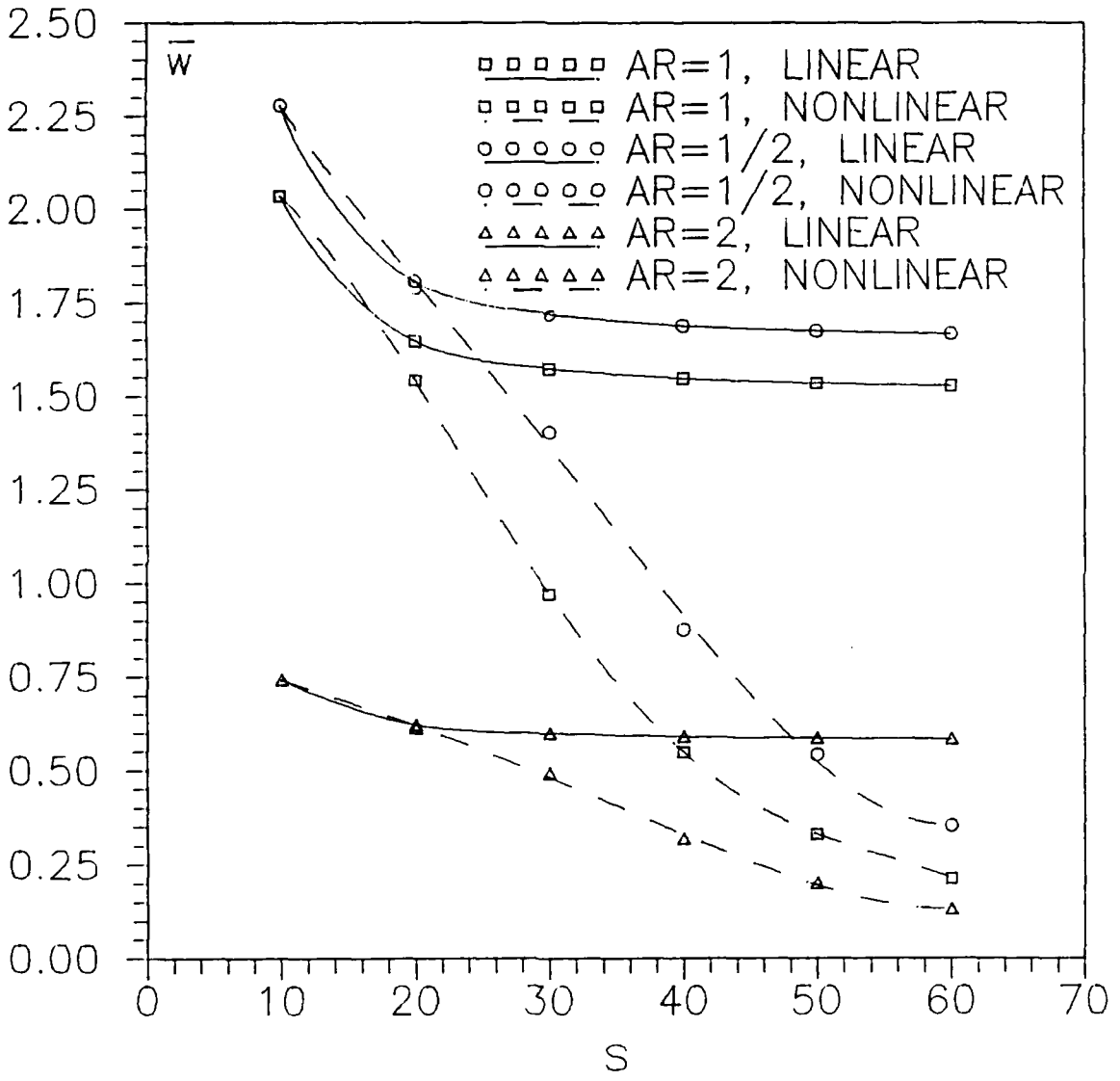

FIGURE 4.5. $\bar{w}$ vs s for a simply supported $[0_{16}/90_8]_s$ plate made of material B.

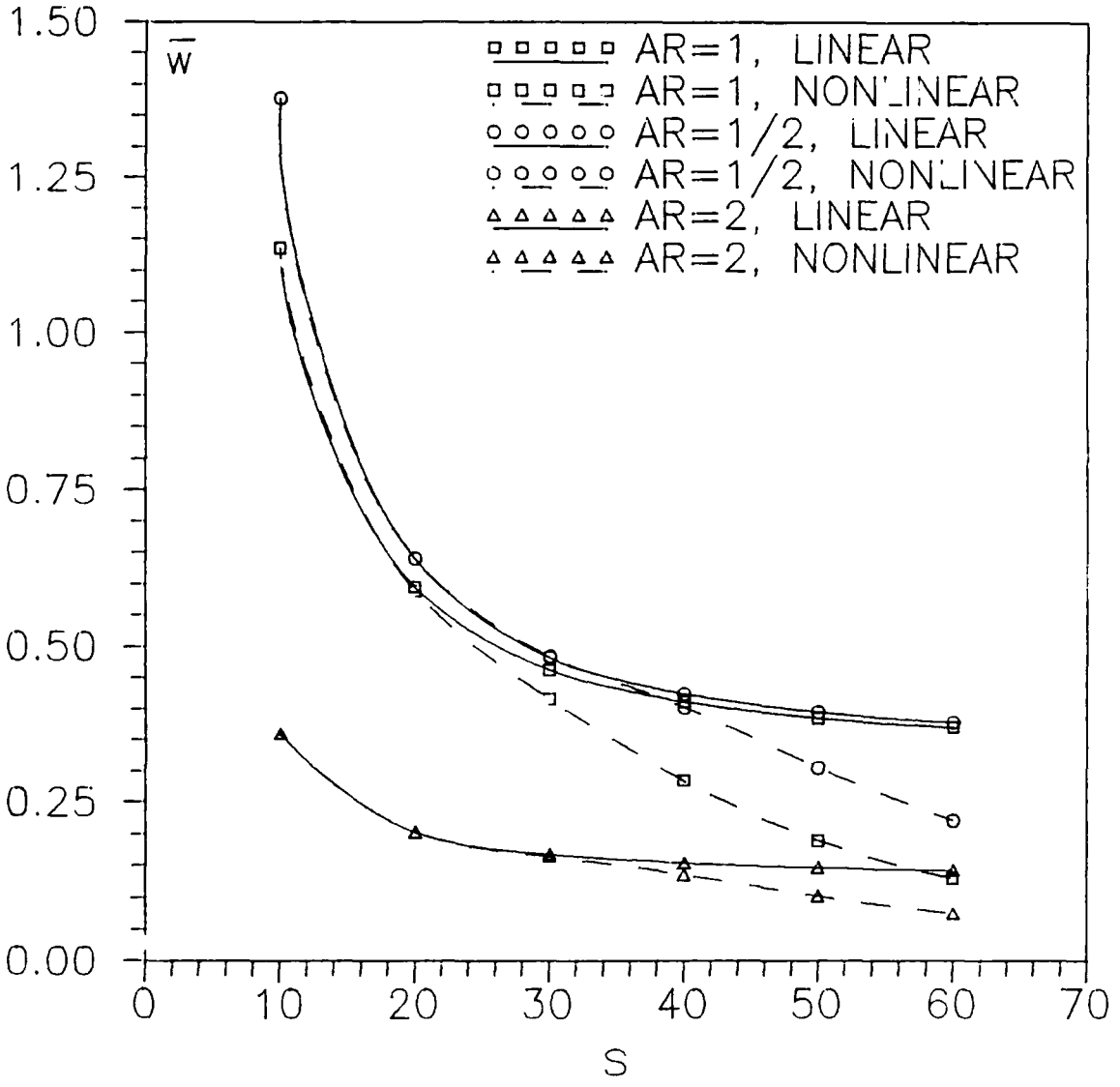

FIGURE 4.6. $\bar{w}$ vs s for a clamped $[0_{12}/45_4/-45_4/90_4]_s$ plate of material B.

looking at S=40 for the linear results, the value of $\bar{w}$ for AR=1/2 is 103% of $\bar{w}$ for AR=1, and $\bar{w}$ for AR=2 is 37% of $\bar{w}$ for AR=1. This compares favorably to the simply supported case. The behavior here, in general, is very similar to the simply supported plate shown in figure 4.5, but the main difference here is that the linear and nonlinear solutions are comparible to a much greater value of S. For an aspect ratio of one half the solutions are comparible up to S=40, for AR=1 up to S=30, and for AR=2 up to S=40. As mentioned in the discussion of figure 4.2, this occurs because the boundary conditions considerably stiffen the plate and the higher order terms present in the nonlinear solution do not come into play to the same extent they do in the simply supported case. All the clamped plates studied exhibited similar behavior.

Effects of Ply Layup.

Next, we look at the effect of ply layup on the response of the plate. Figures 4.7 and 4.8 make the comparison of ply layups by plotting $\bar{w}$ versus S for all ply layups for both linear and nonlinear solutions. The plate shown is of material A with an aspect ratio of one and the ply layups are numbered as shown in table 4.2.

Table 4.2 Layup Numbering System for Figures 4.7 and 4.8.

Ply	Layup
1	$[0_{16}/90_8]_s$
2	$[0_{12}/60_6/-60_6]_s$
3	$[0_{12}/45_6/-45_6]_s$
4	$[0_{12}/45_4/-45_4/90_4]_s$

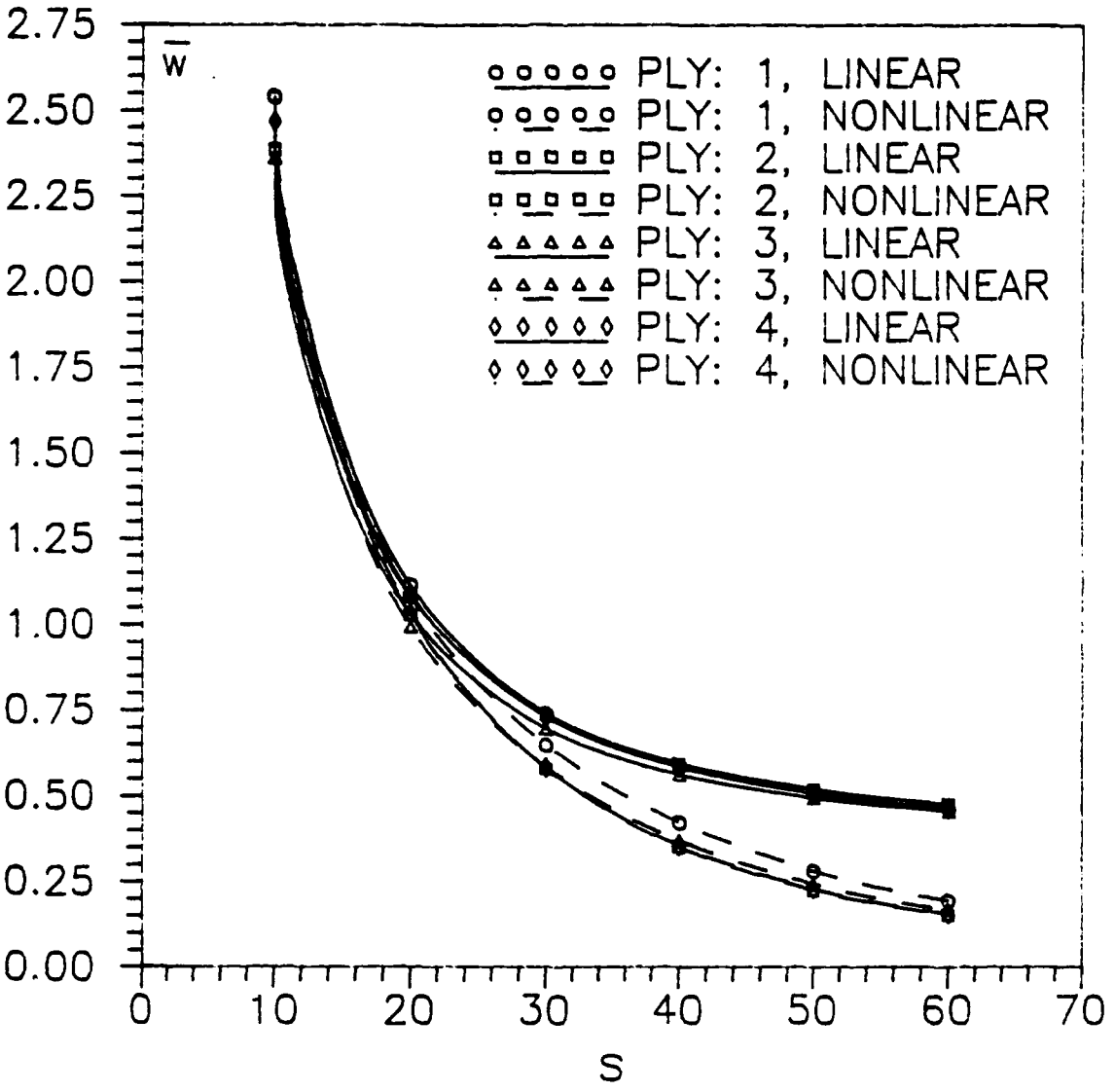

FIGURE 4.7. $\bar{w}$ vs s for a clamped plate of material A with an aspect ratio of 1.

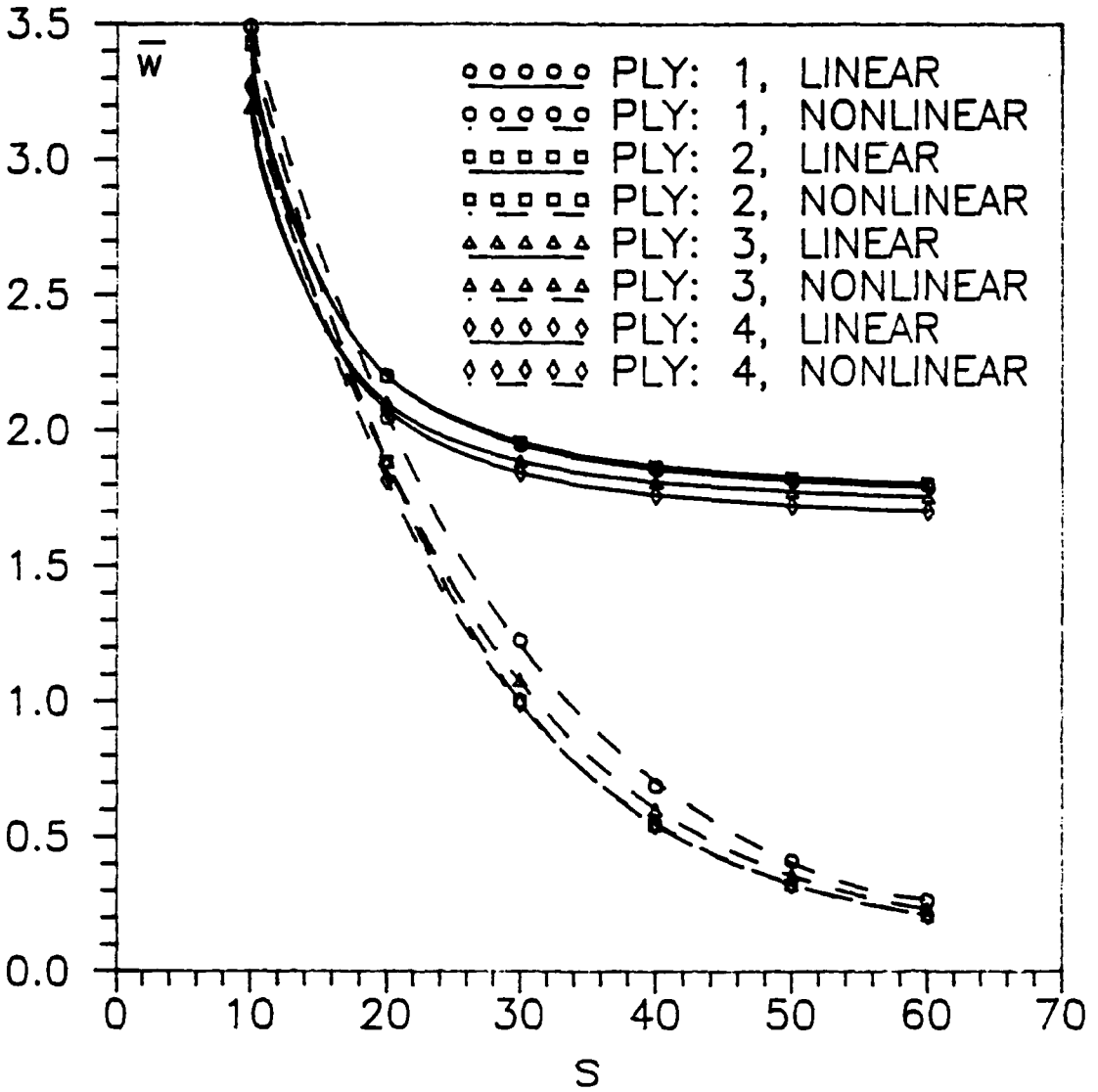

FIGURE 4.8. $\bar{w}$ vs s for a simply supported plate of material A with an aspect ratio of one.

Figure 4.7 is for a clamped plate and figure 4.8 is for a simply supprted plate. As can be seen in both plots, there is not a large difference between the layups. This is due to the fact that for each layup at least 50% of the plies were in the 0° direction, i.e. parrellel to the x-axis, and these plies dominate the response of the structure. However, there are some differences between the layups due to the large differences between some of the smaller A_{ij} and D_{ij} terms as a result of the different ply orientations. But, as can be seen from tables 3.4 and 3.5, these terms are always at least an order of magnitude less than A_{11} or D_{11}, which dominate the plate's response, so the difference in deflection is small. The differences between ply layups is more pronounced for the nonlinear solution than the linear solution. Also, the differences are more pronounced for a thick plate than for a thin plate.

V. CONCLUSIONS

In this thesis the effects of material properties, geometric nonlinearities, thickness, aspect ratio, boundary conditions, and ply layup on the static deflections of a uniformly loaded rectangular composite plate were investigated. Parabolic transverse shear strain was included in the analysis. The plate was analyzed with an existing finite element code incorporating a 4-noded 28 DOF rectangular element. Quarter plate symmetry was used to model the plate.

1. The linear solution asymptotically approaches the classical laminated plate theory (CLPT) solution as the plate gets thinner. This is because as the plate gets thinner the inplane forces begin to dominate the response of the structure and the solution degenerates to a CLPT problem. As the plate gets thicker, the deflection increases from the CLPT solution because the transverse shear effects are coming more and more into play. Therefore, the main difference between the linear solution and the CLPT solution is that the effects of the transverse shear strains have been included.

2. When the transverse shear has a major impact on the response of the plate, i.e. the plate is thick, the difference between the two materials in their transverse material properties becomes more important. As the plate gets thinner, the linear solutions for the different materials approach the same value. Again, this is due to the fact that the inplane forces become dominant and the major difference between the two materials, the E_1/G_{13}

ratio, becomes less important as the magnitude of the transverse shear forces decrease relative to the inplane forces. However, there is always some difference between the solutions created by the differences in the other material parameters.

3. The nonlinear solutions also asymptotically approach a constant value but it is much less than the linear solution and this constant value is not reached until the plate is much thinner. The reason the deflections are so much less in the nonlinear solution than the linear solutions is because the higher order terms present in the inplane deflections translate into increased membrane stiffness which plays a greater role as the plate gets thinner when the inplane stresses begin to dominate the structural response. However, for thick plates there is virtually no difference between the linear and nonlinear solution. All ply layups and aspect ratios investigated exhibited similar behavior.

4. For a clamped plate with a linear solution, the deflection does not approach a constant value until the plate is quite thin. However, the most striking feature about the clamped plate is the linear and nonlinear solution are quite close compared to the simply supported case. This closeness is due to the significant stiffening which the clamped boundary condition imparts to the plate. Consequently, the higher order terms do not play as large a role in the deflections and ensuing strains and stresses. This closeness of the linear and nonlinear solutions was exhibited for all ply layups and aspect ratios investigated.

5. The slope of the load-displacement curve gets more nonlinear and flatter, as the plate gets thinner. This occurs because the higher order terms in the assumed

displacement function are coming more into play as the membrane forces begin to dominate the solution. However, for a thick plate the displacement increases linearly with load. This is because, for thick plates, the linear and nonlinear solutions are nearly identical.

6. For aspect ratios of one half and one, the deflections are quite similar. This is due to the fact that for these two aspect ratios, there are a greater number of fibers in the direction of the short dimension of the plate for the ply layups considered here. The short dimension of the plate has a greater influence on the response of the plate and so, when the short dimension of an orthotropic plate with an aspect ratio of one half is equal to the dimensions of a square othotropic plate of the same ply layup, their responses are very similar. The nonlinear solutions all converge to roughly the same value for all aspect ratios. This is because the higher order terms in the inplane displacement function significantly stiffen the plate and reduce transverse deflection. For a clamped plate, the linear and nonlinear solutions are comparible until the plate is much thinner than for a simply supported plate. This occurs because the boundary conditions considerably stiffen the plate and the higher order terms present in the nonlinear solution do not come into play to the same extent they do in the simply supported case. All clamped plates exhibit similar behavior.

7. In this research, ply layup does not have a large effect on the deflection of the plate since at least 50% of the plies are in the 0° direction, i.e. parrellel to the x-axis, and these plies dominate the response of the plate. However, there are small differences in deflection between the layups. These differences are more pronounced for the

nonlinear solution than the linear solution and are more pronounced for a thick plate than for a thin plate. Also, it was observed that the maximum transverse shear stress usually occurred between the plies with the maximum angle difference between them.

Appendix A

Material Properties Comparisons

This appendix presents a complete set of curves of nondimesionalized displacement, $\overline{w}$, versus thickness ratio, S, for all ply layups and aspect ratios. Linear and nonlinear solutions for both materials are presented on each graph. The displacement is nondimensionalized according to Eqn (A.1):

$$\overline{w} = \frac{w_c h^3 E_1}{q_o a^4} \times 10 \qquad (A.1)$$

where

w_c = center displacement
h = plate thickness
E_1 = Young's modulus in fiber direction
q_o = total load on plate
a = characteristic inplane dimension

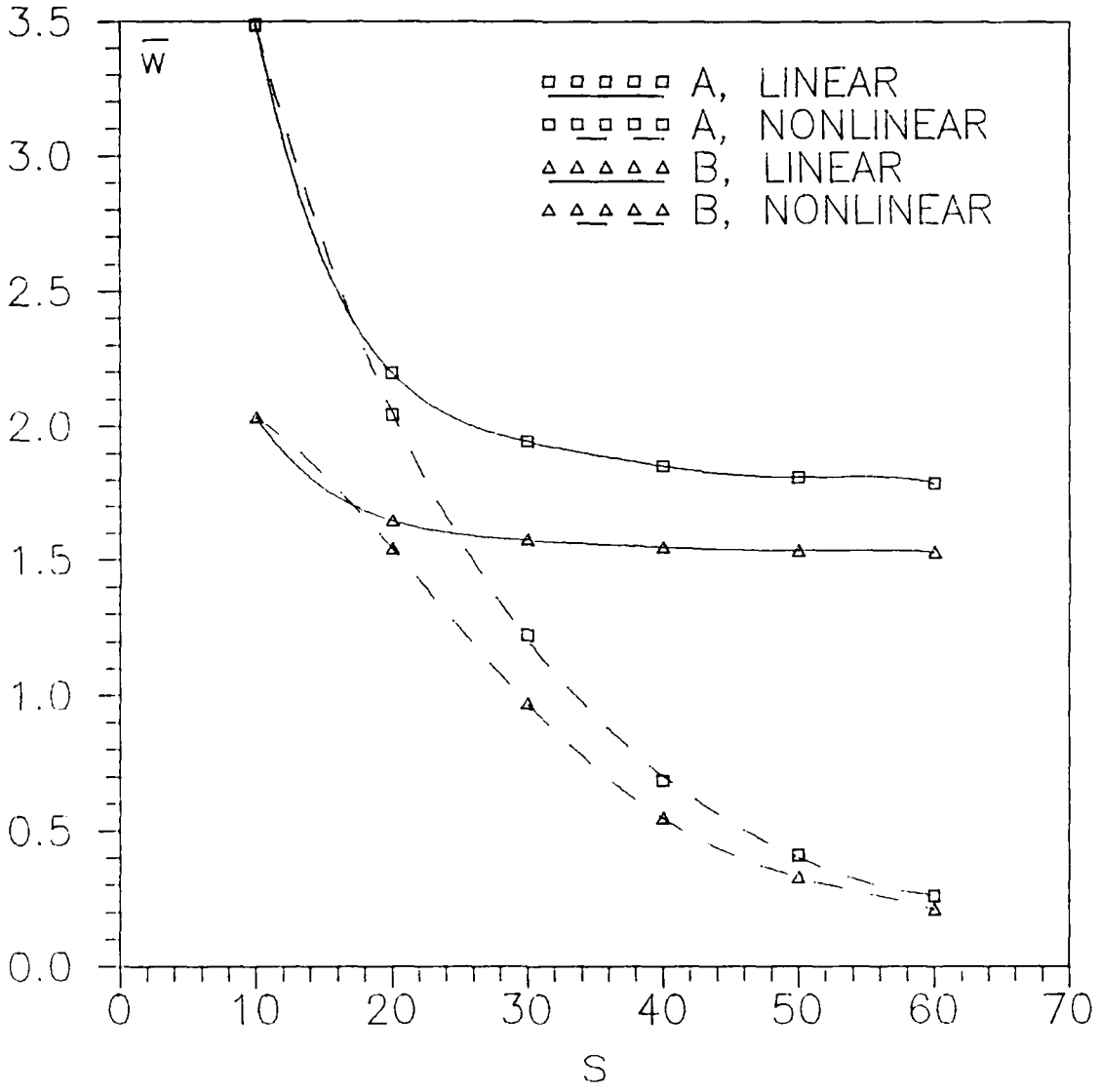

Figure A.1. $\bar{w}$ vs s for a simply supported $[0_{16}/90_8]_s$ plate with an aspect ratio of 1

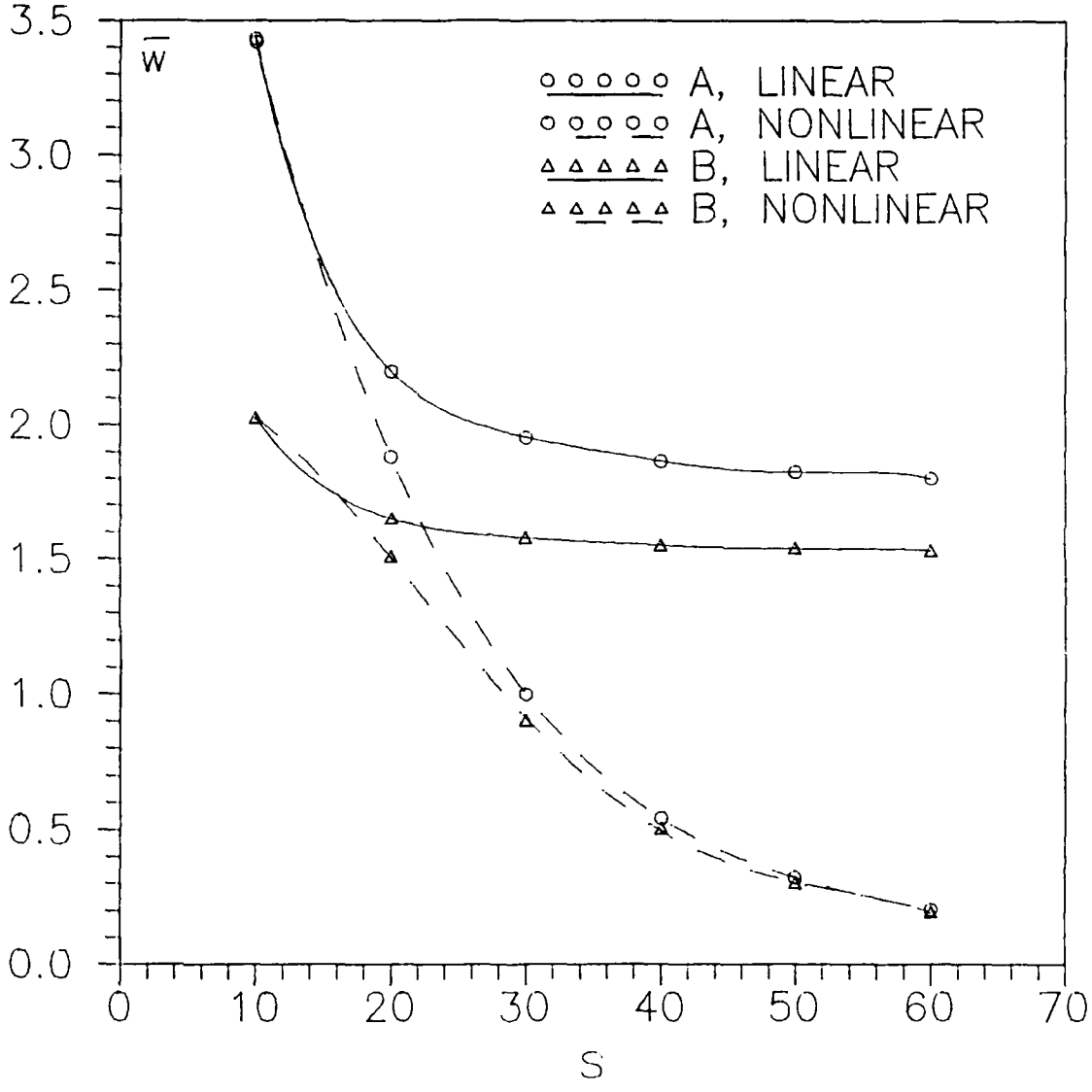

Figure A.2. $\bar{w}$ vs s for a simply supported $[0_{12}/60_6/-60_6]_s$ plate with an aspect ratio of 1

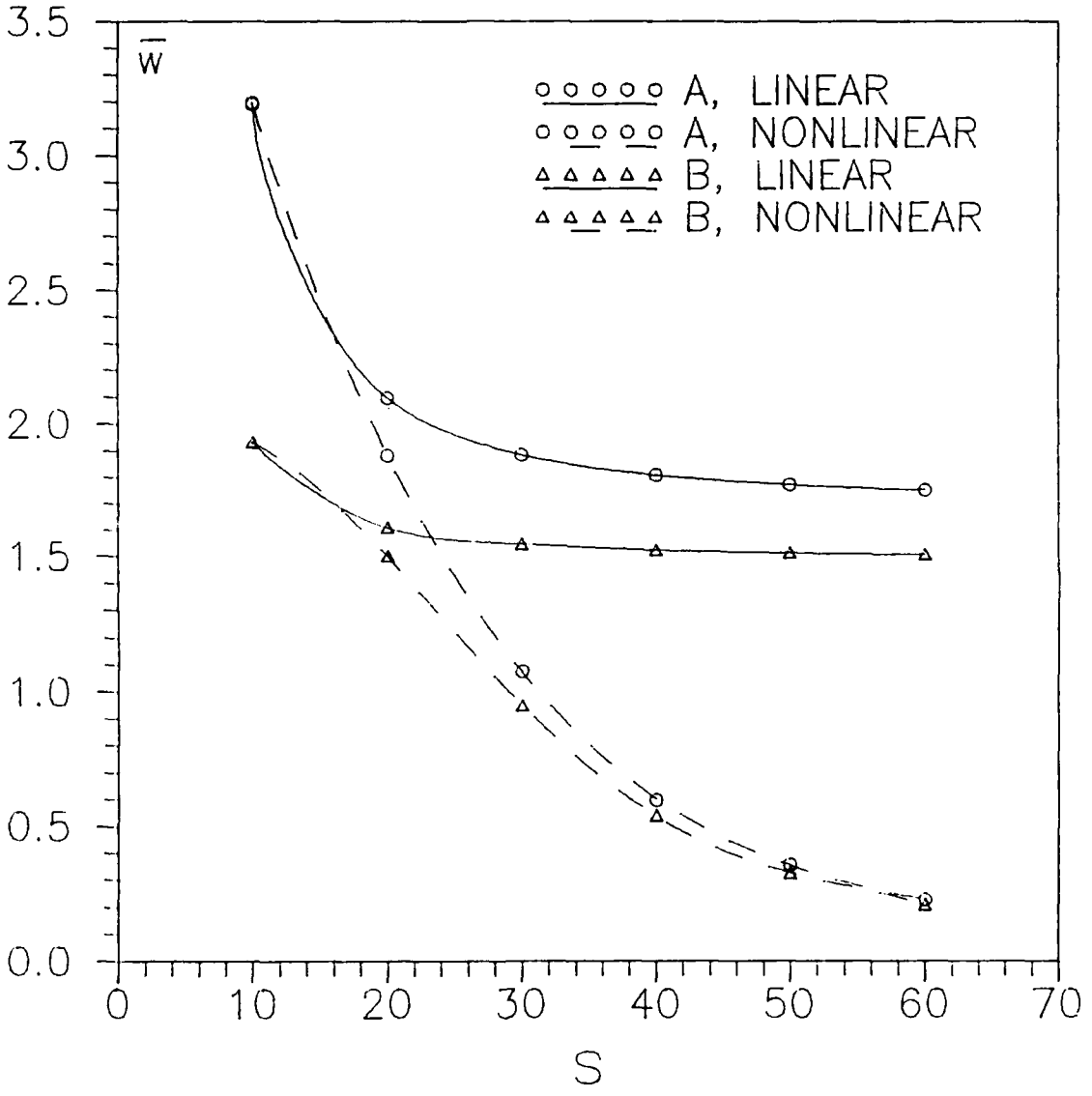

Figure A.3. $\bar{w}$ *vs s for a simply supported* $[0_{12}/45_6/-45_6]_s$ plate with an aspect ratio of 1

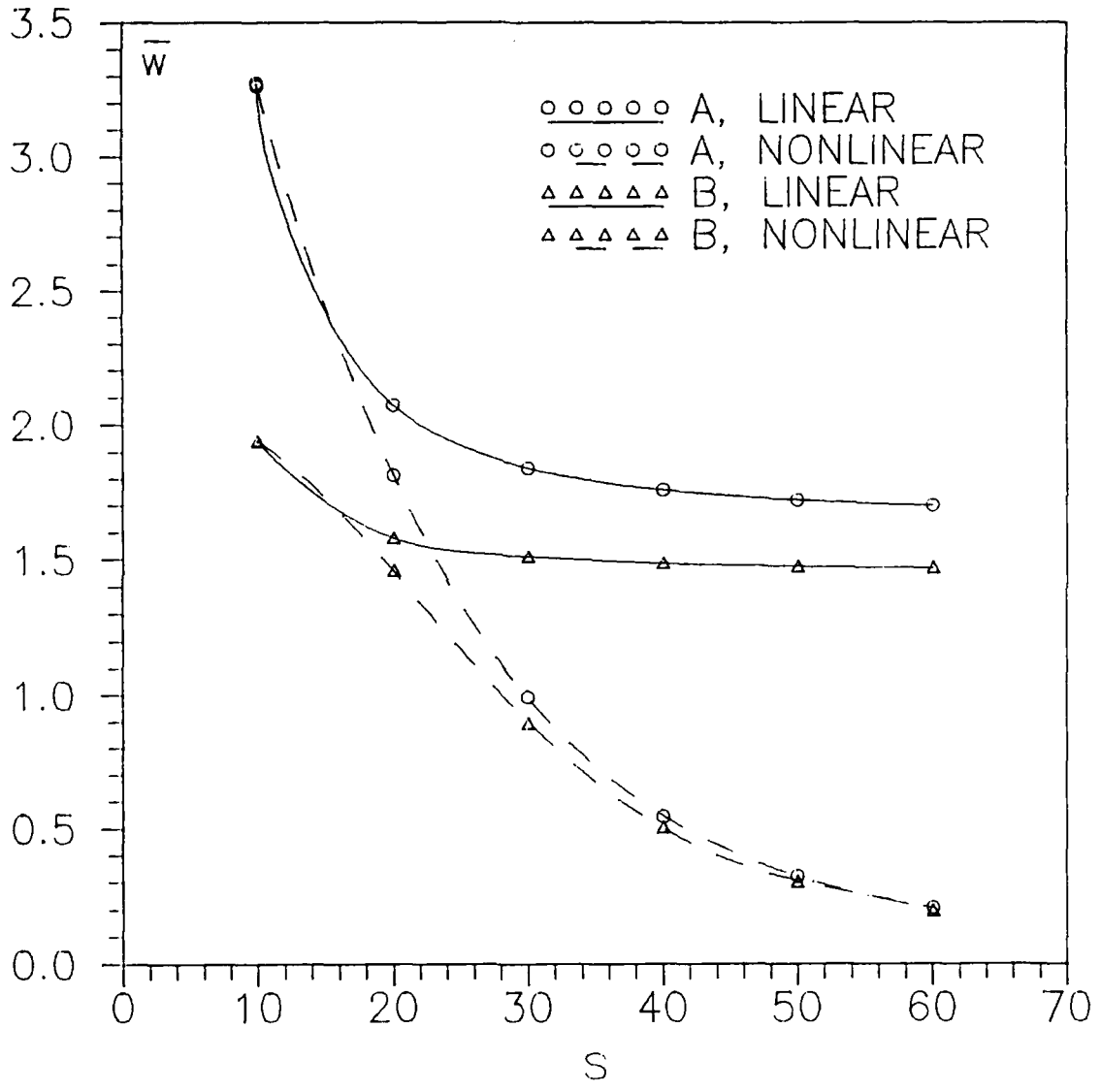

Figure A.4. $\bar{w}$ vs s for a simply supported $[0_{12}/45_4/-45_4/90_4]_s$ plate with an aspect ratio of 1

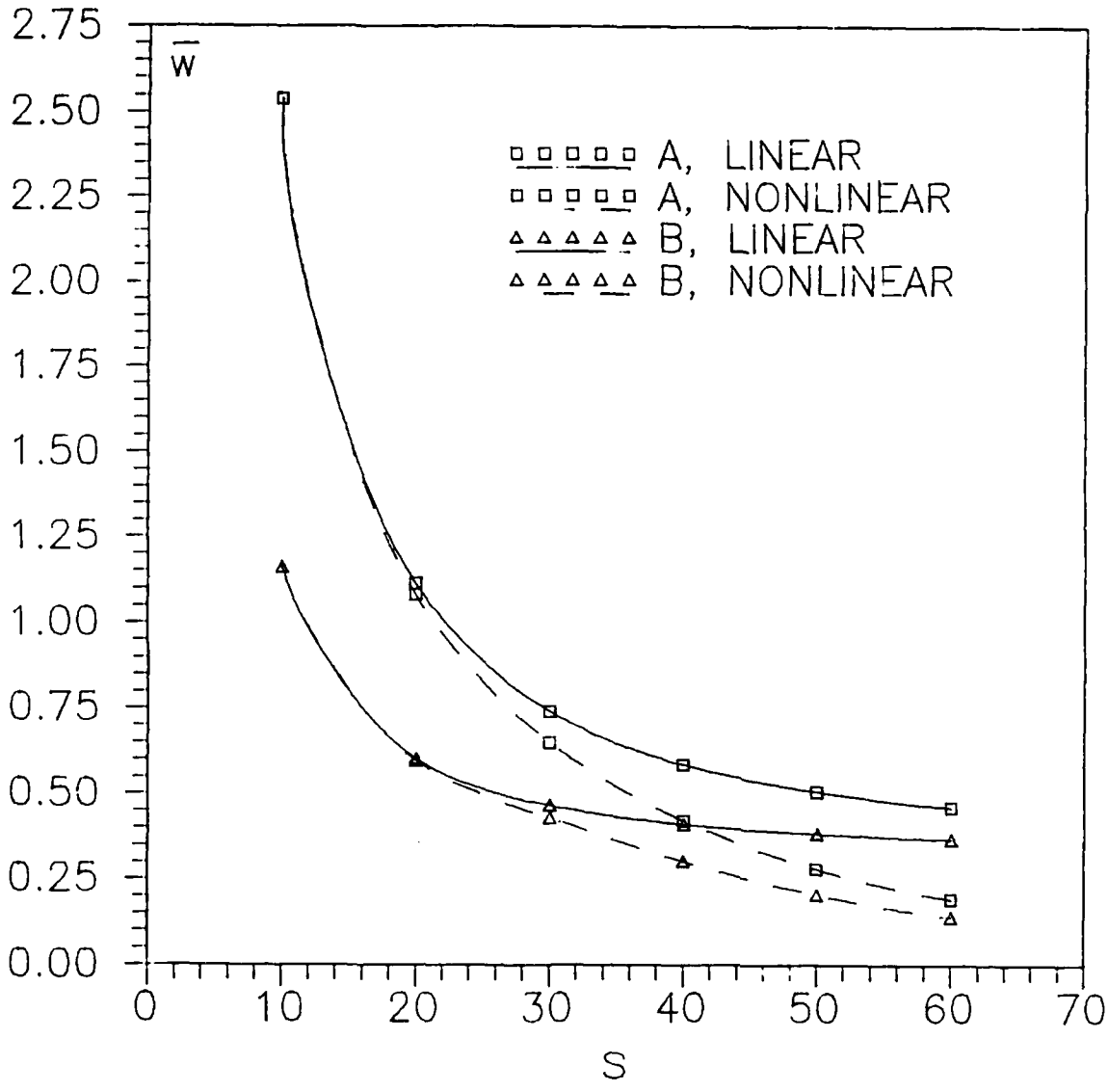

Figure A.5. $\bar{w}$ vs s for a clamped $[0_{16}/90_8]_s$ plate with an aspect ratio of 1

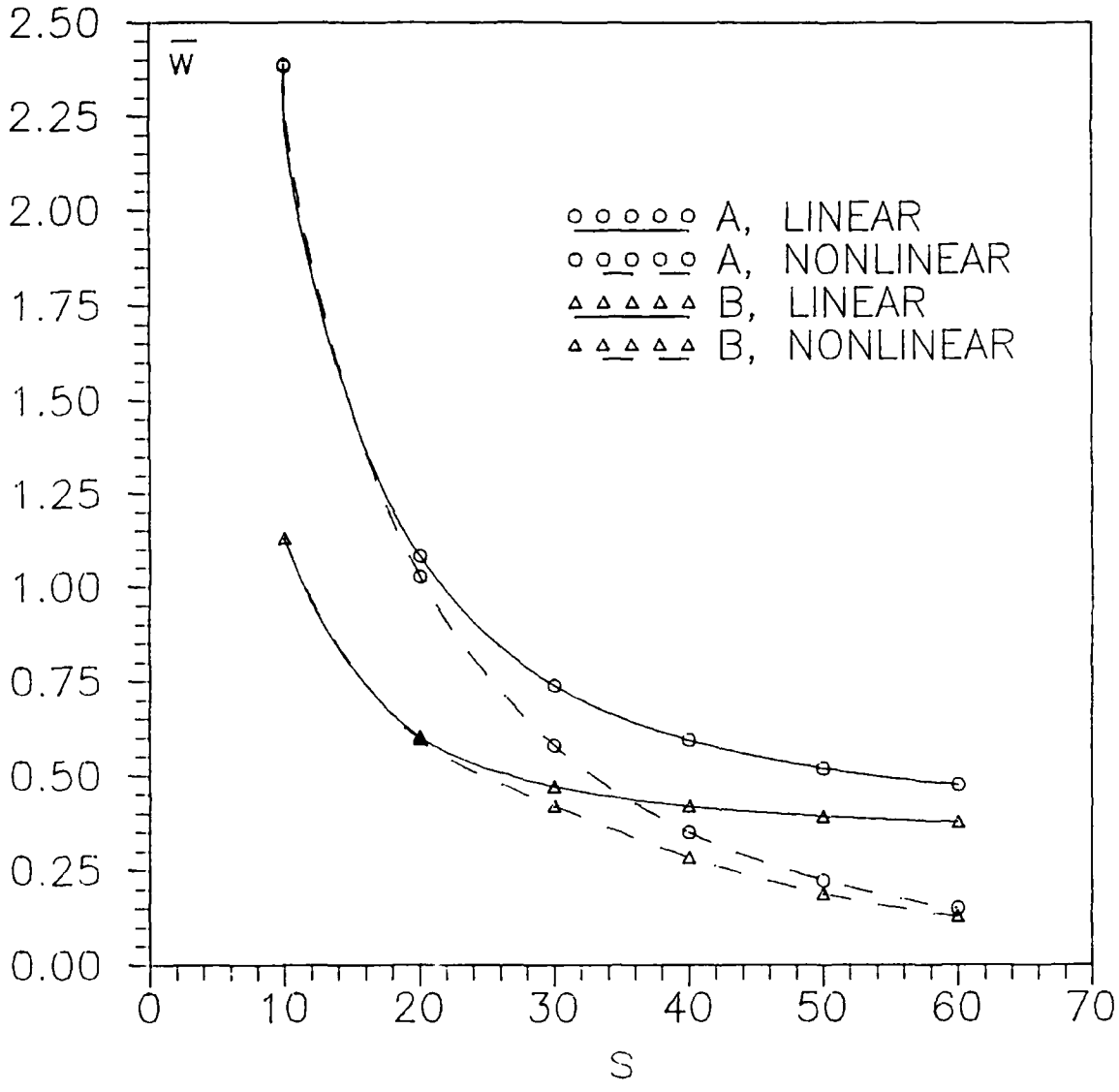

Figure A.6. $\overline{w}$ vs s for a clamped $[0_{12}/60_6/-60_6]_s$ plate with an aspect ratio of 1

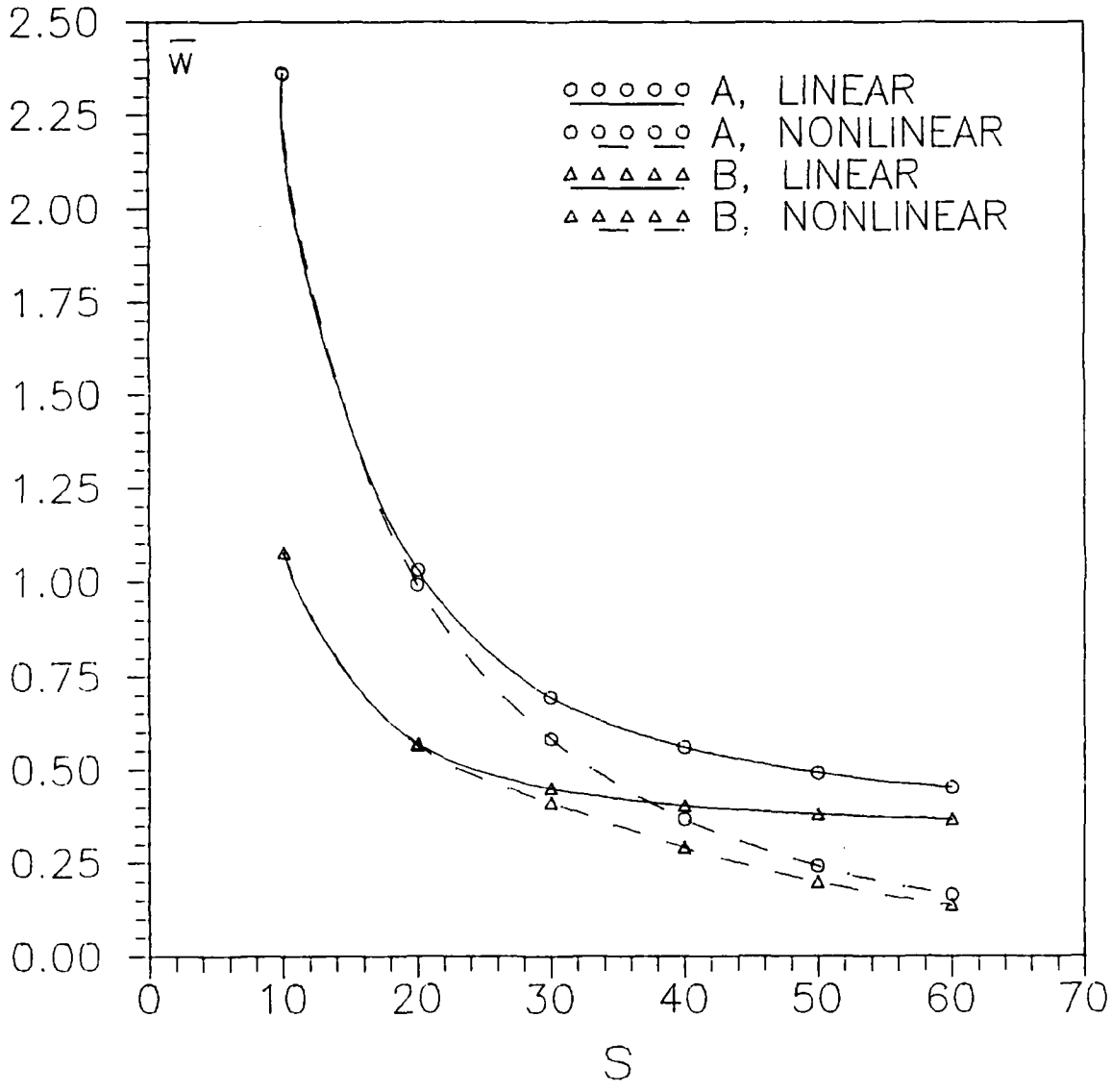

Figure A.7. $\bar{w}$ vs s for a clamped $[0_{12}/45_6/-45_6]_s$ plate with an aspect ratio of 1

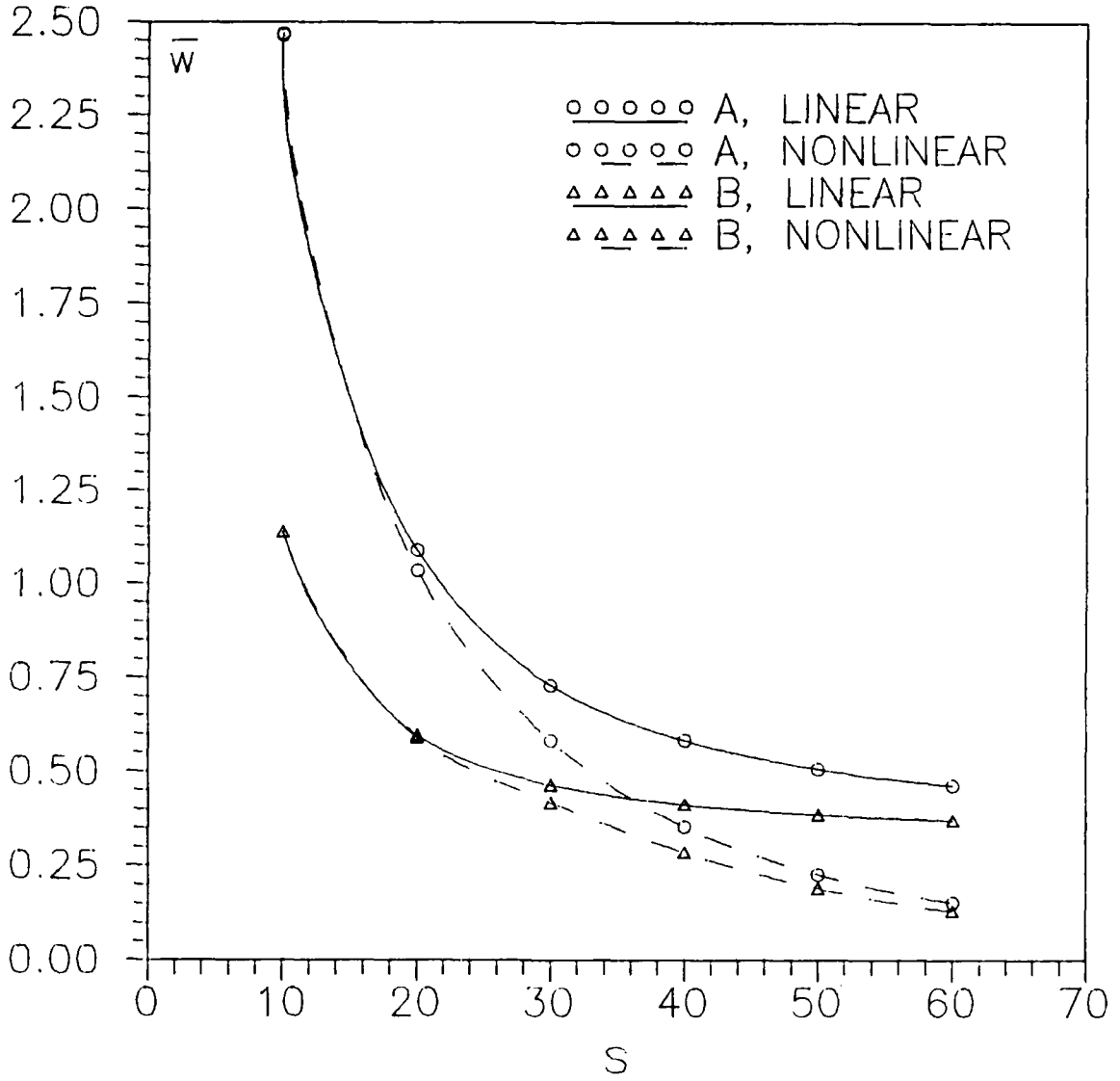

Figure A.8. $\bar{w}$ vs s for a clamped $[0_{12}/45_4/-45_4/90_4]_s$ plate with an aspect ratio of 1

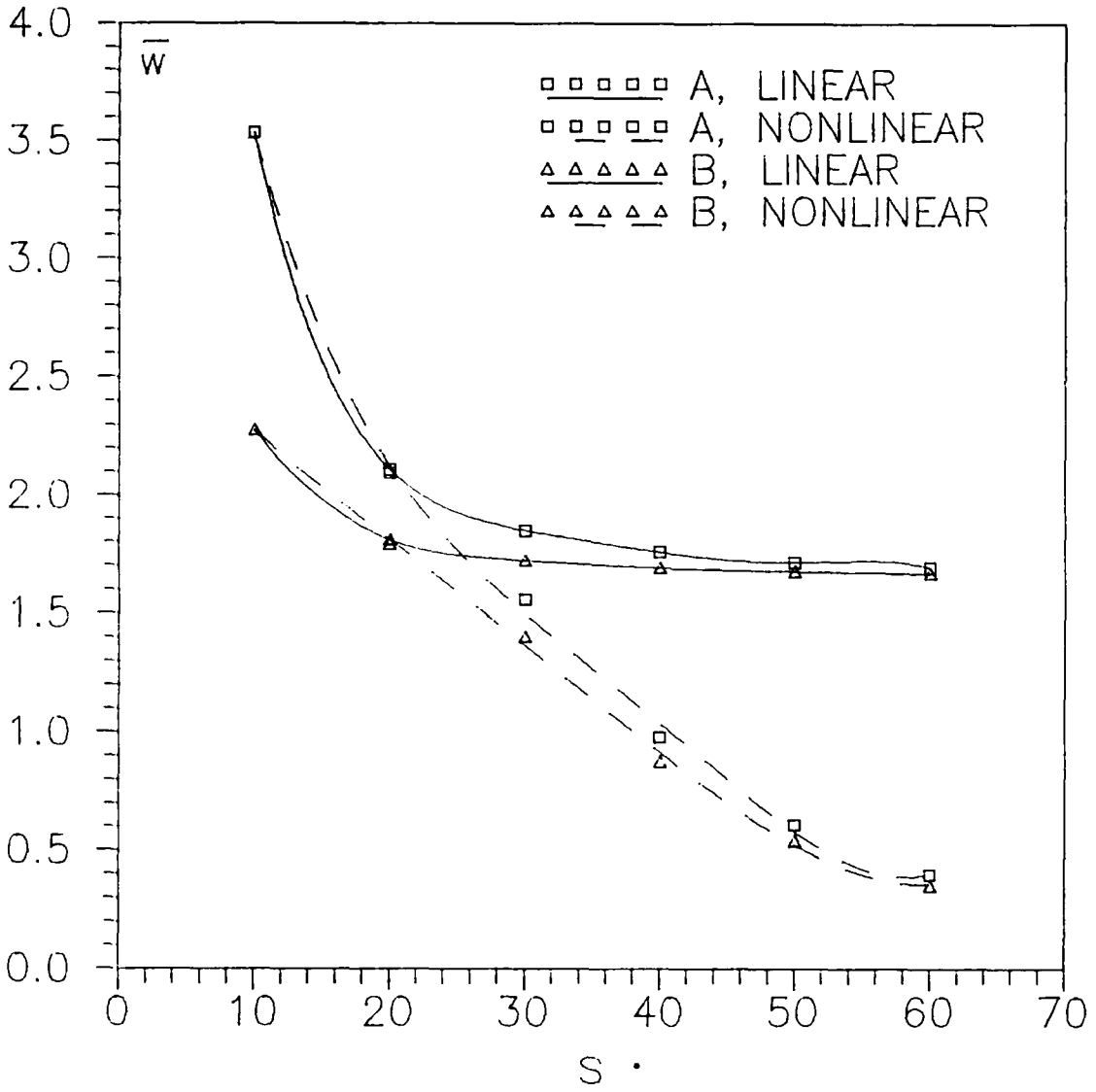

Figure A.9. $\bar{w}$ vs s for a simply supported $[0_{16}/90_8]_s$ plate with an aspect ratio of 1/2

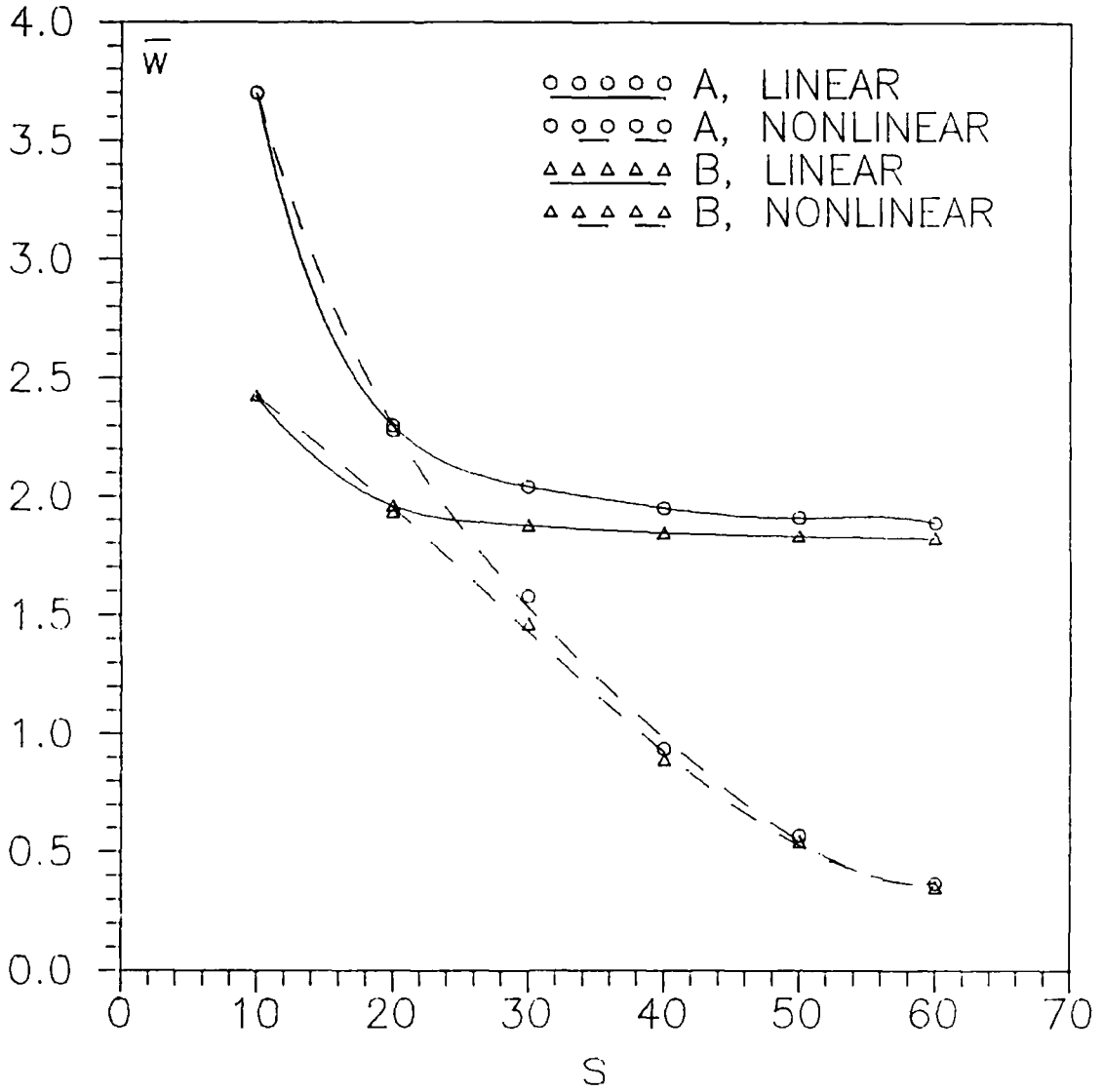

Figure A.10. $\bar{w}$ vs s for a simply supported $[0_{12}/60_6/-60_6]_s$ plate with an aspect ratio of 1/2

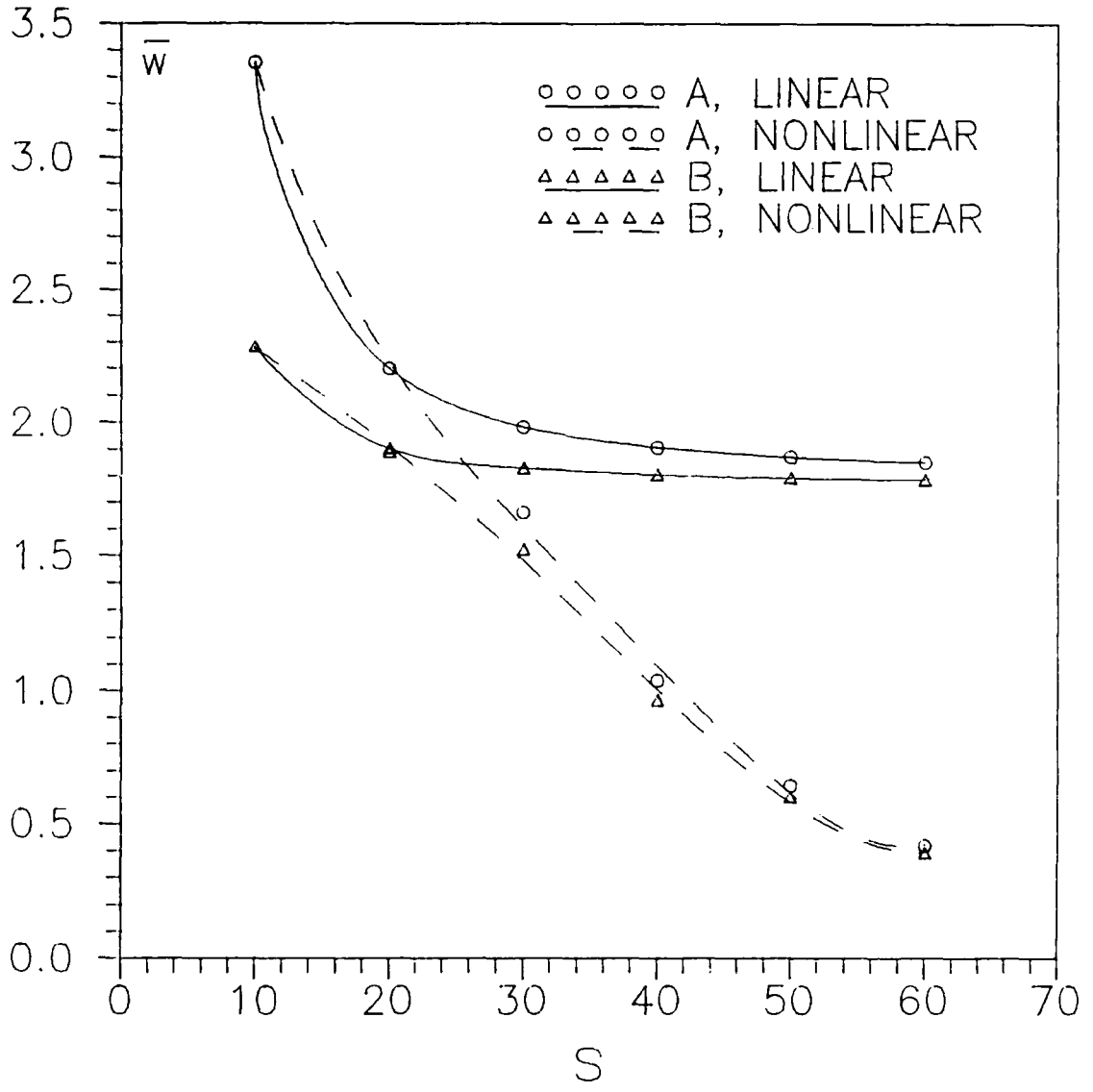

Figure A.11. $\bar{w}$ vs s for a simply supported $[0_{12}/45_6/-45_6]_s$ plate with an aspect ratio of 1/2

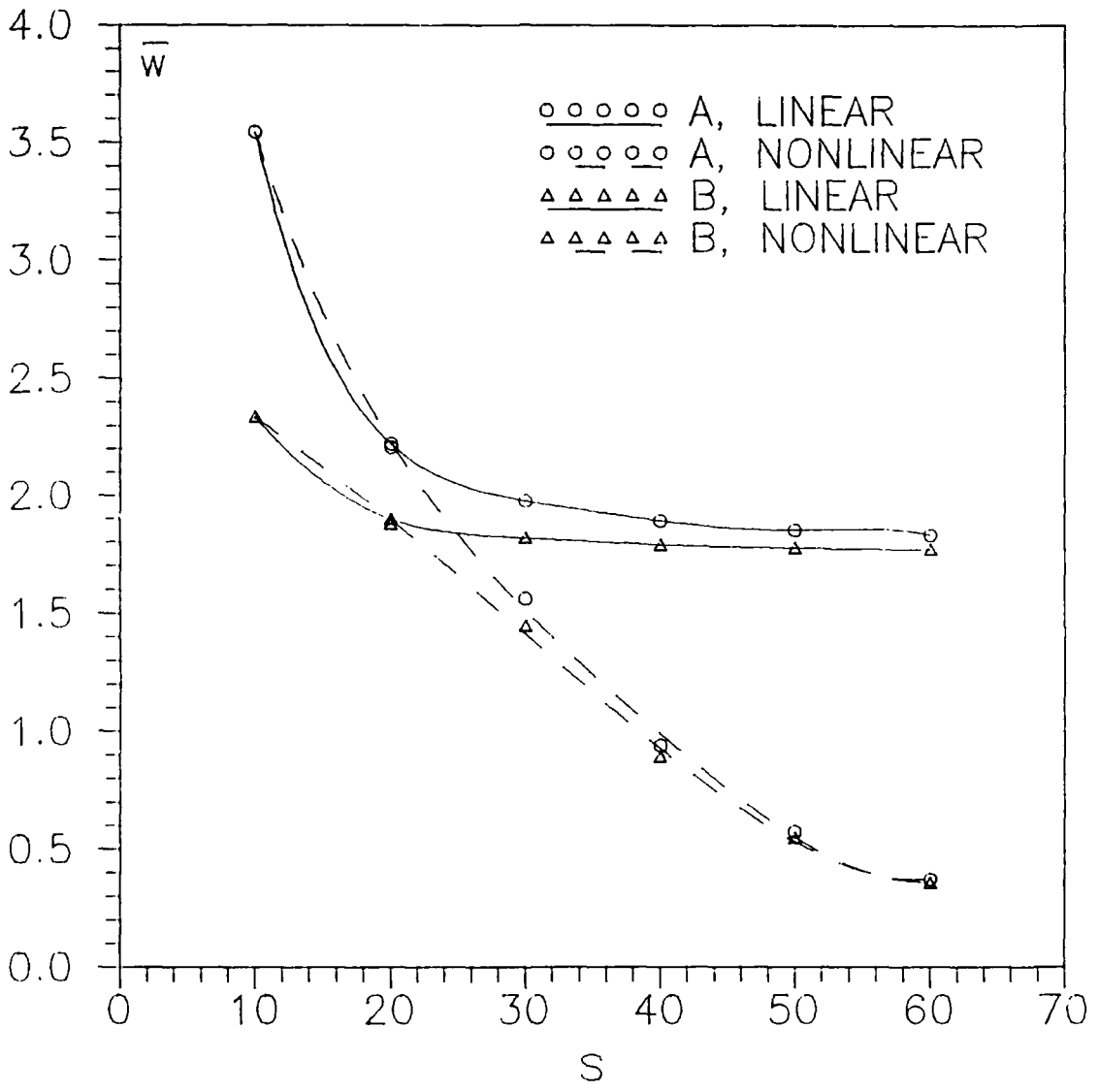

Figure A.12. $\bar{w}$ vs s for a simply supported $[0_{12}/45_4/-45_4/90_4]_s$ plate with an aspect ratio of 1/2

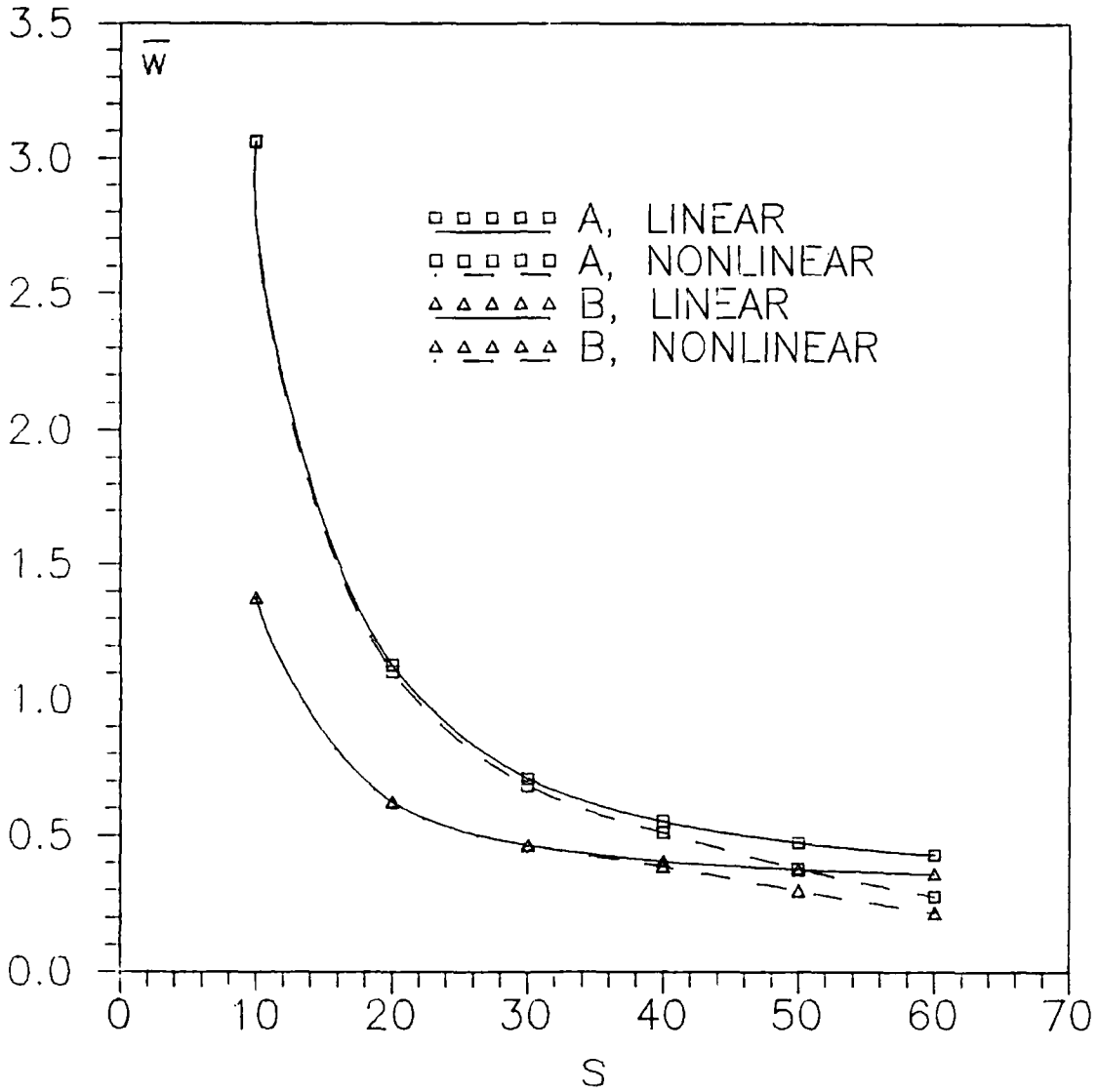

Figure A.13. $\overline{w}$ vs s for a clamped $[0_{16}/90_8]_s$ plate with an aspect ratio of 1/2

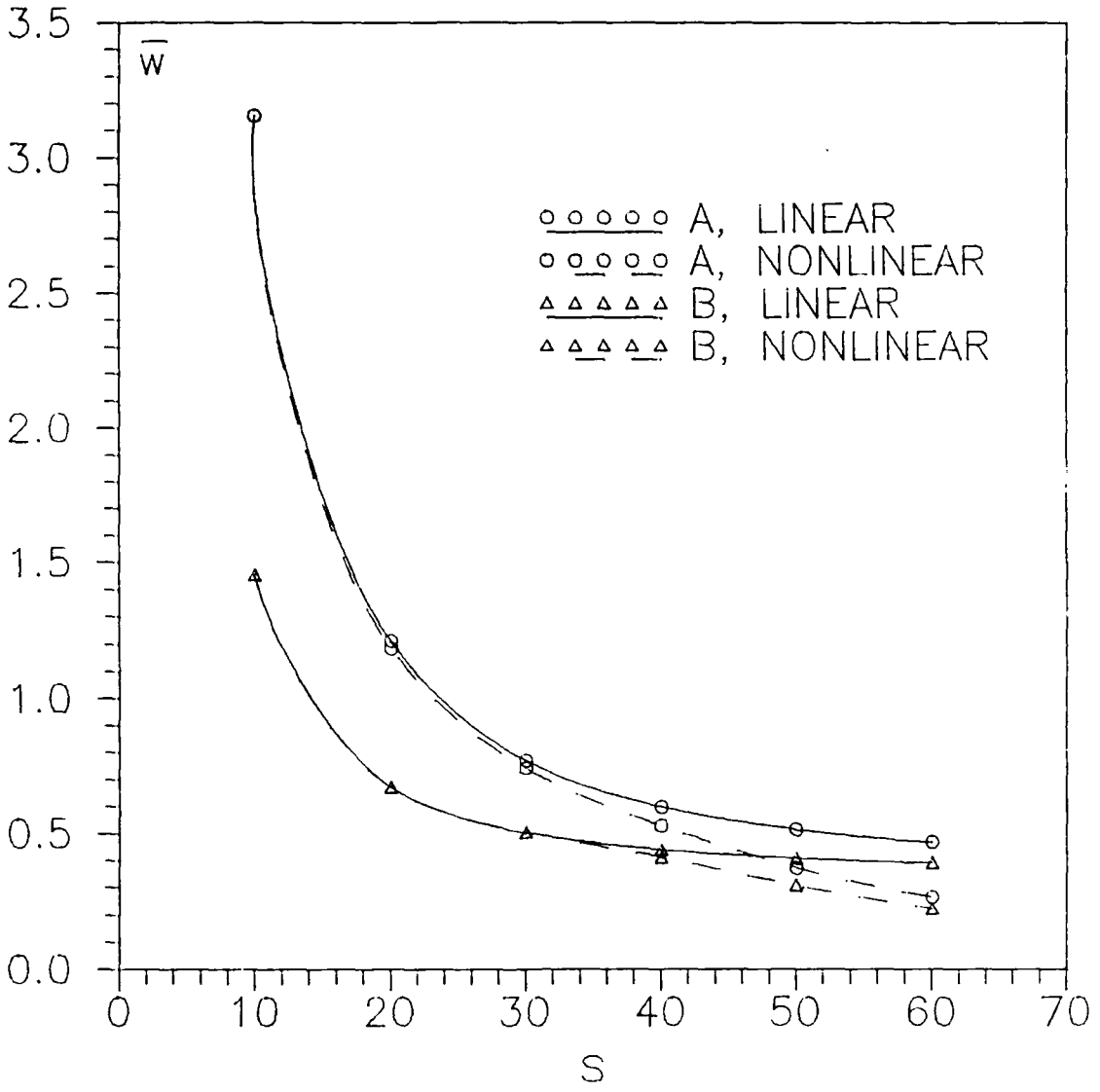

Figure A.14. $\bar{w}$ vs s for a clamped $[0_{12}/60_6/-60_6]_s$ plate with an aspect ratio of 1/2

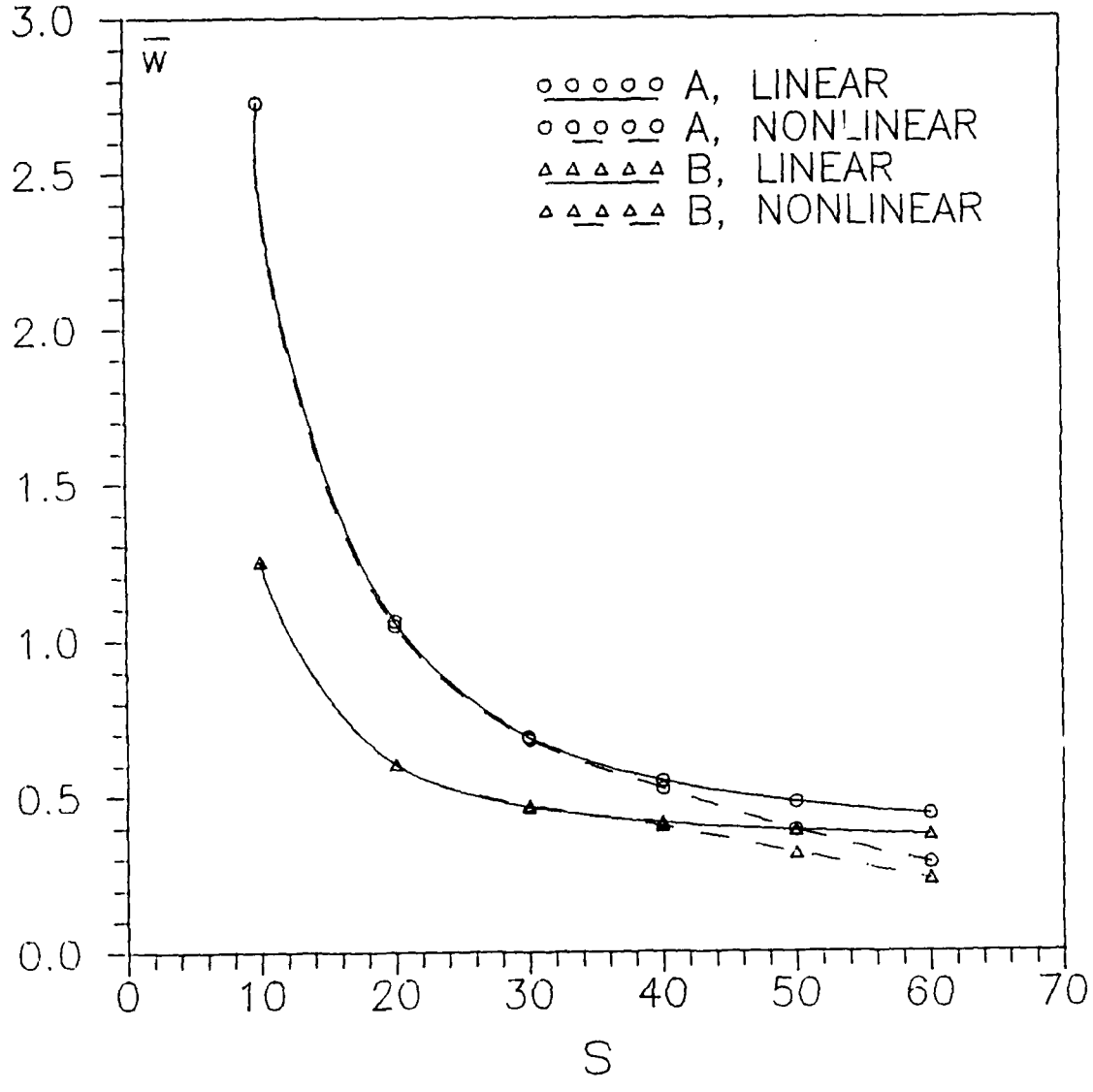

Figure A.15. $\bar{w}$ vs s for a clamped $[0_{12}/45_6/-45_6]_s$ plate with an aspect ratio of 1/2

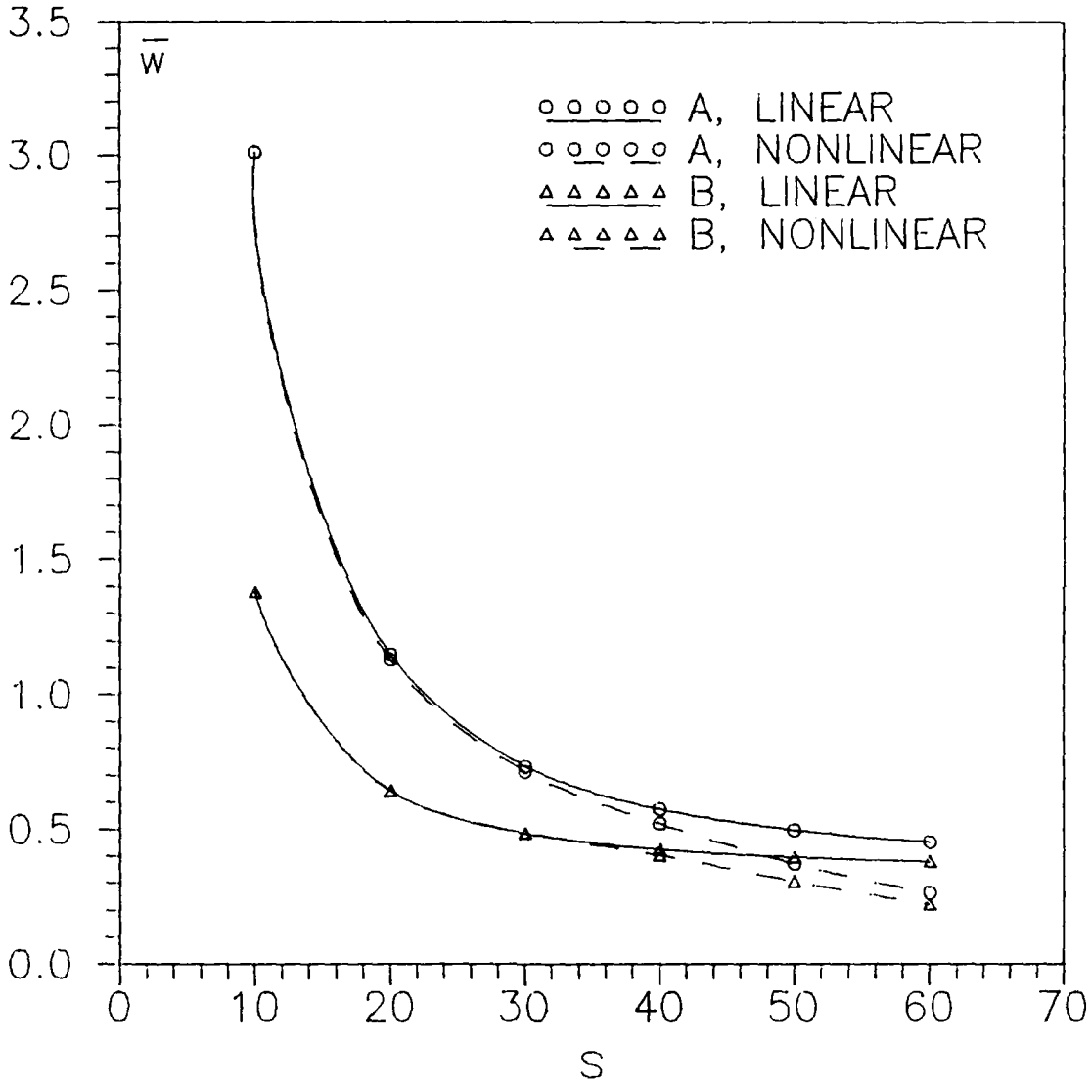

Figure A.16. $\bar{w}$ vs s for a clamped $[0_{12}/45_4/-45_4/90_4]_s$ plate with an aspect ratio of 1/2

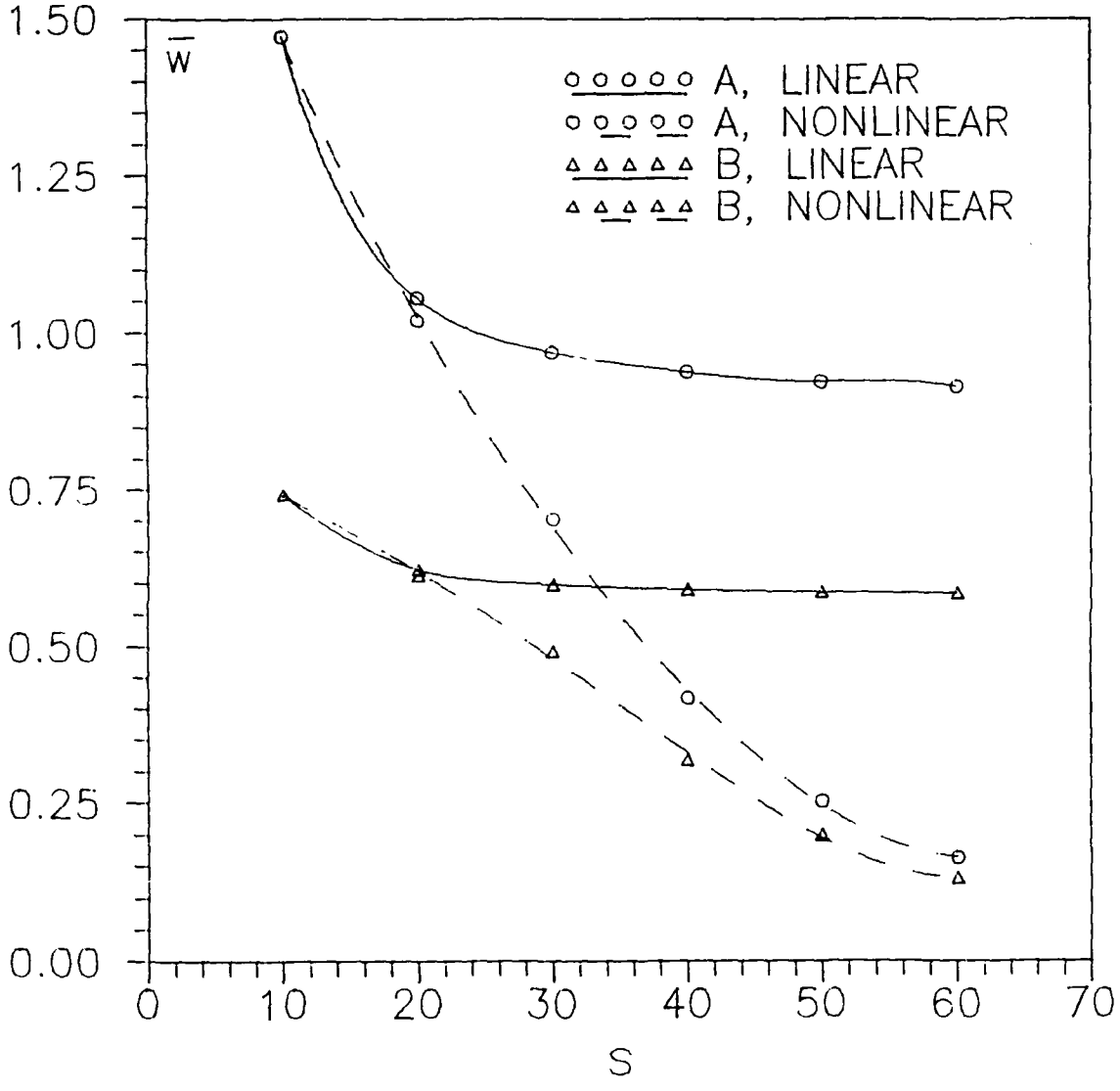

Figure A.17. $\bar{w}$ vs s for a simply supported $[0_{16}/90_8]_s$ plate with an aspect ratio of 2

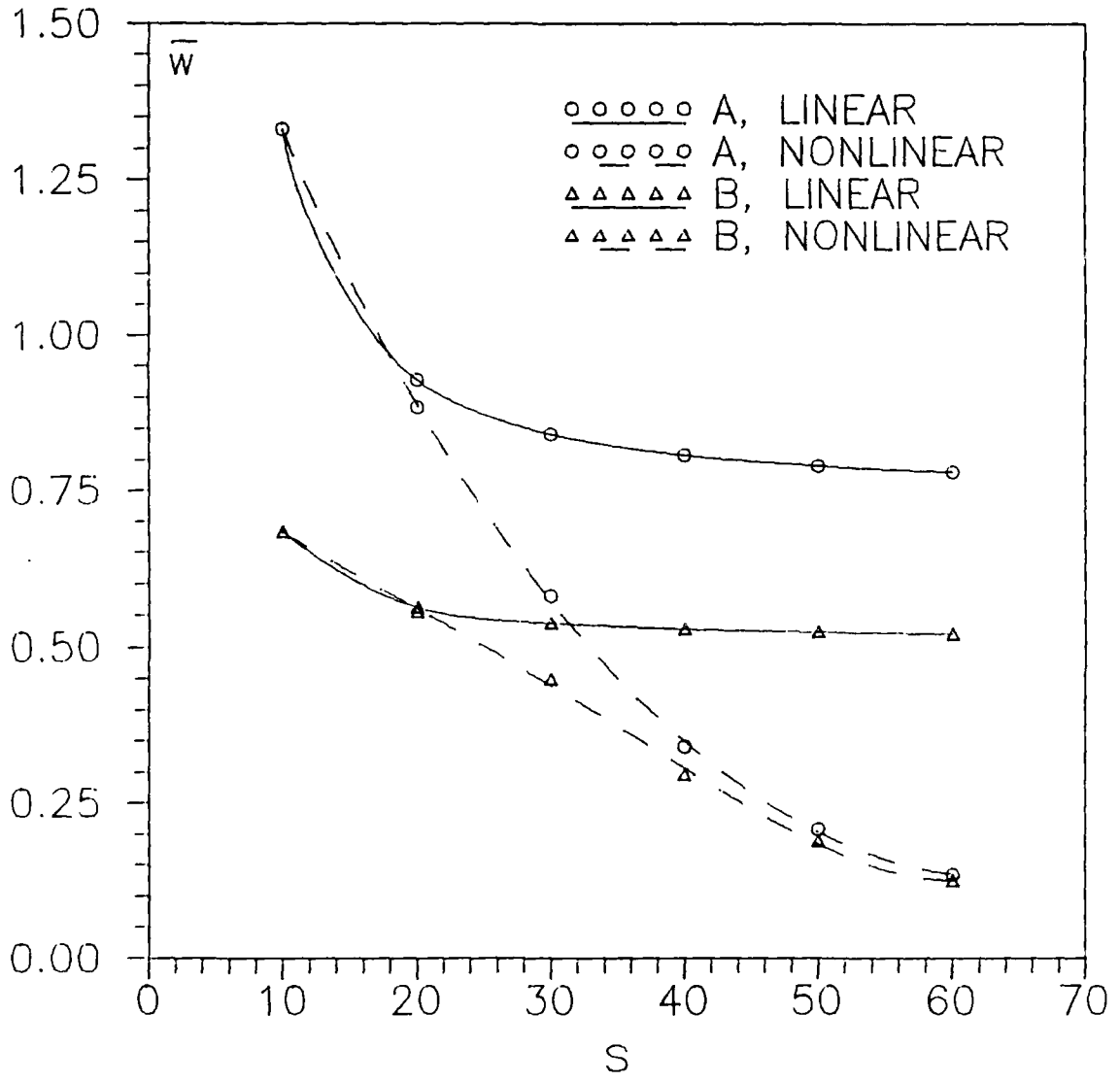

Figure A.18. $\bar{w}$ vs s for a simply supported $[0_{12}/60_6/-60_6]_s$ plate with an aspect ratio of 2

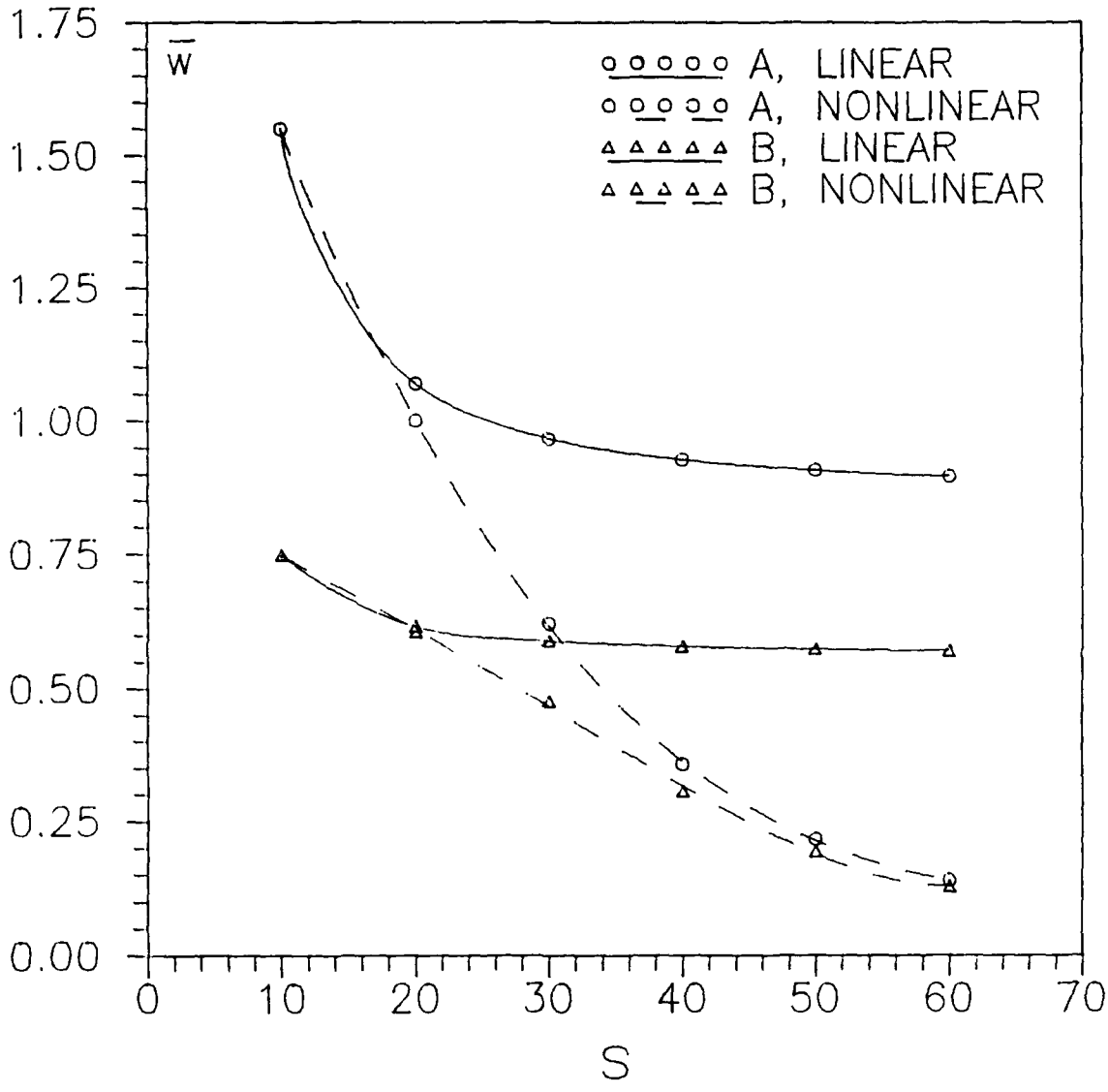

Figure A.19. $\bar{w}$ vs s for a simply supported $[0_{12}/45_6/-45_6]_s$ plate with an aspect ratio of 2

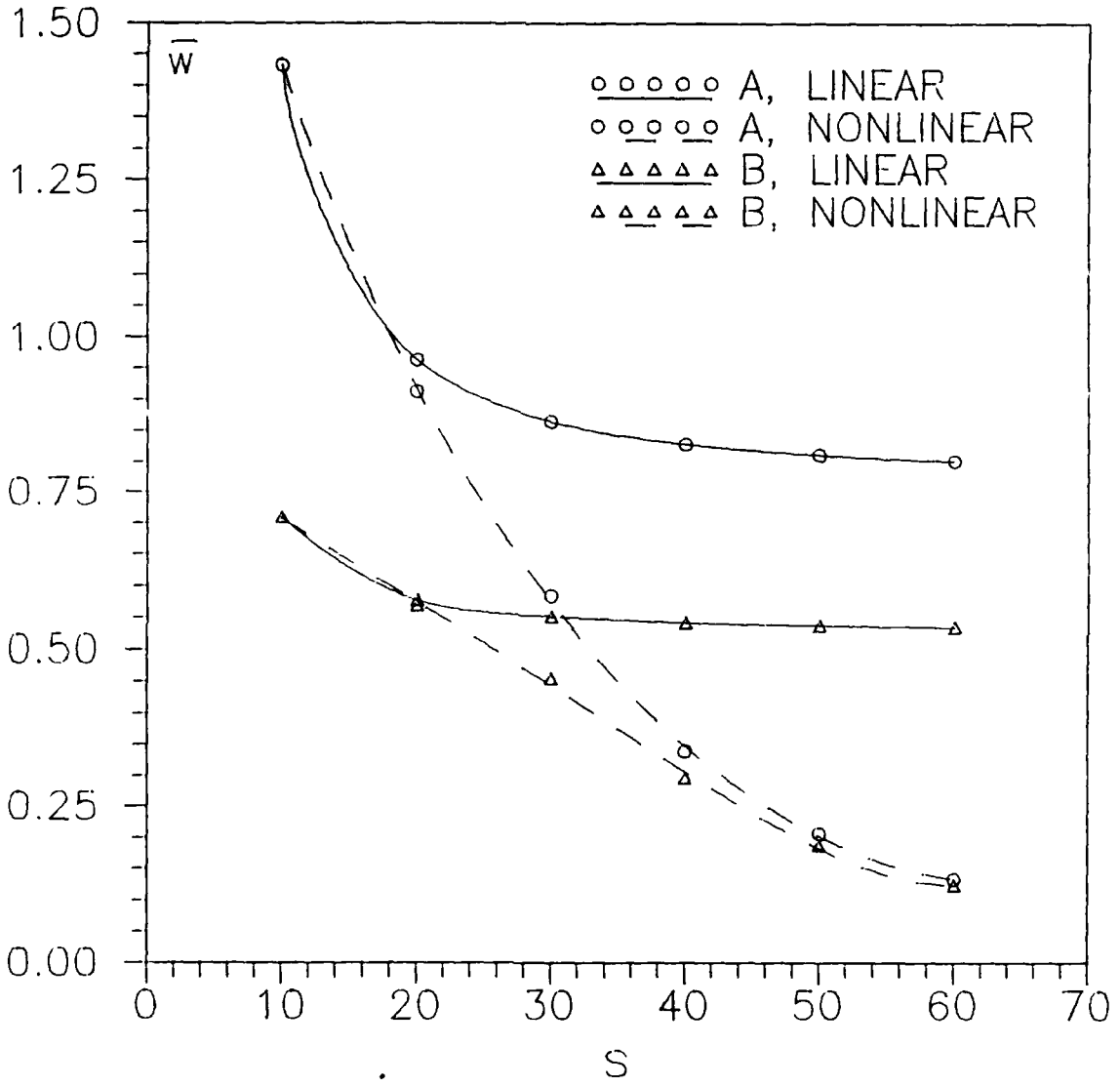

Figure A.20. $\bar{w}$ vs s for a simply supported $[0_{12}/45_4/-45_4/90_4]_s$ plate with an aspect ratio of 2

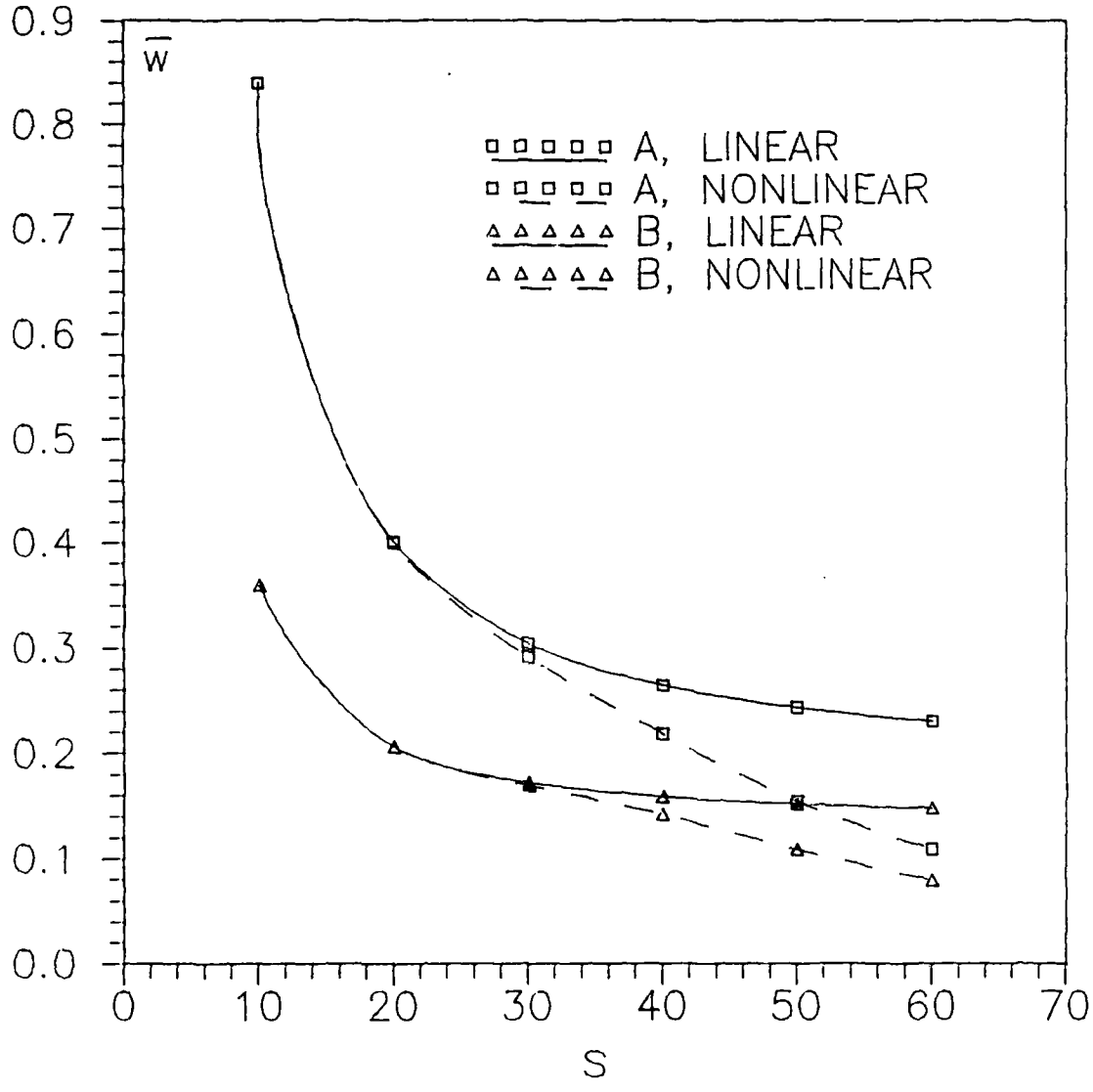

Figure A.21. $\bar{w}$ vs s for a clamped $[0_{16}/90_8]_s$ plate with an aspect ratio of 2

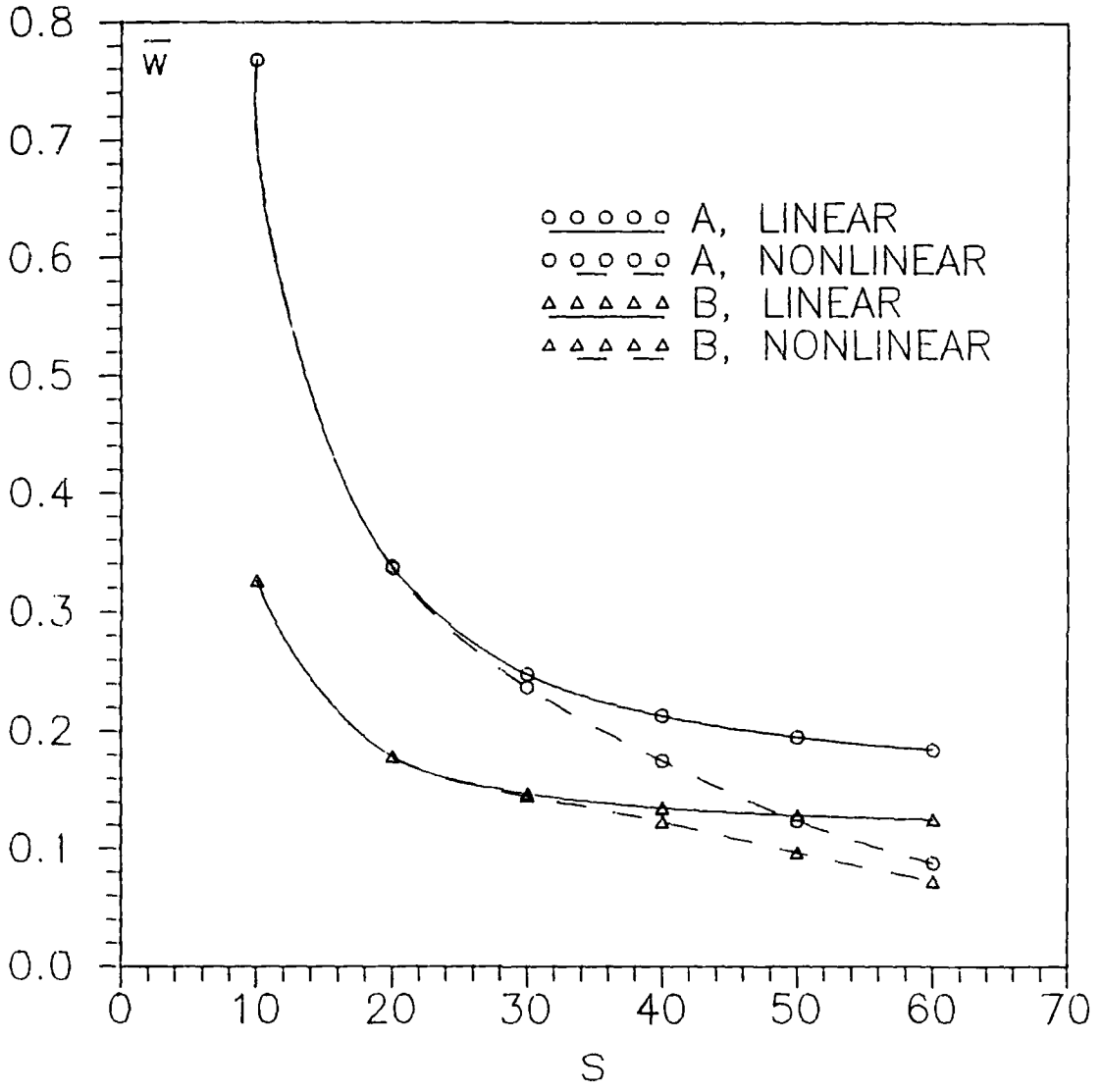

Figure A.22. $\bar{w}$ vs s for a clamped $[0_{12}/60_6/-60_6]_s$ plate with an aspect ratio of 2

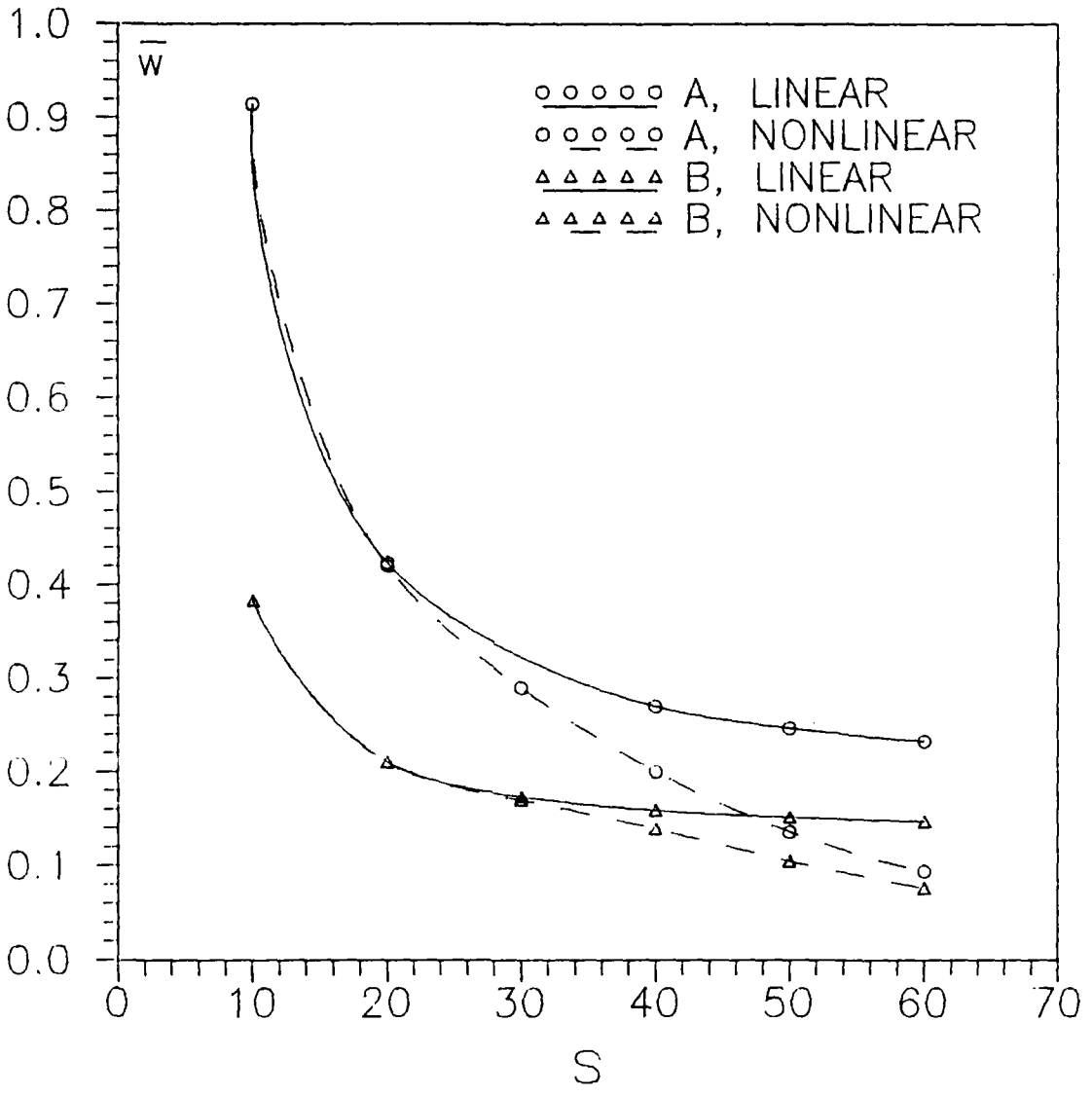

Figure A.23. $\bar{w}$ vs s for a clamped $[0_{12}/45_6/-45_6]_s$ plate with an aspect ratio of 2

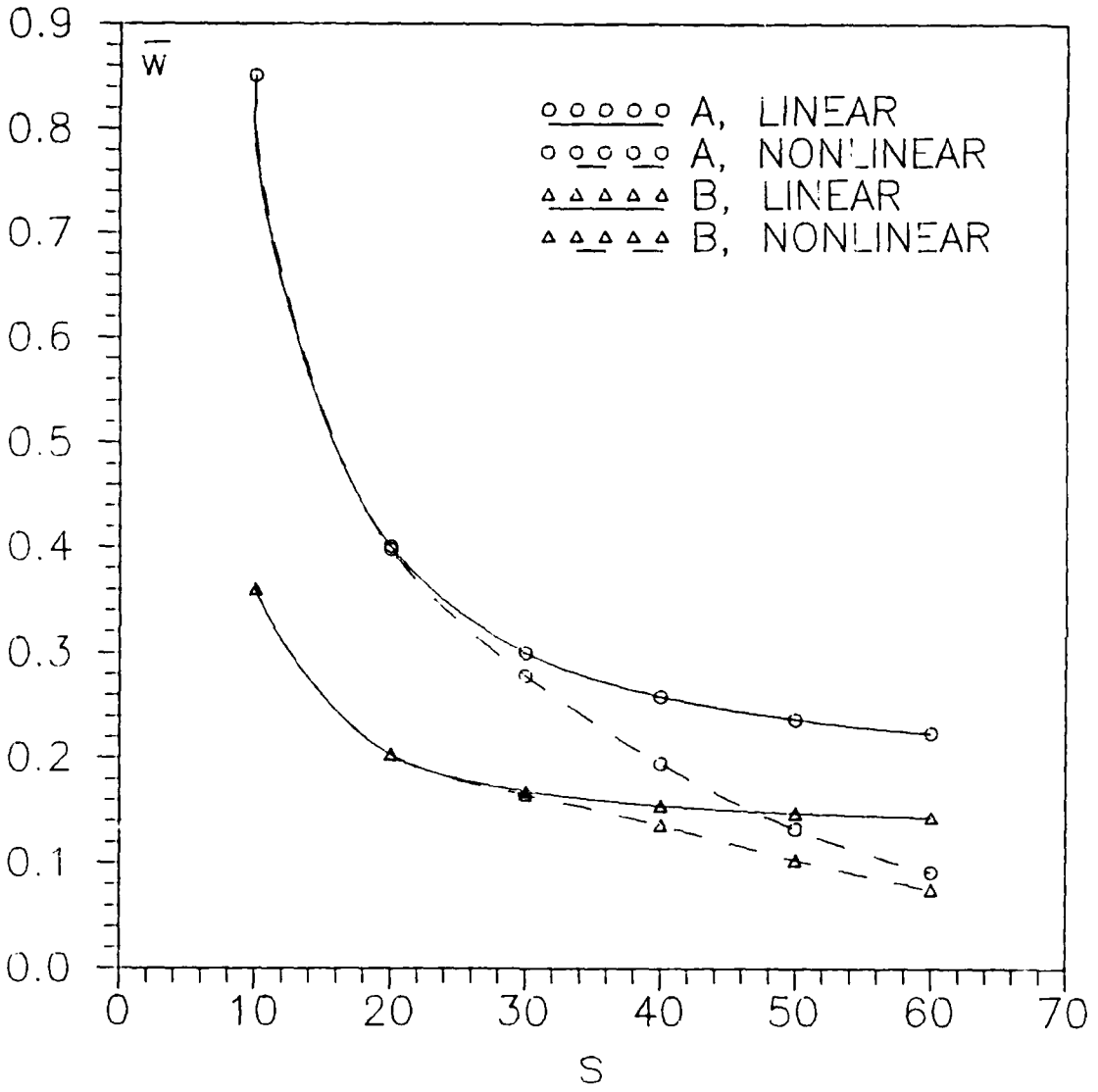

Figure A.24. $\bar{w}$ vs s for a clamped $[0_{12}/45_4/-45_4/90_4]_s$ plate with an aspect ratio of 2

Appendix B

Nondimensionalized Load-Displacement Curves

This appendix presents a complete set of curves of nondimesionalized displacement, $\bar{w}$, versus nondimensionalized load, $\bar{q}$, for all ply layups and aspect ratios. Nonlinear solutions for both materials are presented on each graph for thickness ratios of 10, 30, and 60. The displacement and load are nondimensionalized according to Eqn (B.1):

$$\bar{w} = \frac{w_c h^3 E_1}{q_o a^4} \times 10 \qquad \bar{q} = \frac{q_o}{E_1} \times 10^6 \qquad \text{(B.1)}$$

where

w_c = center displacement
h = plate thickness
E_1 = Young's modulus in fiber direction
q_o = total load on plate
a = characteristic inplane dimension

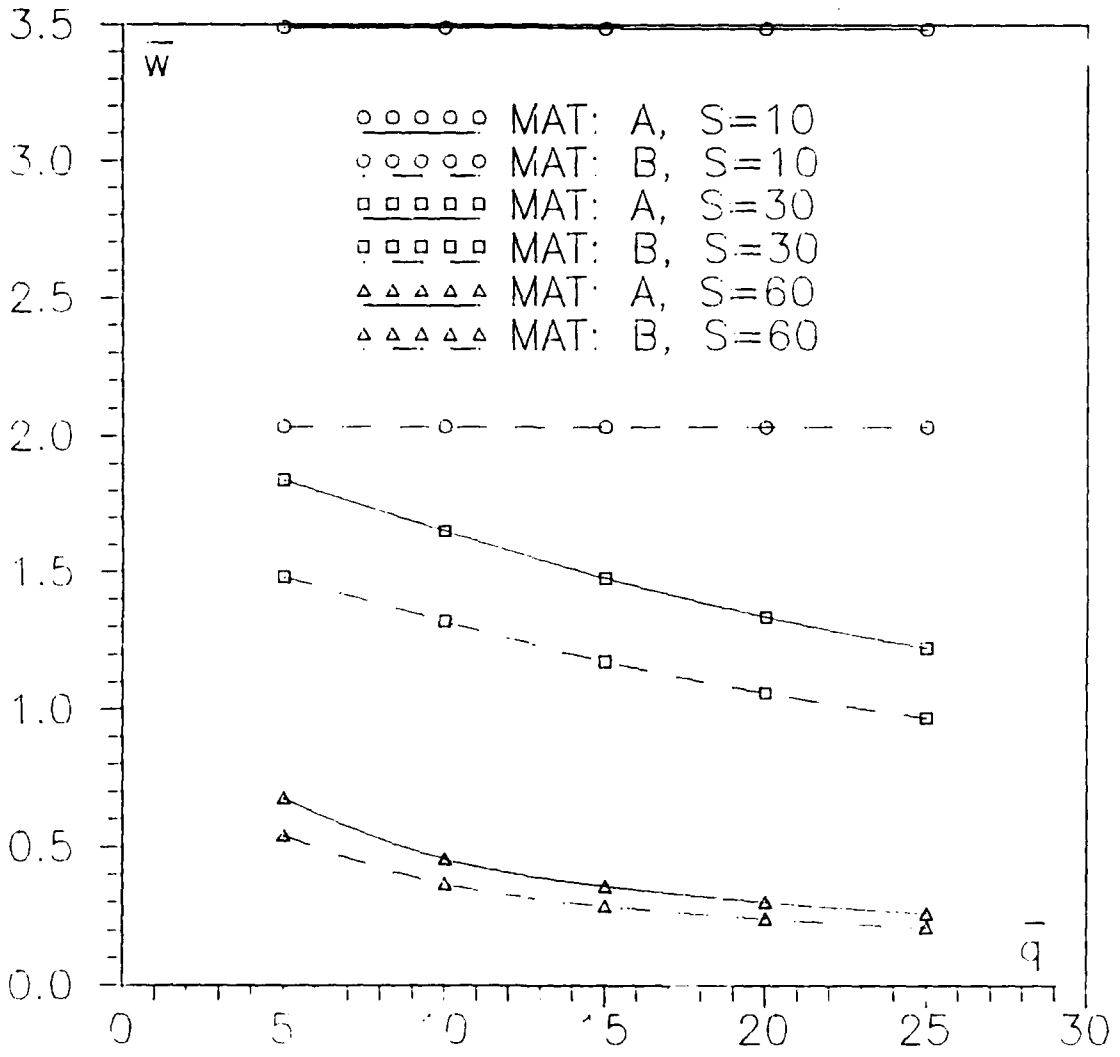

Figure B.1. $\bar{w}$ vs $\bar{q}$ for a simply supported $[0_{16}/90_8]_s$ plate with an aspect ratio of 1

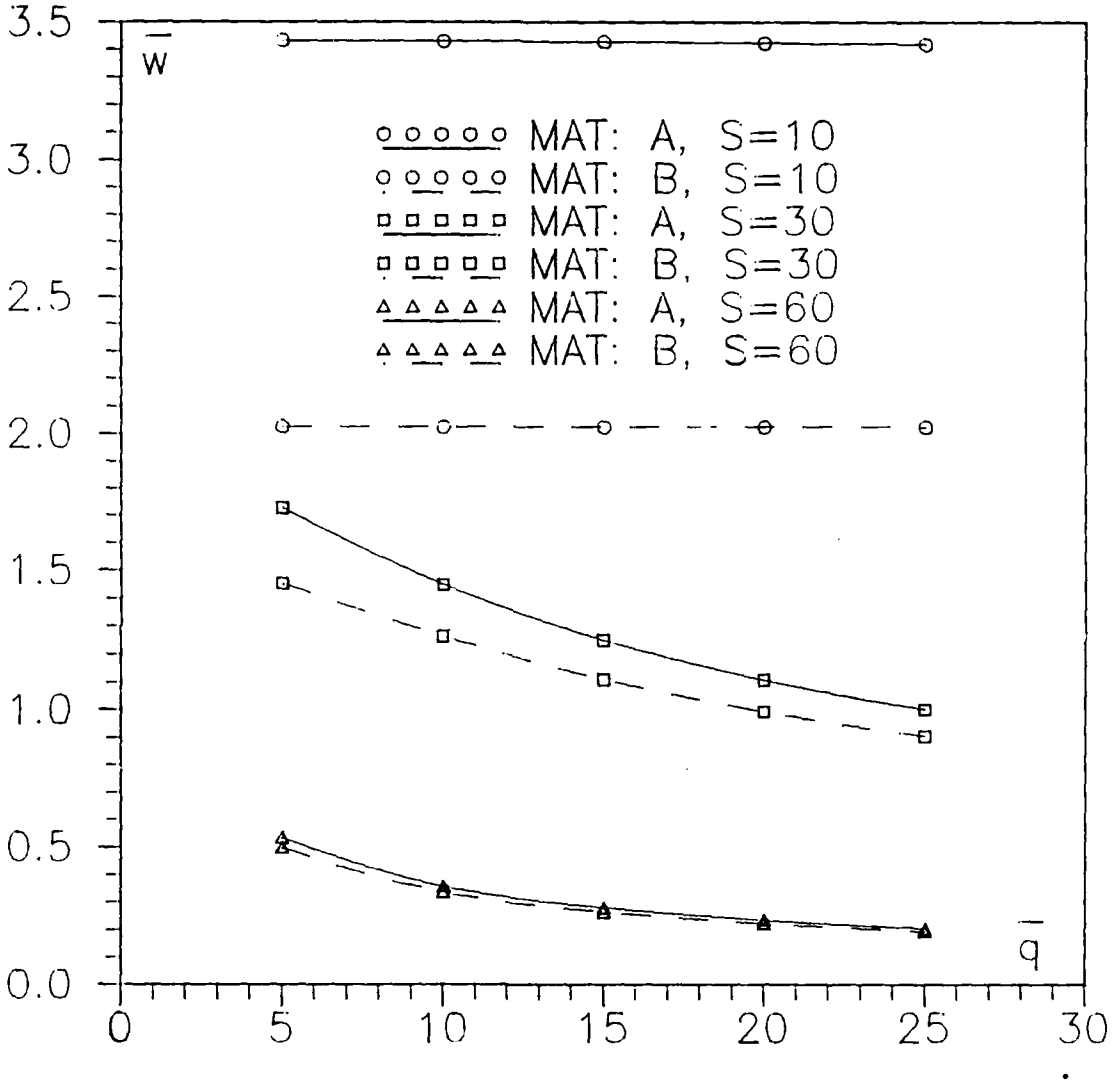

Figure B.2. $\bar{w}$ vs $\bar{q}$ for a simply supported $[0_{12}/60_6/-60_6]_s$ plate with an aspect ratio of 1

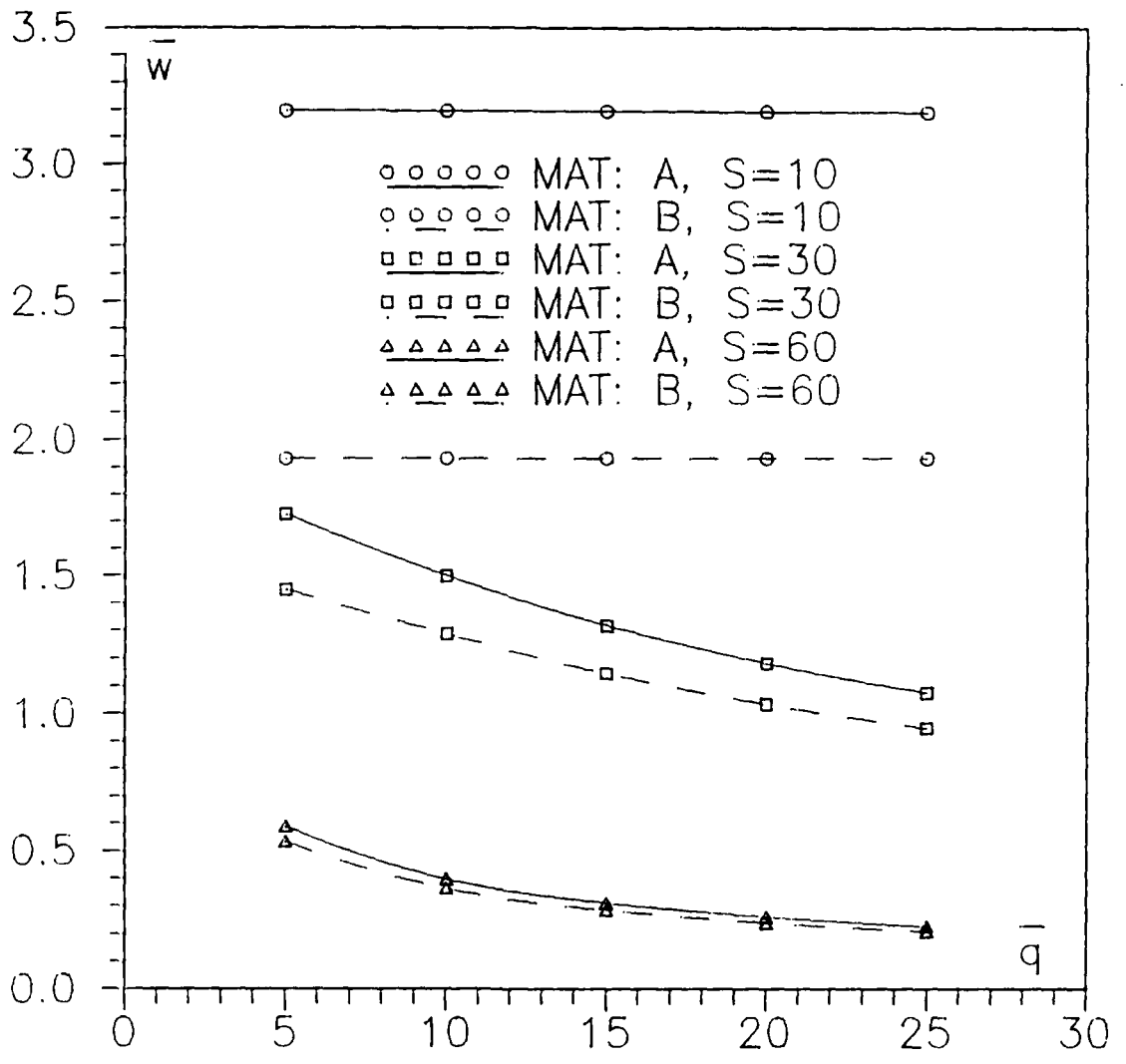

Figure B.3. $\bar{w}$ vs $\bar{q}$ for a simply supported $[0_{12}/45_6/-45_6]_s$ plate with an aspect ratio of 1

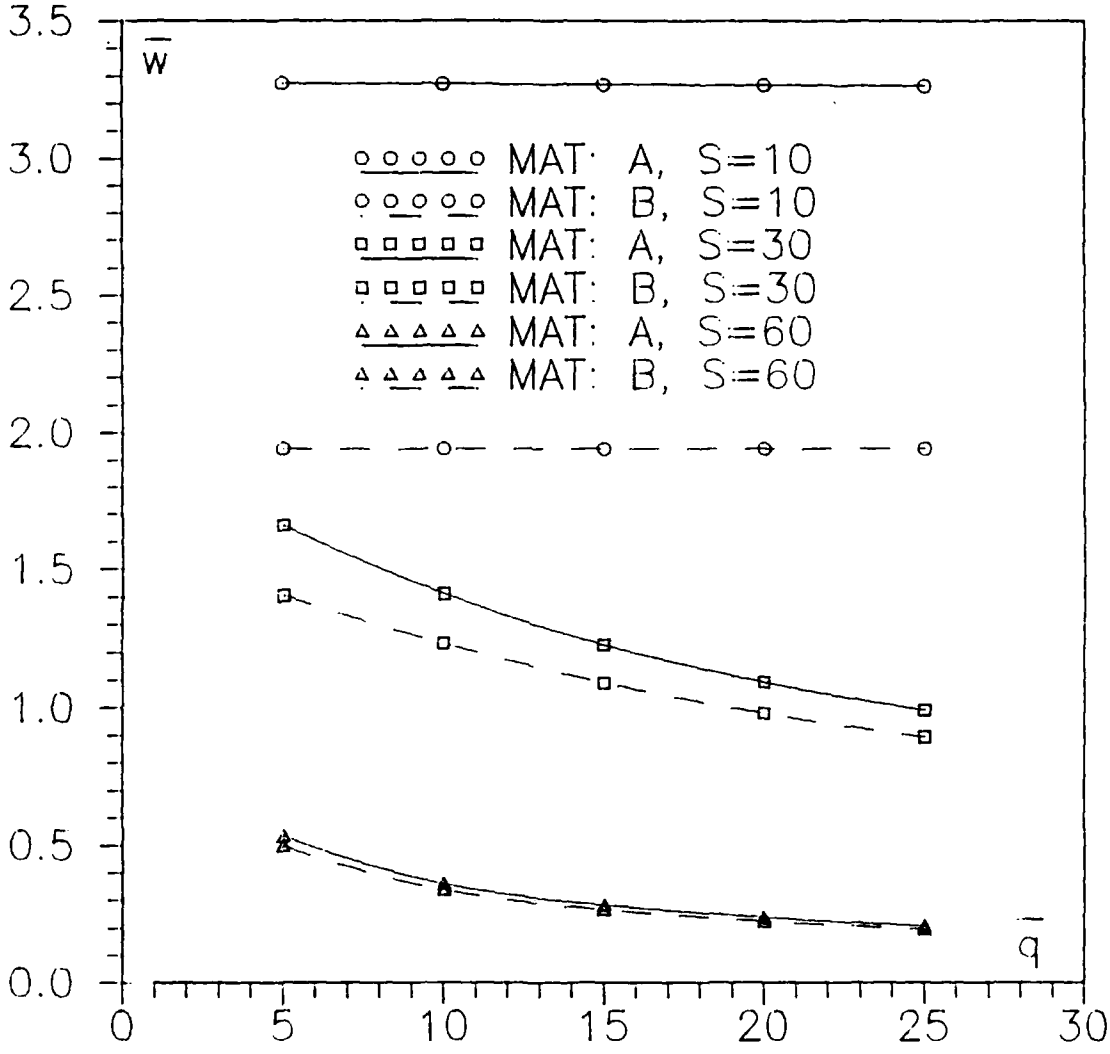

Figure B.4. $\bar{w}$ vs $\bar{q}$ for a simply supported $[0_{12}/45_4/-45_4/90_4]_s$ plate with an aspect ratio of 1

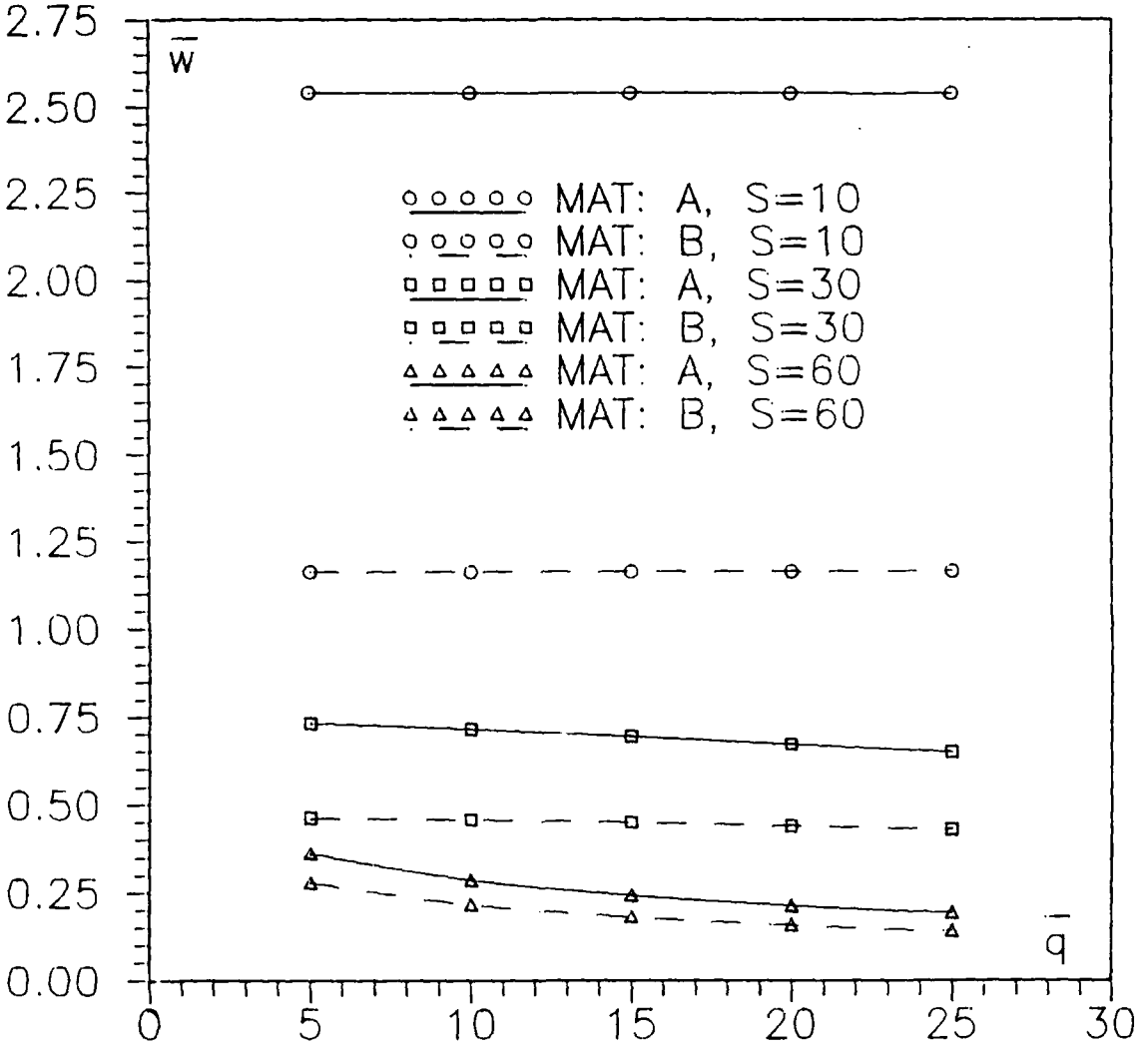

Figure B.5. $\bar{w}$ vs $\bar{q}$ for a clamped $[0_{16}/90_8]_s$ plate with an aspect ratio of 1

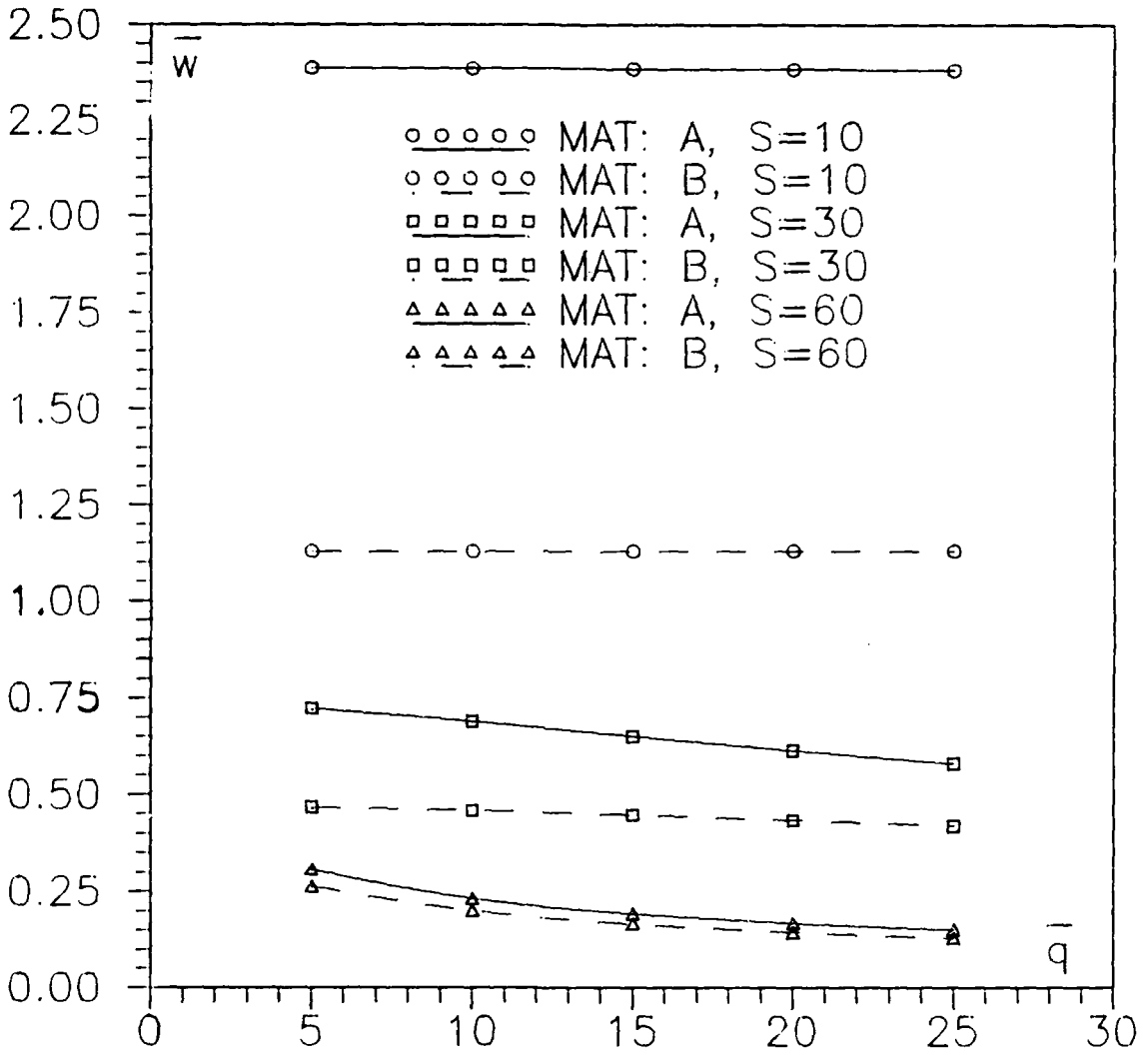

Figure B.6. $\bar{w}$ vs $\bar{q}$ for a clamped $[0_{12}/60_6/-60_6]_s$ plate with an aspect ratio of 1

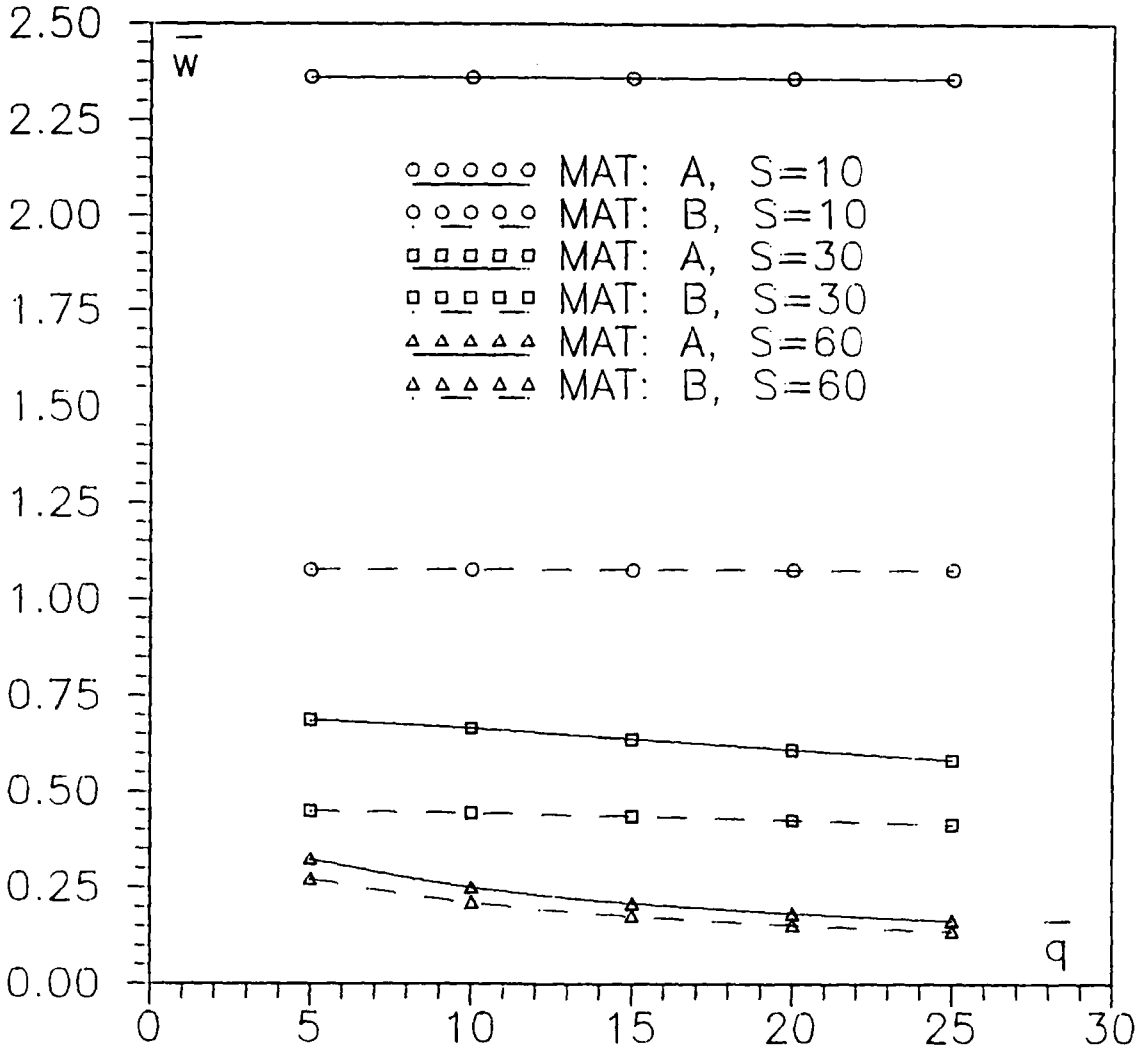

Figure B.7. $\bar{w}$ vs $\bar{q}$ for a clamped $[0_{12}/45_6/-45_6]_s$ plate with an aspect ratio of 1

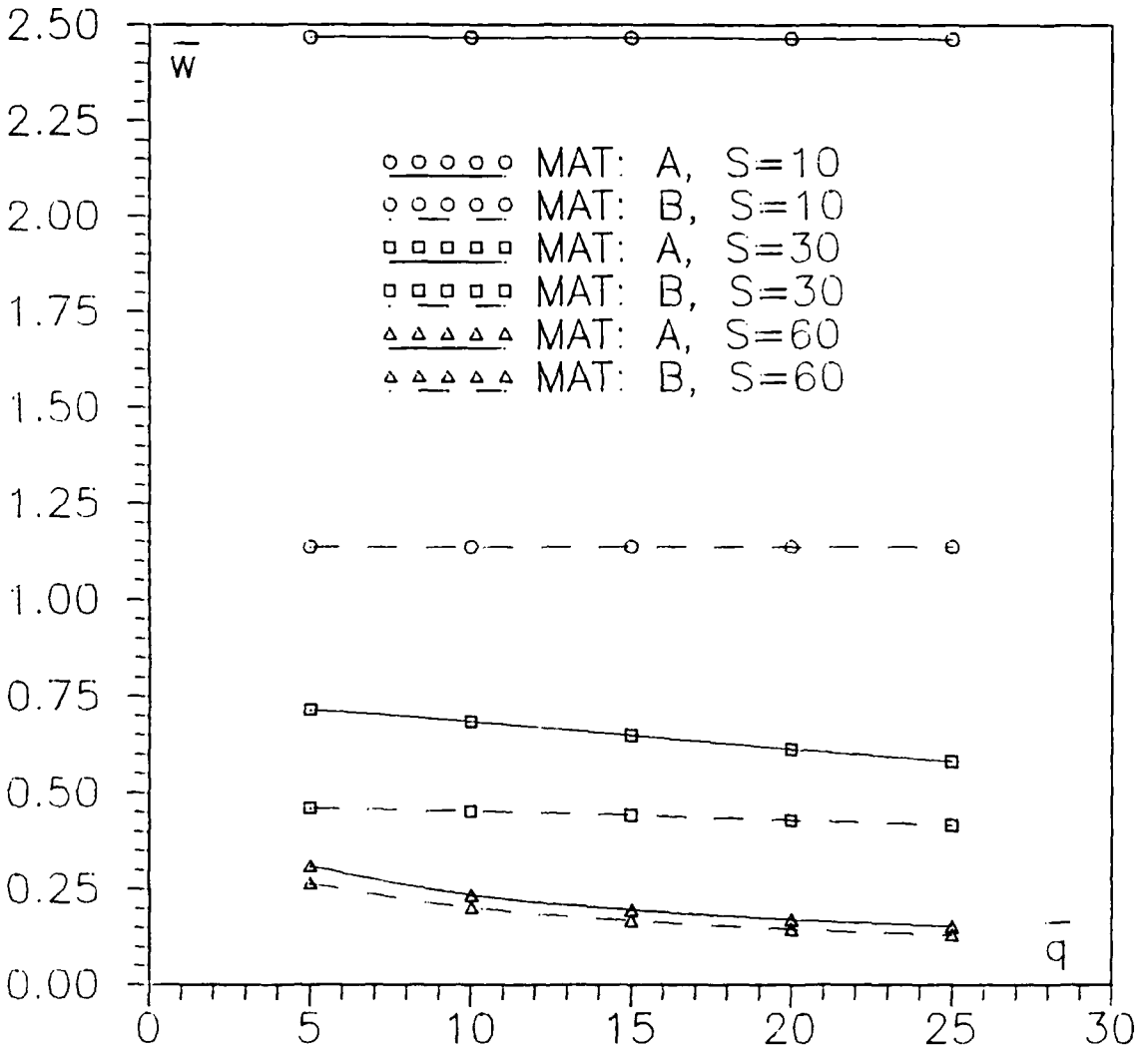

Figure B.8. $\bar{w}$ vs $\bar{q}$ for a clamped $[0_{12}/45_4/-45_4/90_4]_s$ plate with an aspect ratio of 1

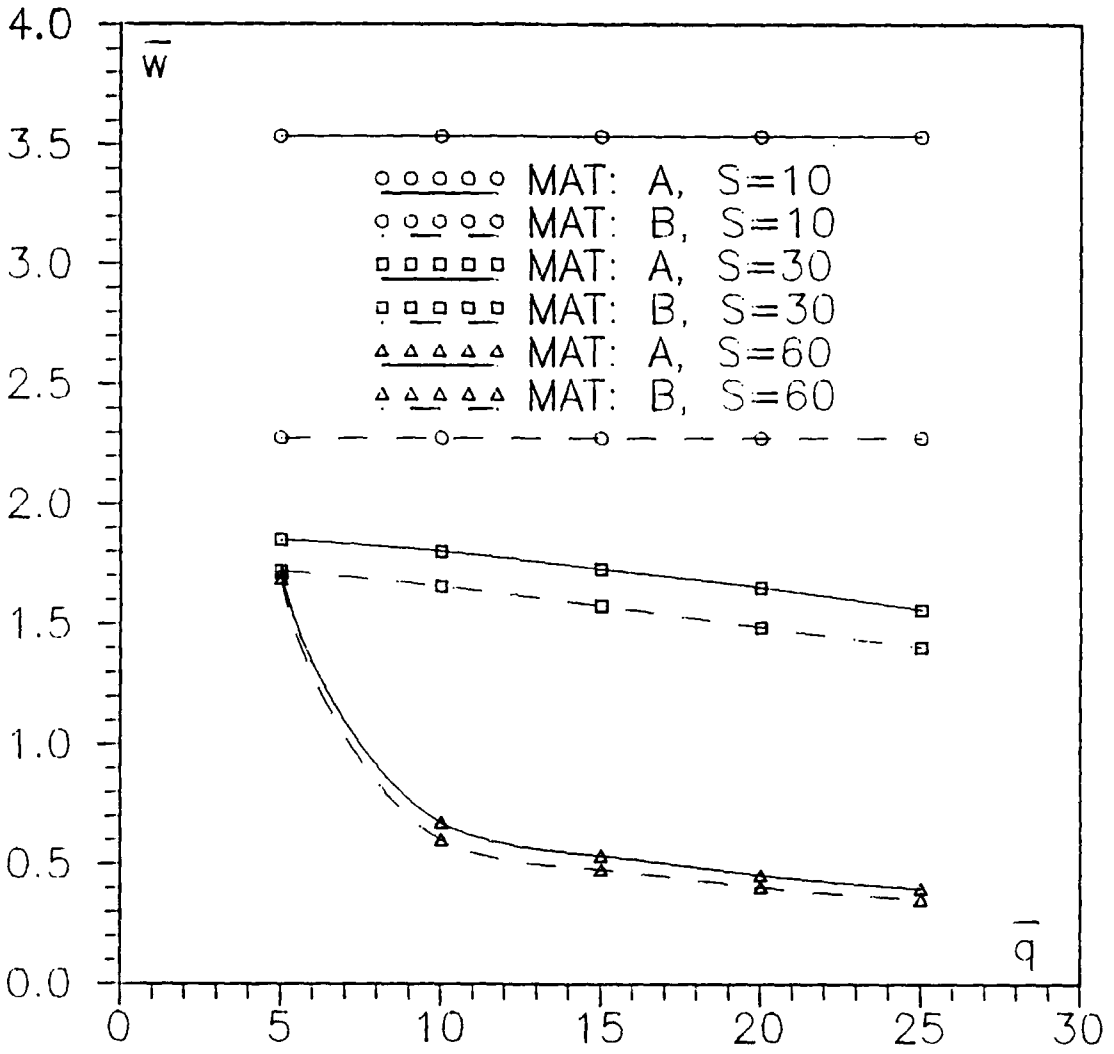

Figure B.9. $\bar{w}$ vs $\bar{q}$ for a simply supported $[0_{16}/90_8]_s$ plate with an aspect ratio of 1/2

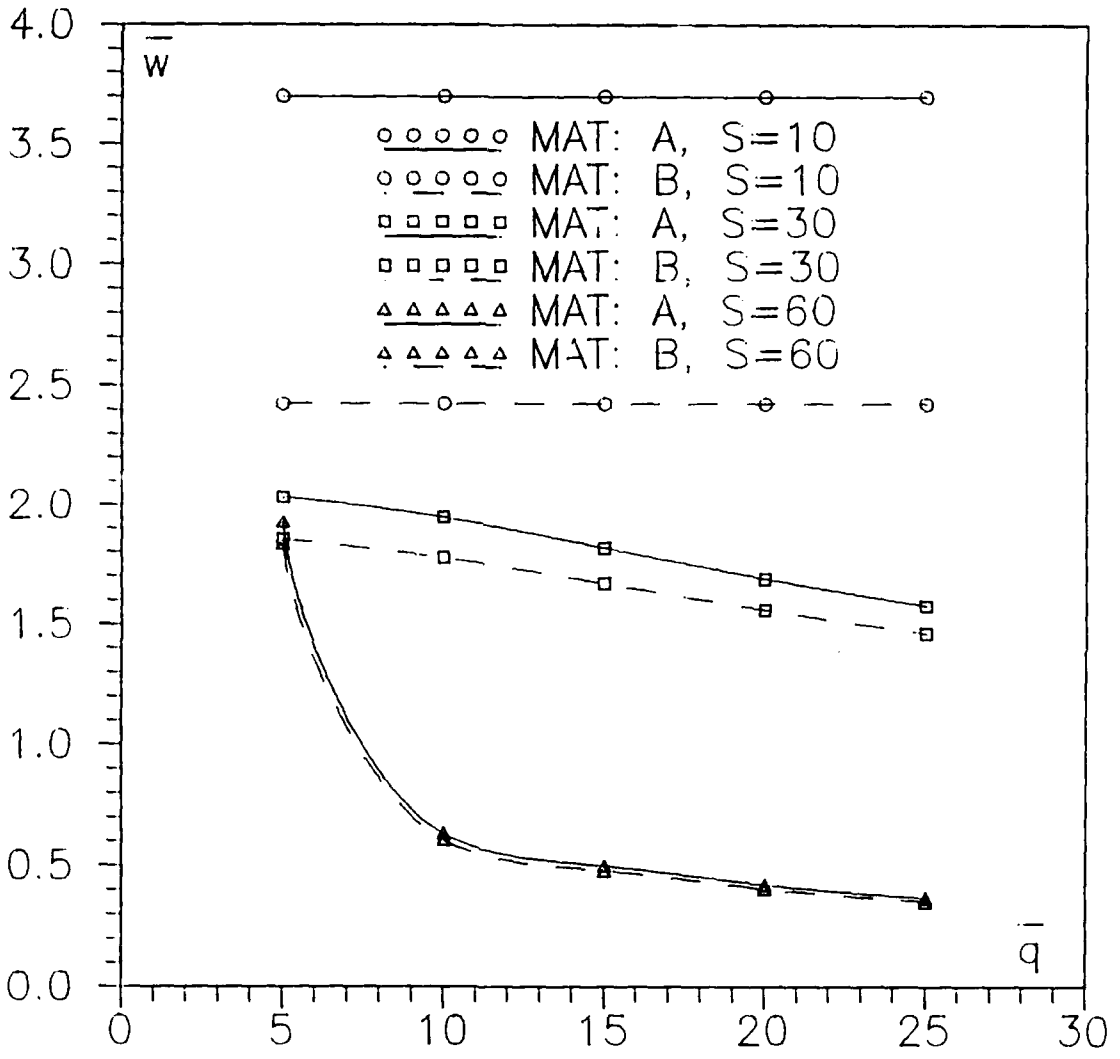

Figure B.10. $\bar{w}$ vs $\bar{q}$ for a simply supported $[0_{12}/60_6/-60_6]_s$ plate with an aspect ratio of 1/2

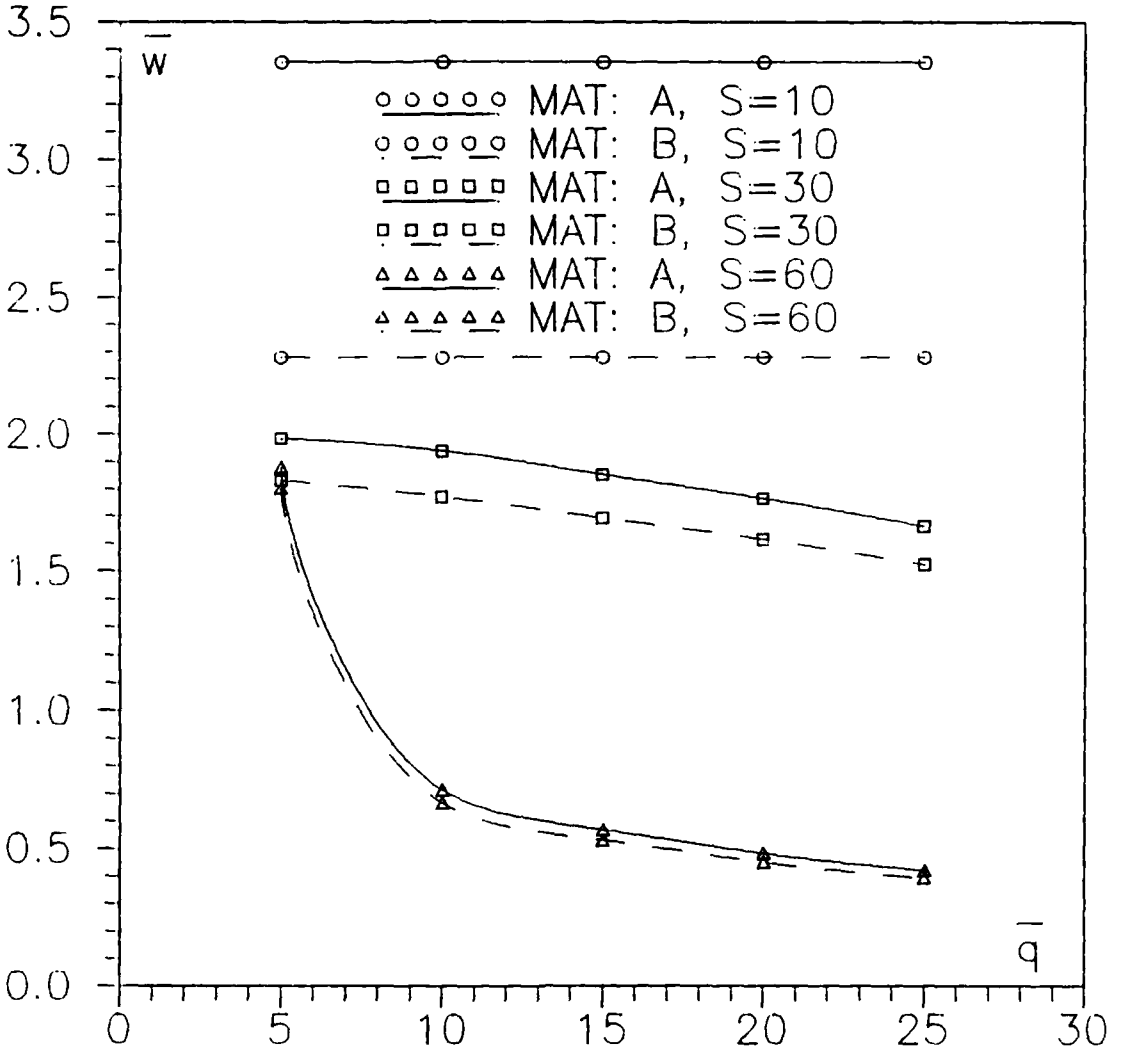

Figure B.11. $\bar{w}$ vs $\bar{q}$ for a simply supported $[0_{12}/45_6/-45_6]_s$ plate with an aspect ratio of 1/2

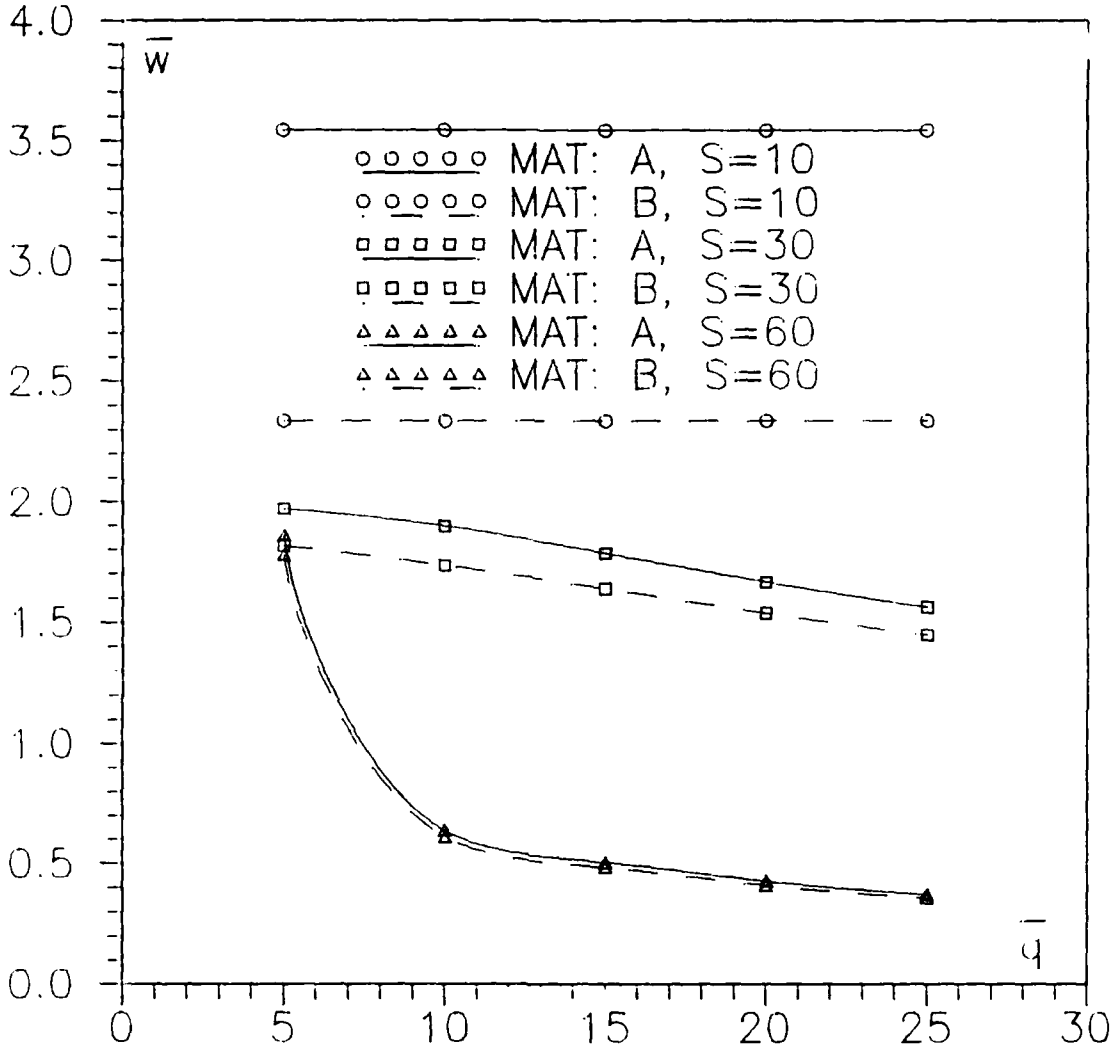

Figure B.12. $\bar{w}$ vs $\bar{q}$ for a simply supported $[0_{12}/45_4/-45_4/90_4]_s$ plate with an aspect ratio of 1/2

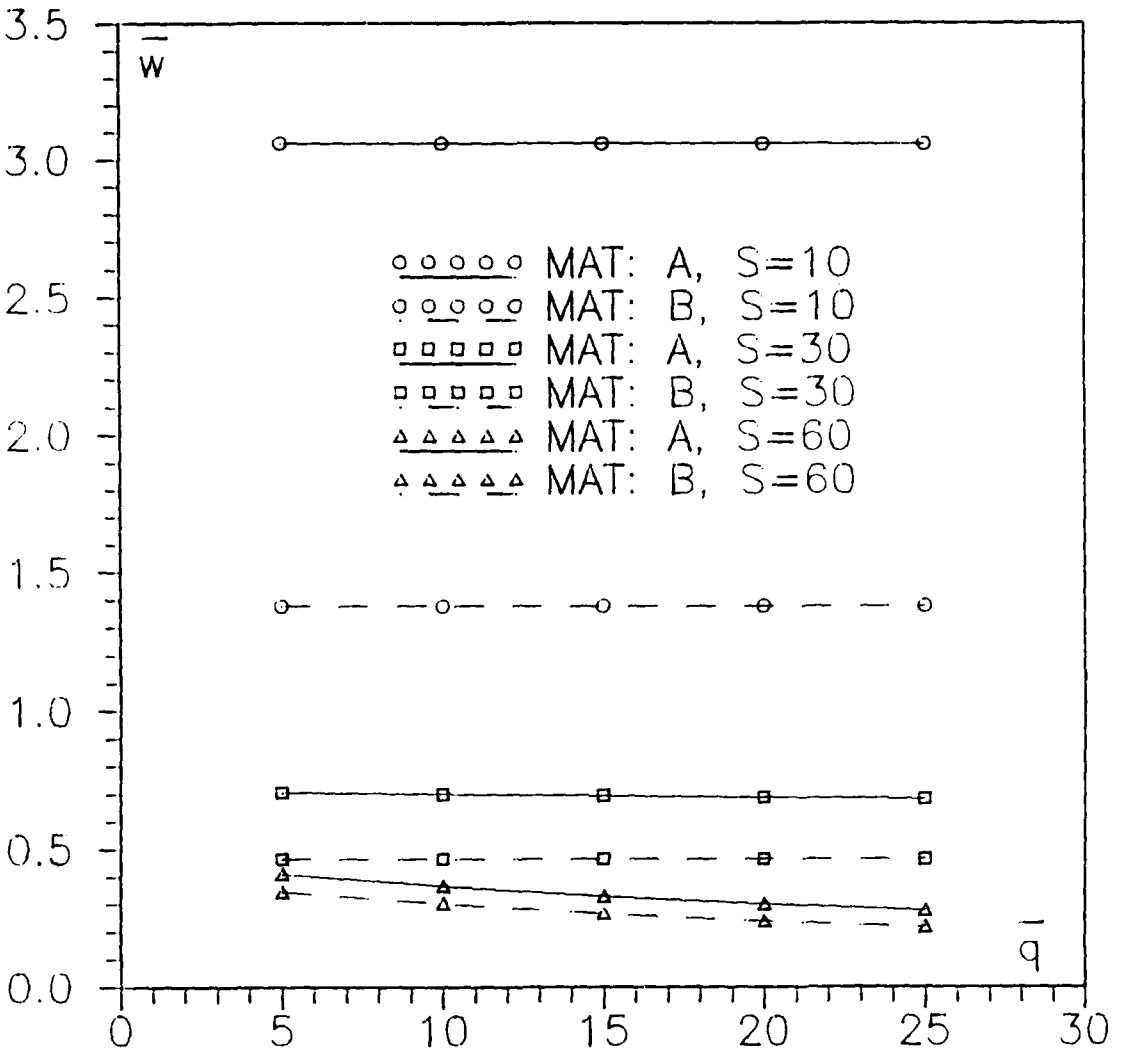

Figure B.13. $\bar{w}$ vs $\bar{q}$ for a clamped $[0_{16}/90_8]_s$ plate with an aspect ratio of 1/2

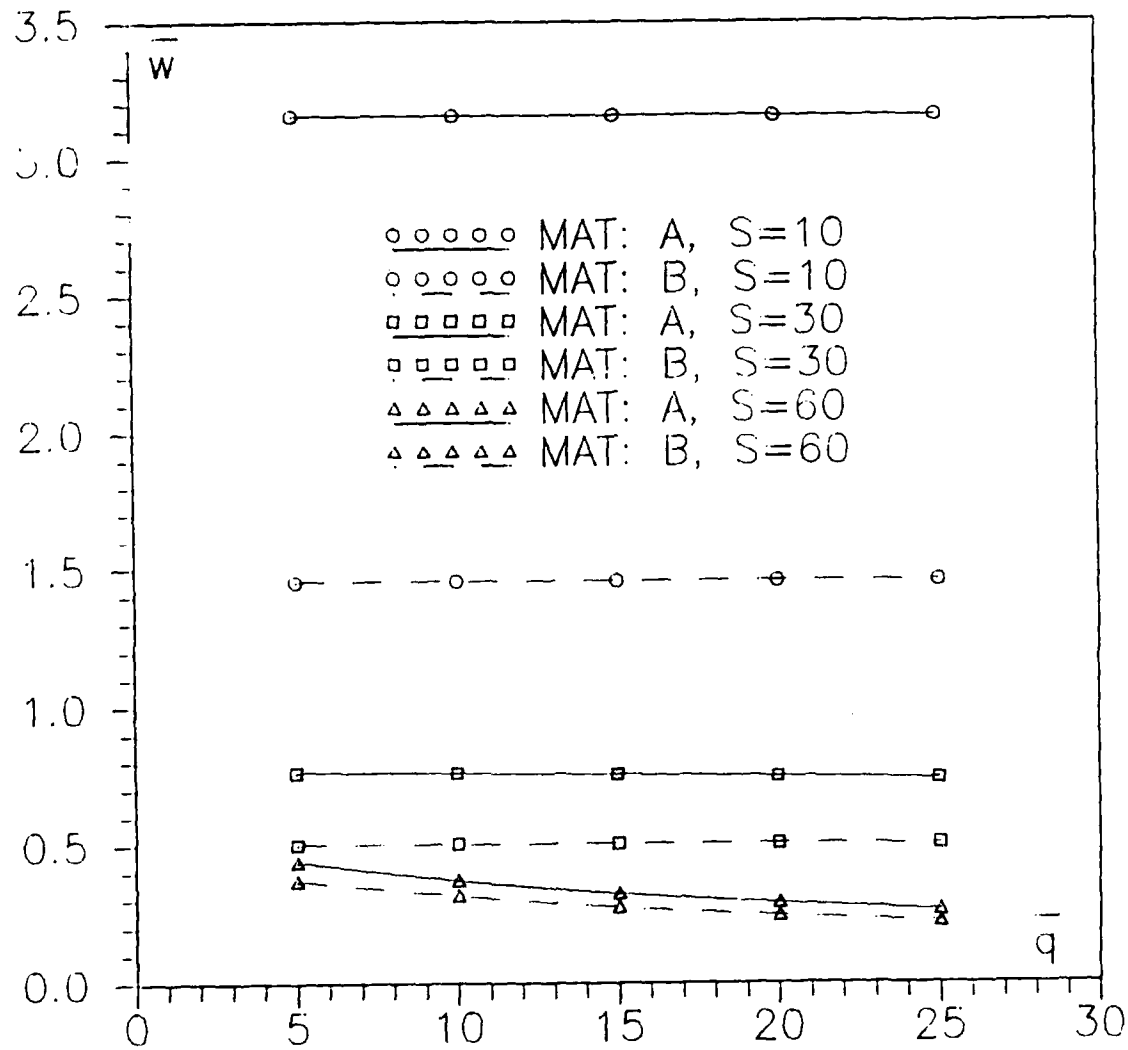

Figure B.14. $\bar{w}$ vs $\bar{q}$ for a clamped $[0_{12}/60_6/-60_6]_s$ plate with an aspect ratio of 1/2

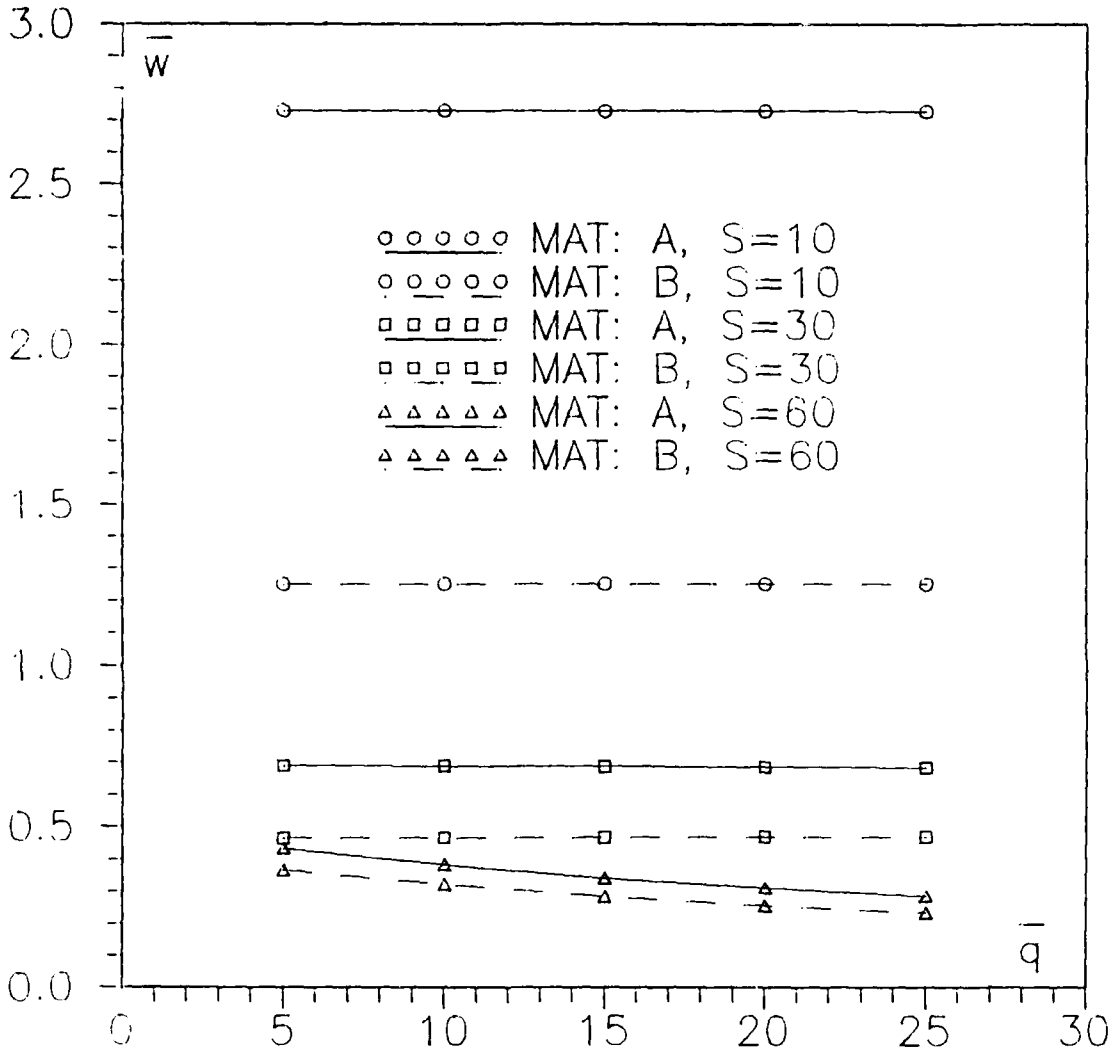

Figure B.15. $\bar{w}$ vs $\bar{q}$ for a clamped $[0_{12}/45_6/-45_6]_s$ plate with an aspect ratio of 1/2

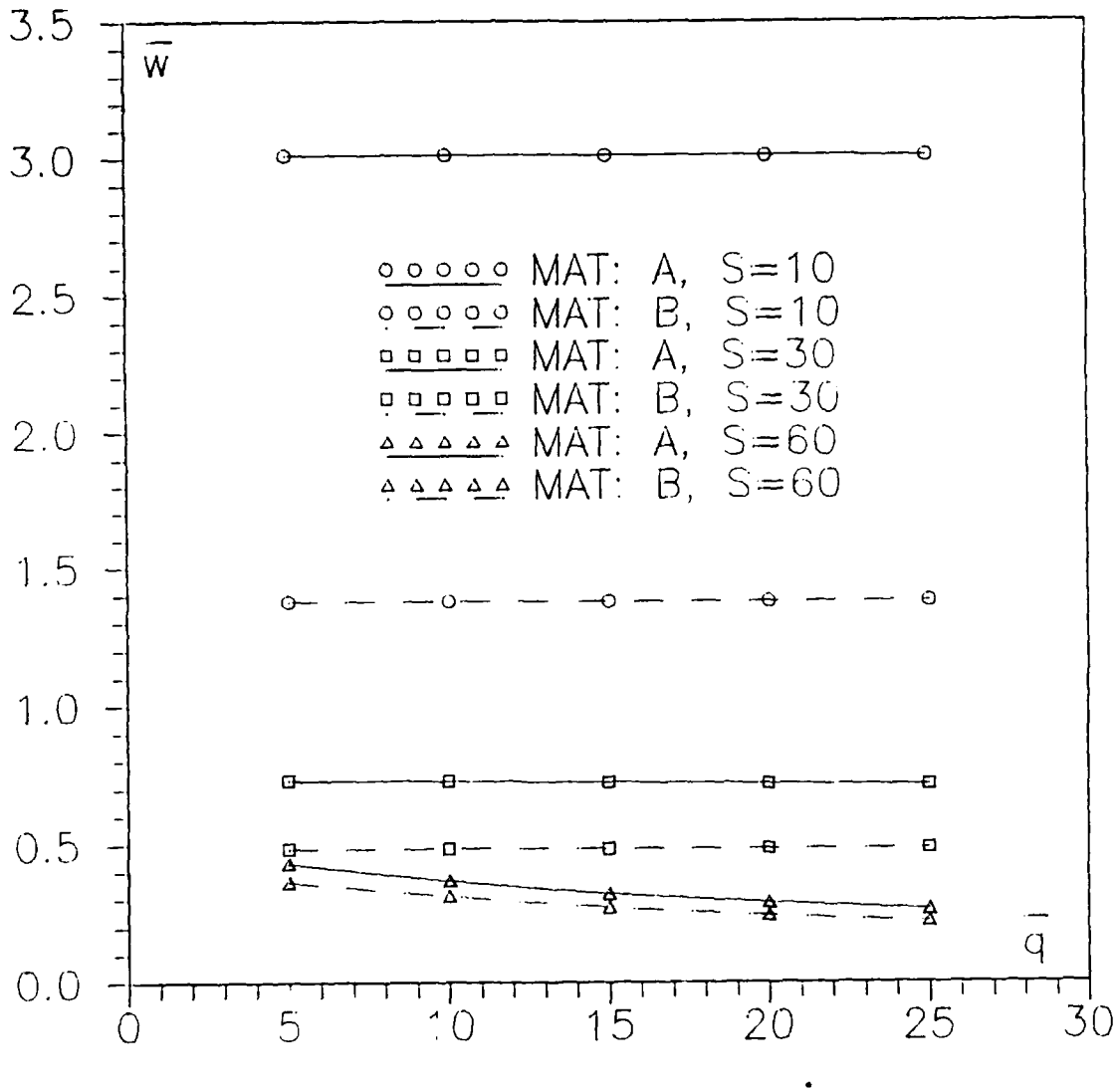

Figure B.16. $\bar{w}$ vs $\bar{q}$ for a clamped $[0_{12}/45_4/-45_4/90_4]_s$ plate with an aspect ratio of 1/2

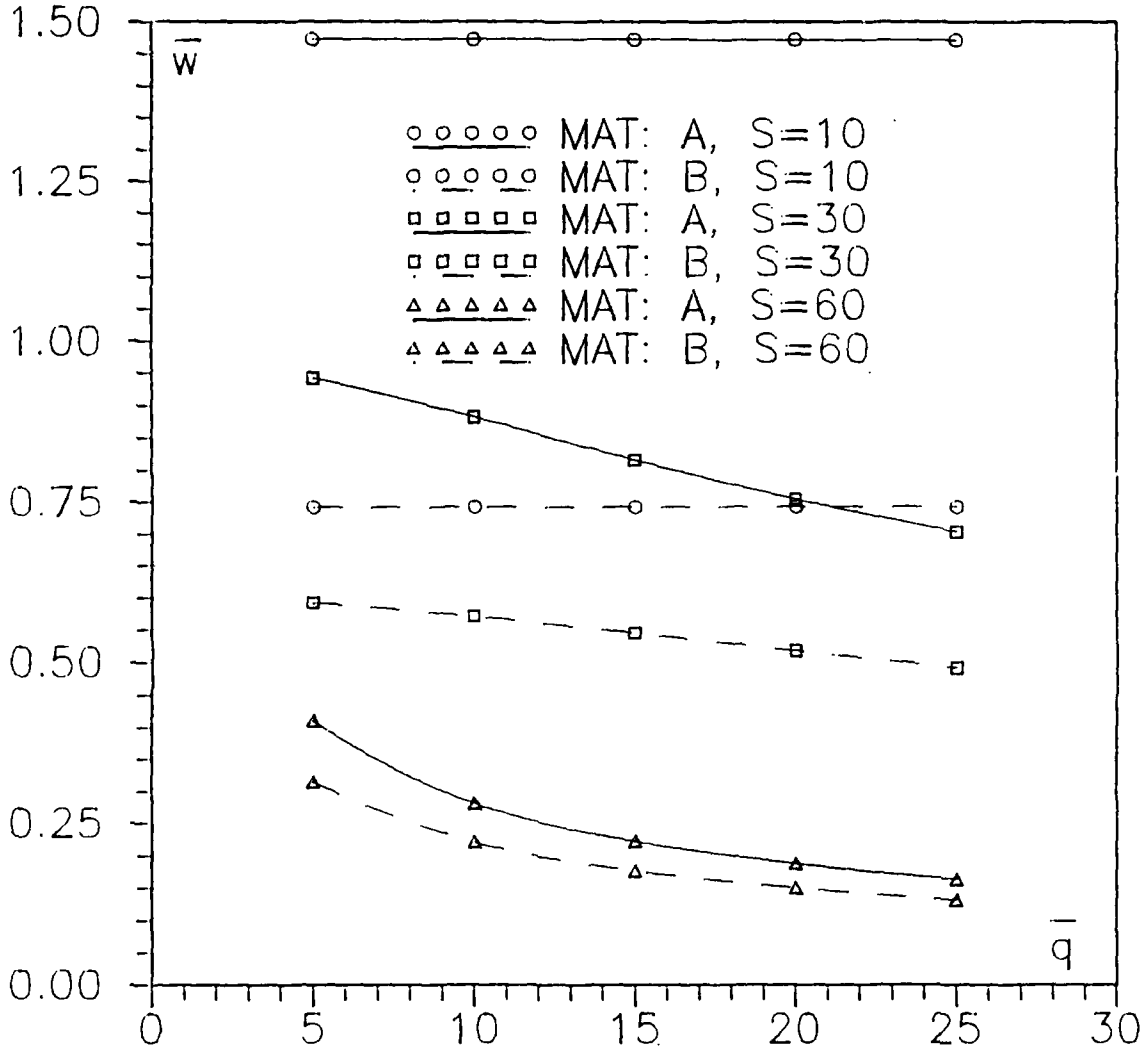

Figure B.17. $\bar{w}$ vs $\bar{q}$ for a simply supported $[0_{16}/90_8]_s$ plate with an aspect ratio of 2

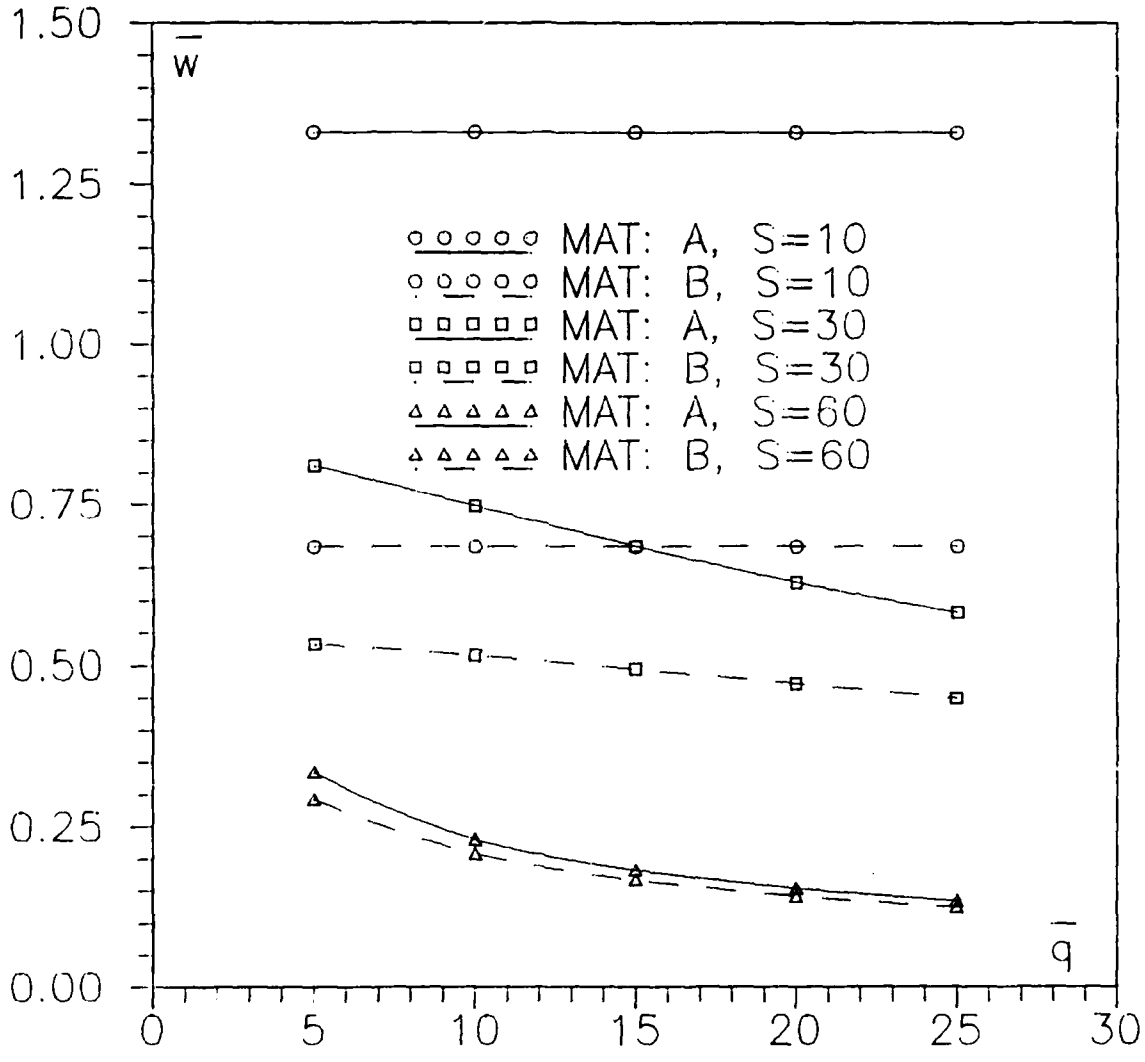

Figure B.18. $\bar{w}$ vs $\bar{q}$ for a simply supported $[0_{12}/60_6/-60_6]_s$ plate with an aspect ratio of 2

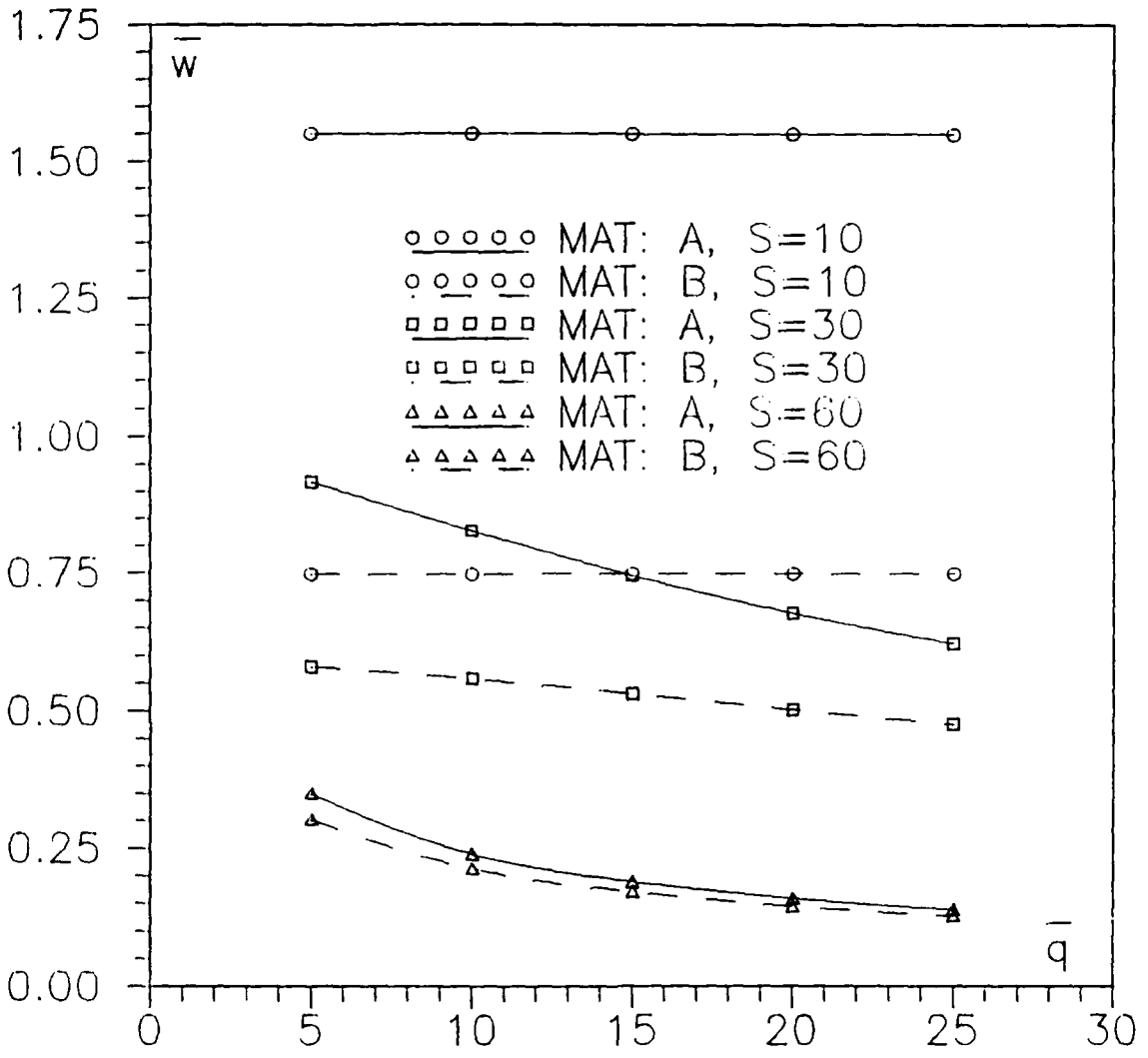

Figure B.19. $\bar{w}$ vs $\bar{q}$ for a simply supported $[0_{12}/45_6/-45_6]_s$ plate with an aspect ratio of 2

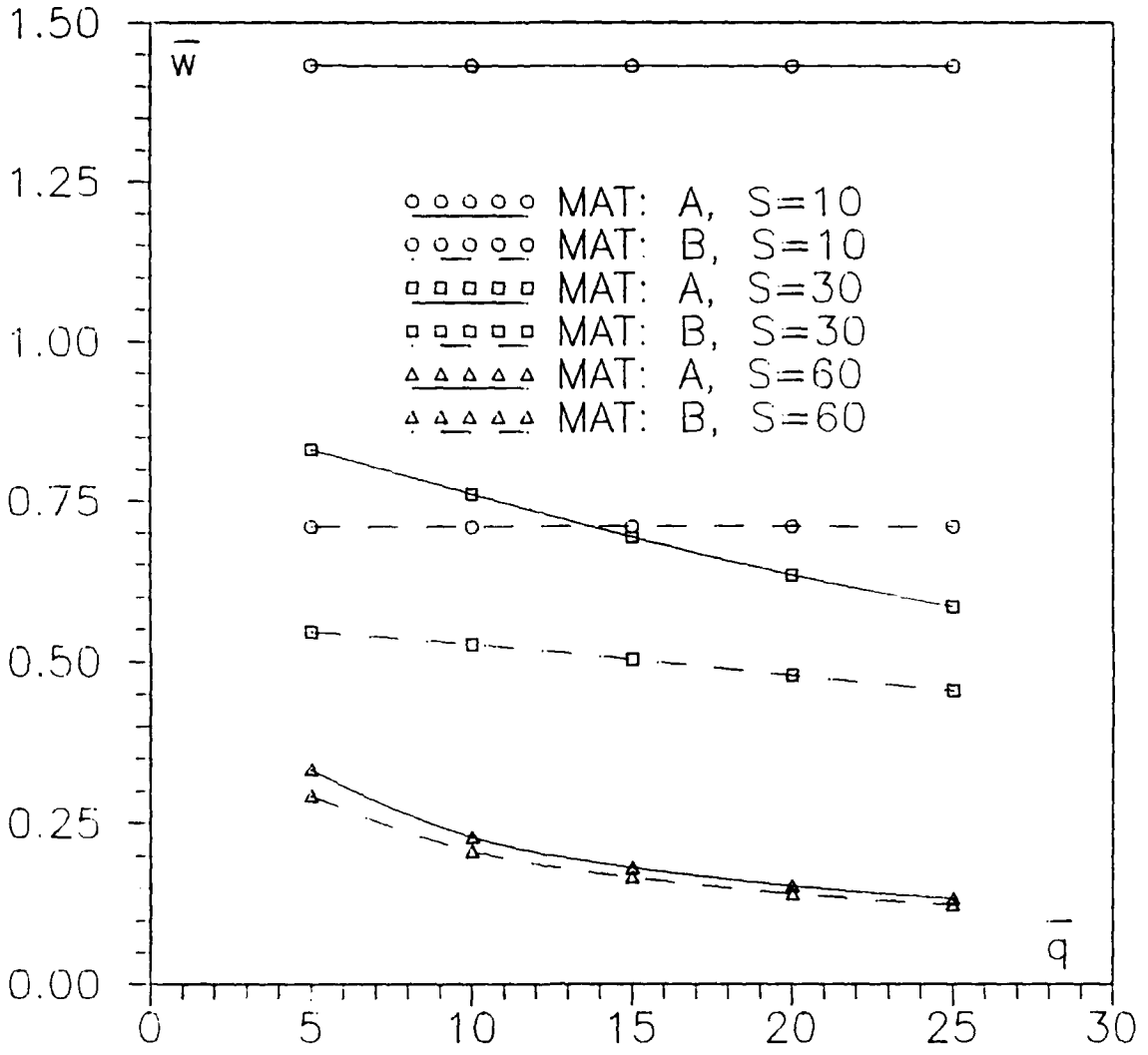

Figure B.20. $\bar{w}$ vs $\bar{q}$ for a simply supported $[0_{12}/45_4/-45_4/90_4]_s$ plate with an aspect ratio of 2

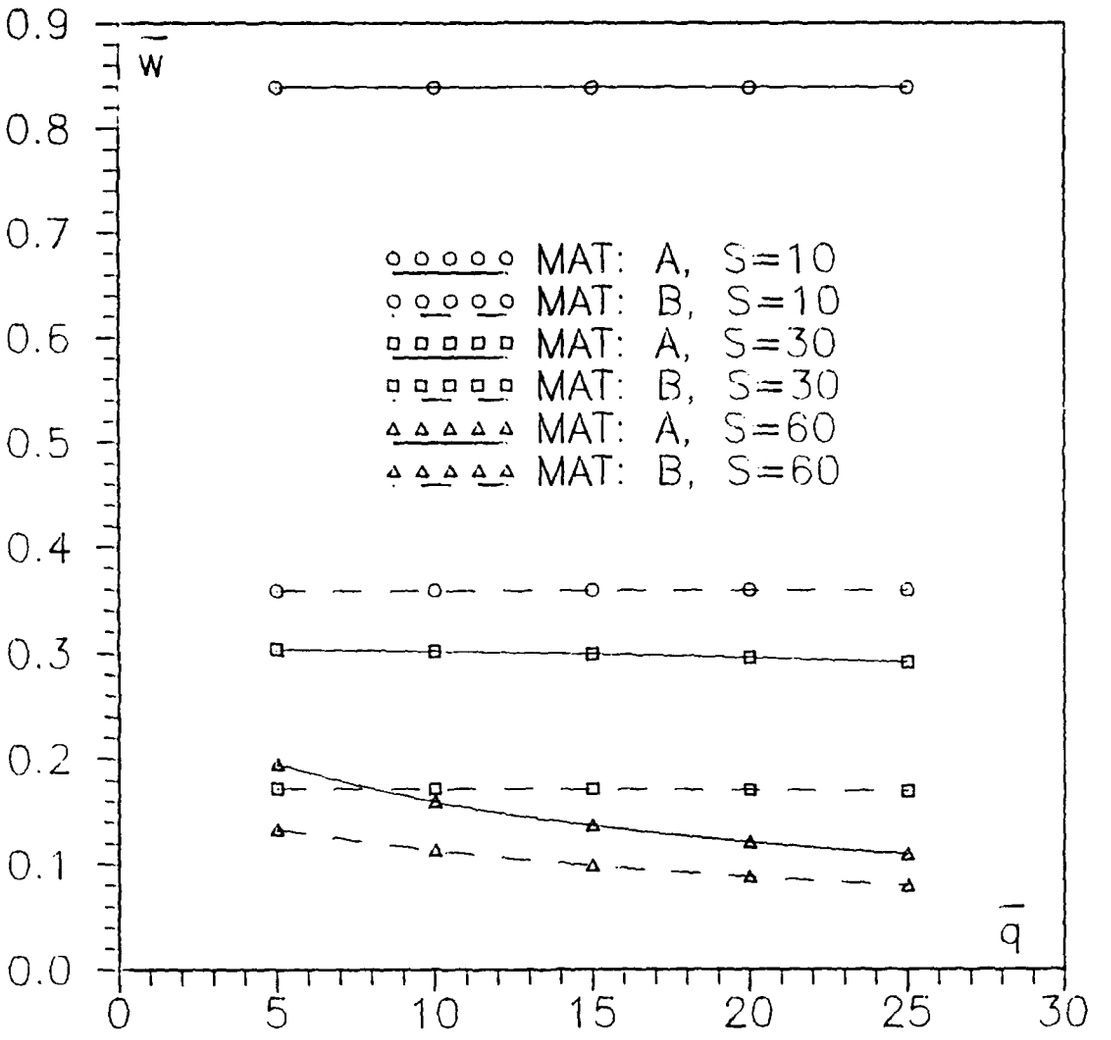

Figure B.21. $\bar{w}$ vs $\bar{q}$ for a clamped $[0_{16}/90_8]_s$ plate with an aspect ratio of 2

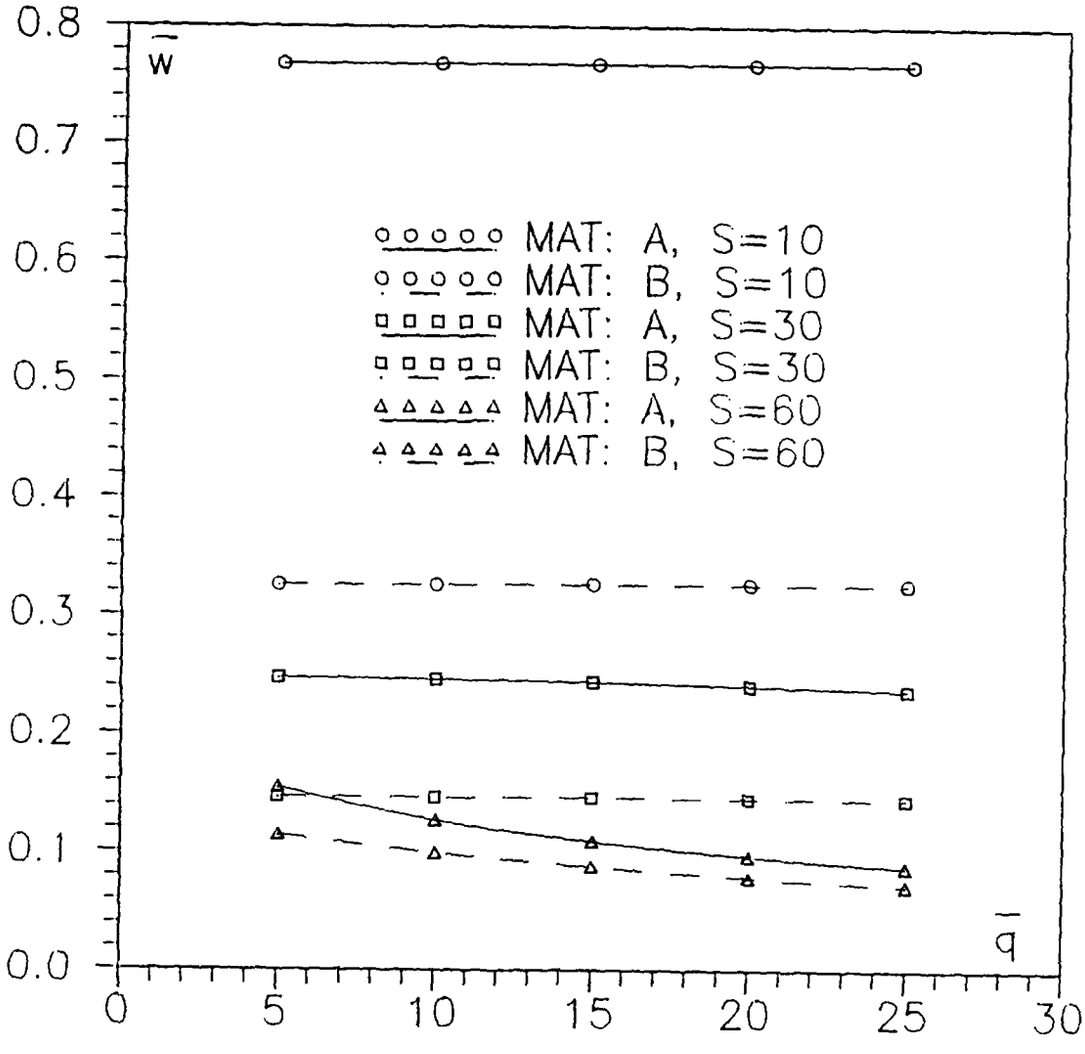

Figure B.22. $\bar{w}$ vs $\bar{q}$ for a clamped $[0_{12}/60_6/-60_6]_s$ plate with an aspect ratio of 2

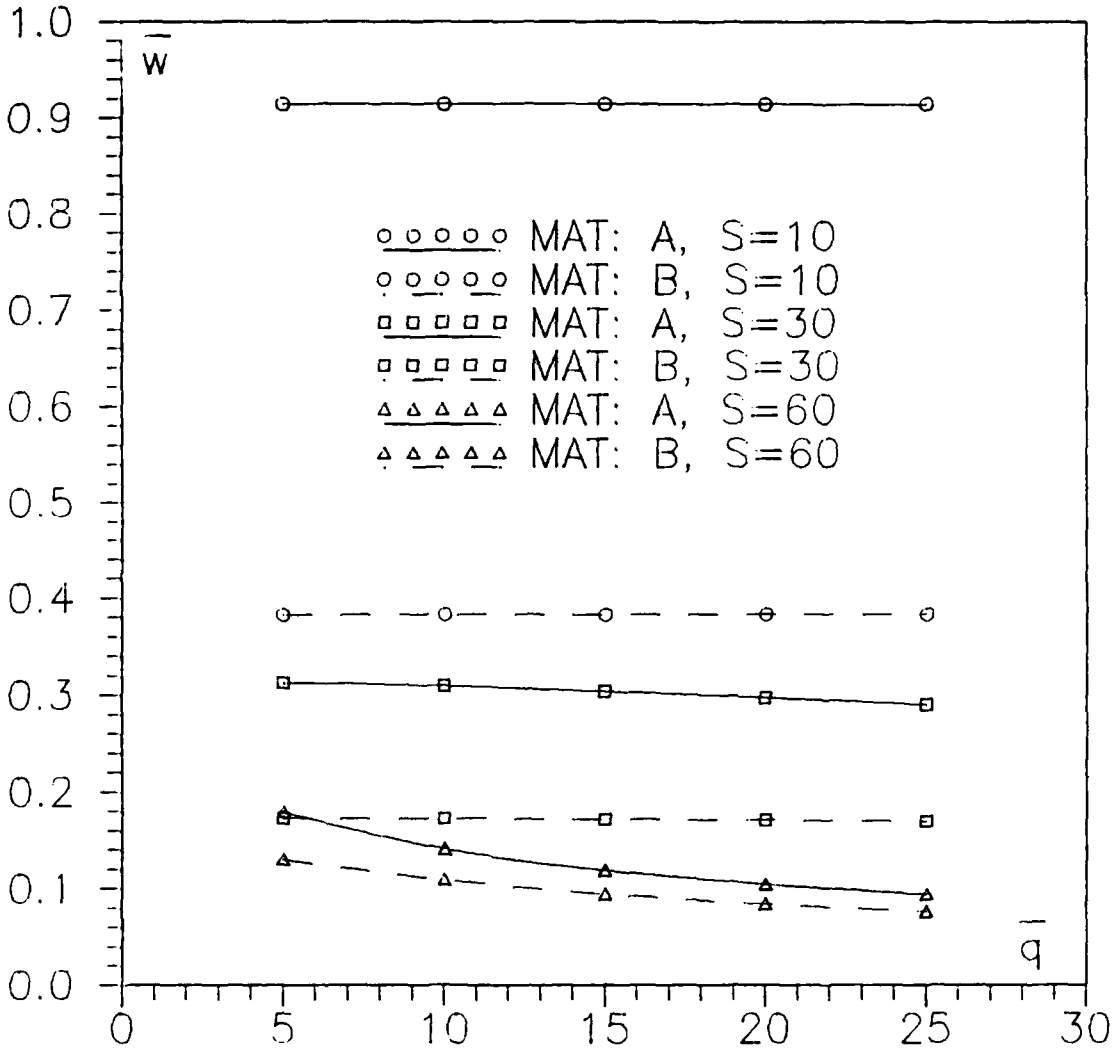

Figure B.23. $\bar{w}$ vs $\bar{q}$ for a clamped $[0_{12}/45_6/-45_6]_s$ plate with an aspect ratio of 2

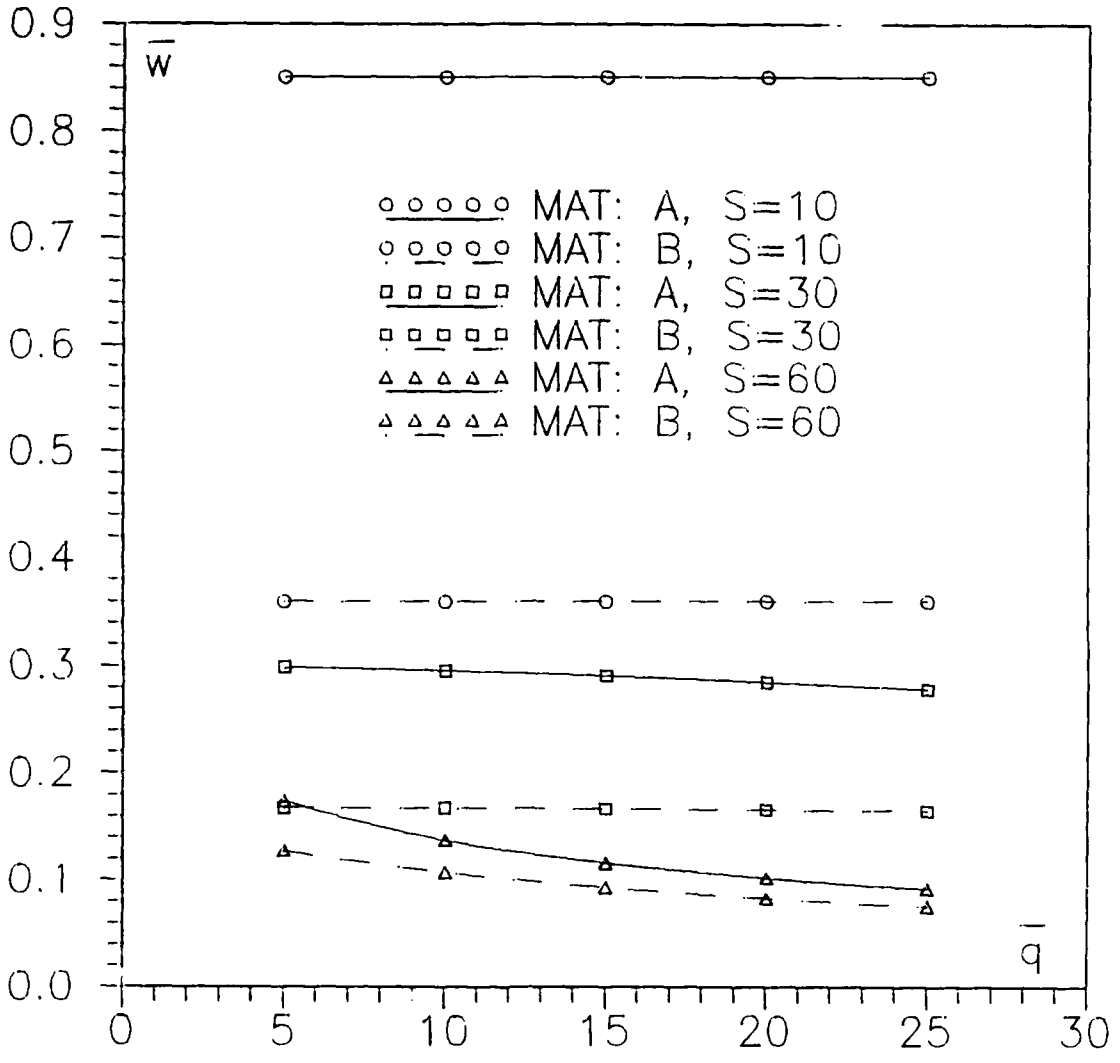

Figure B.24. $\bar{w}$ vs $\bar{q}$ for a clamped $[0_{12}/45_4/-45_4/90_4]_s$ plate with an aspect ratio of 2

Appendix C

Aspect Ratio Comparisons

This appendix presents a complete set of curves of nondimesionalized displacement, $\bar{w}$, versus thickness ratio, S, for all ply layups. Linear and nonlinear solutions for each aspect ratio are presented on each graph. The displacement is nondimensionalized according to Eqn (C.1):

$$\bar{w} = \frac{w_c h^3 E_1}{q_o a^4} \times 10 \qquad (C.1)$$

where

w_c = center displacement

h = plate thickness

E_1 = Young's modulus in fiber direction

q_o = total load on plate

a = characteristic inplane dimension

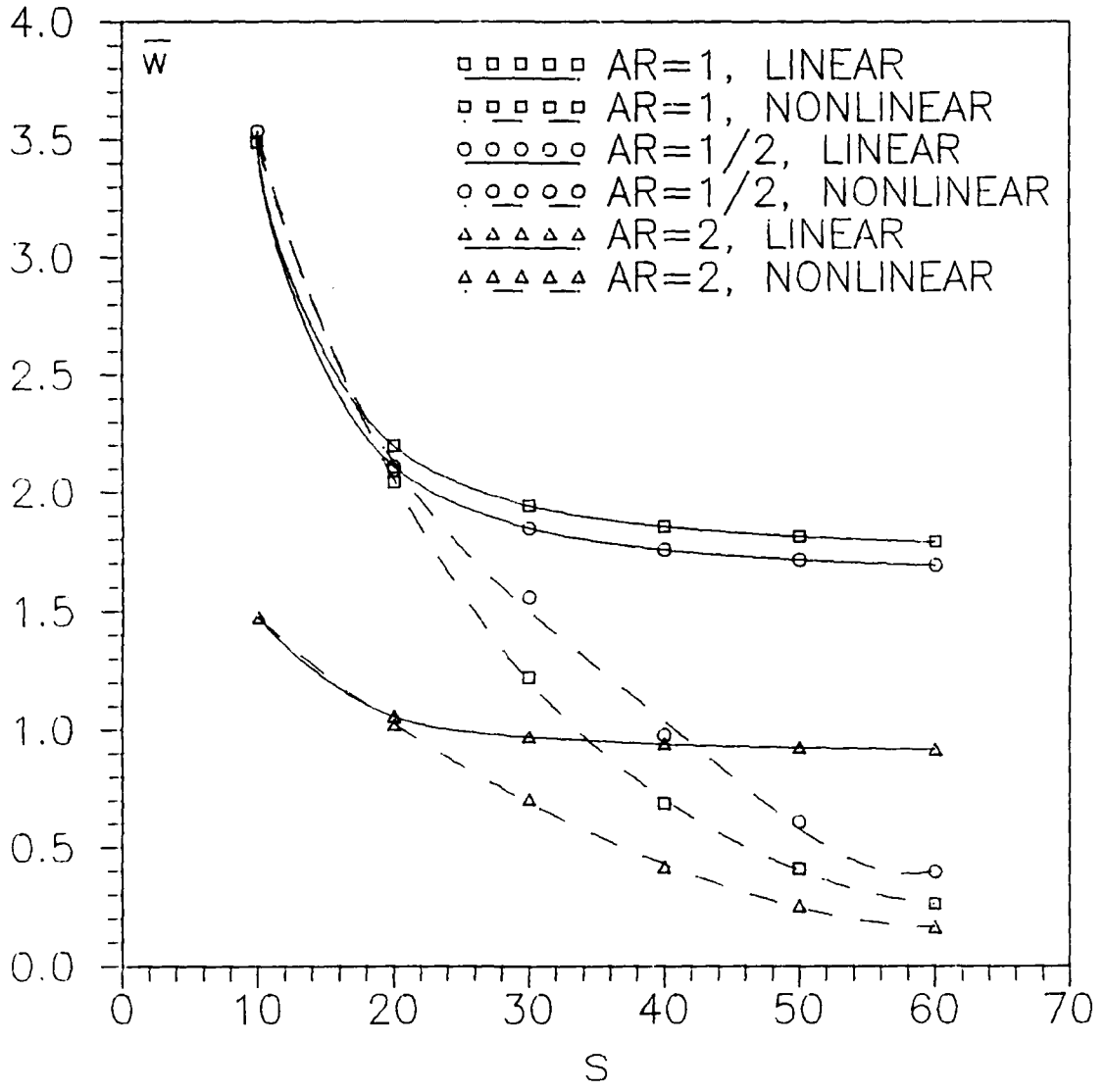

Figure C.1. $\bar{w}$ vs s for a simply supported $[0_{16}/90_8]_s$ plate made of material A

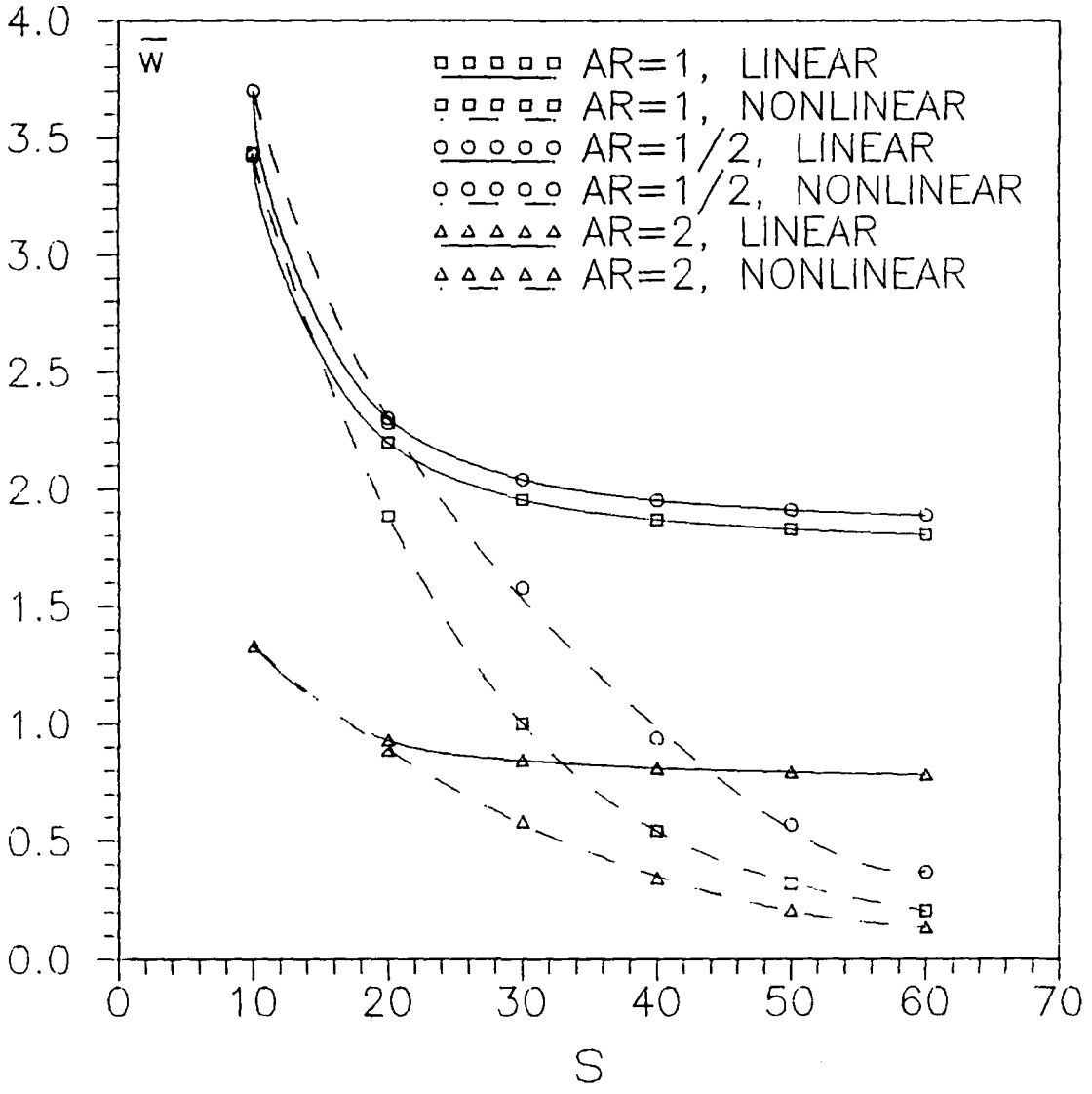

Figure C.2. $\bar{w}$ vs s for a simply supported $[0_{12}/60_6/-60_6]_s$ plate made of material A

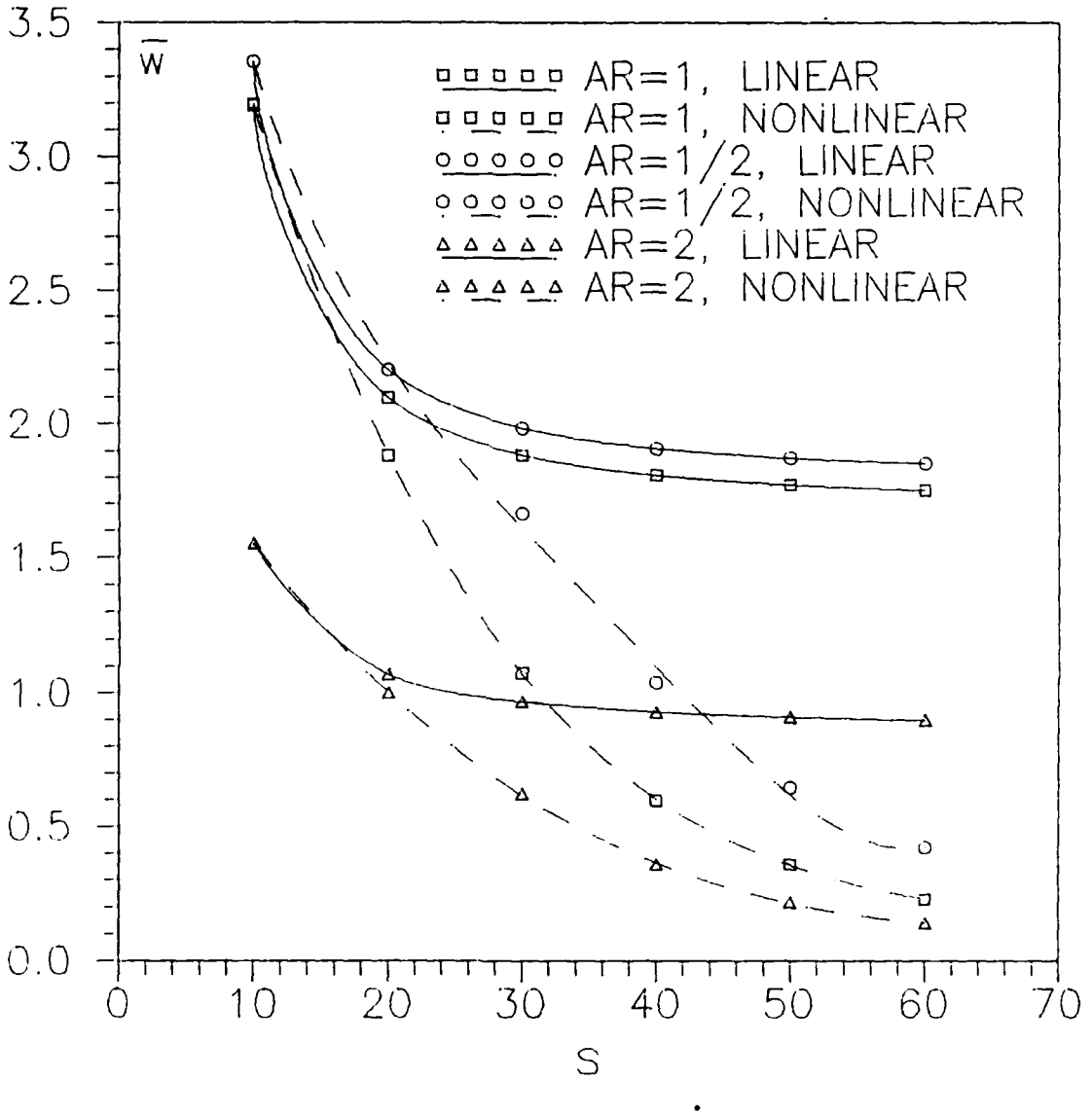

Figure C.3. $\bar{w}$ vs s for a simply supported $[0_{12}/45_6/-45_6]_s$ plate made of material A

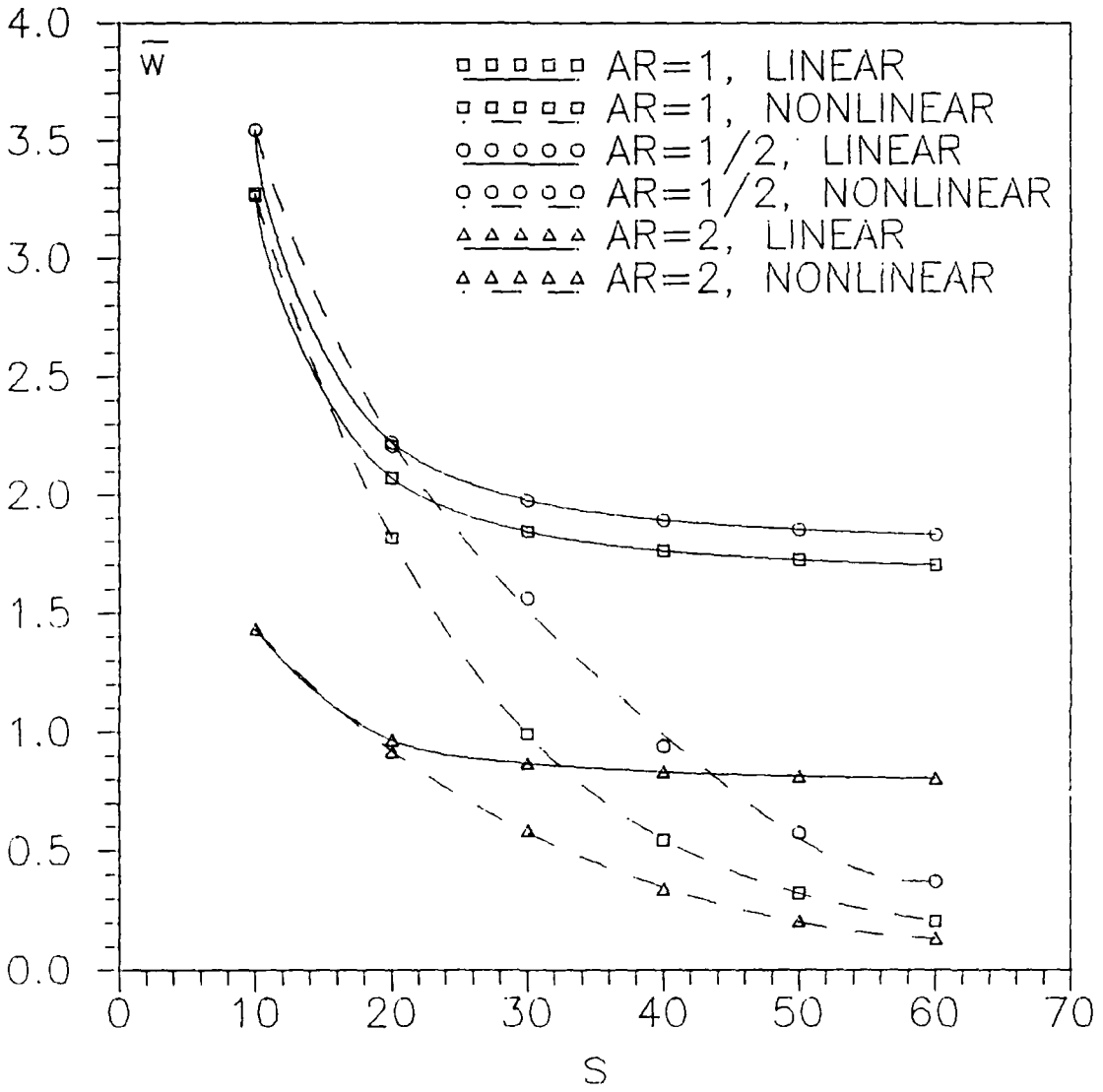

Figure C.4. $\bar{w}$ vs s for a simply supported $[0_{12}/45_4/-45_4/90_4]_s$ plate made of material A

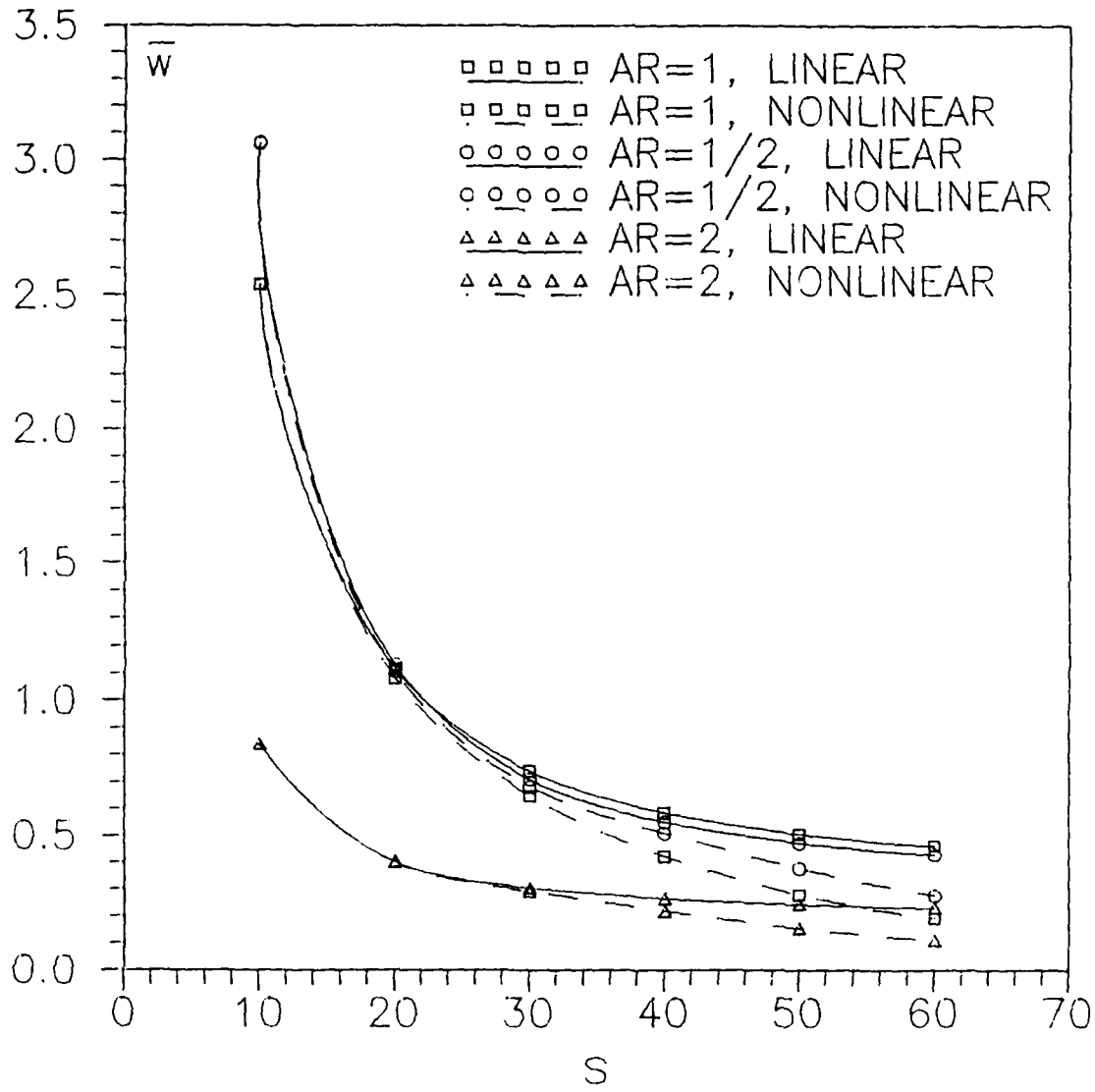

Figure C.5. $\bar{w}$ vs s for a clamped $[0_{16}/90_8]_s$ plate made of matrerial A

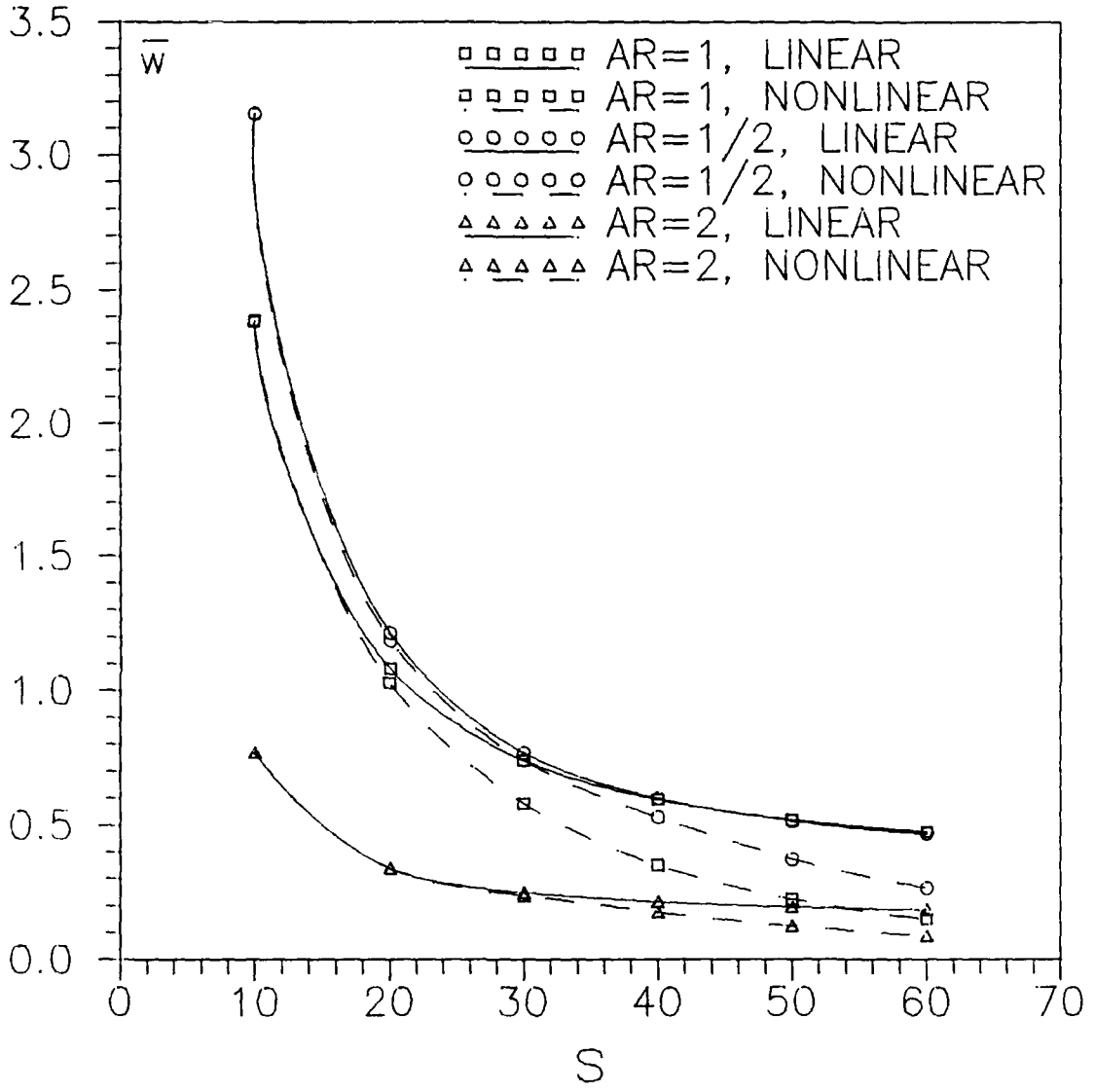

Figure C.6. $\bar{w}$ vs s for a clamped $[0_{12}/60_6/-60_6]_s$ plate made of material A

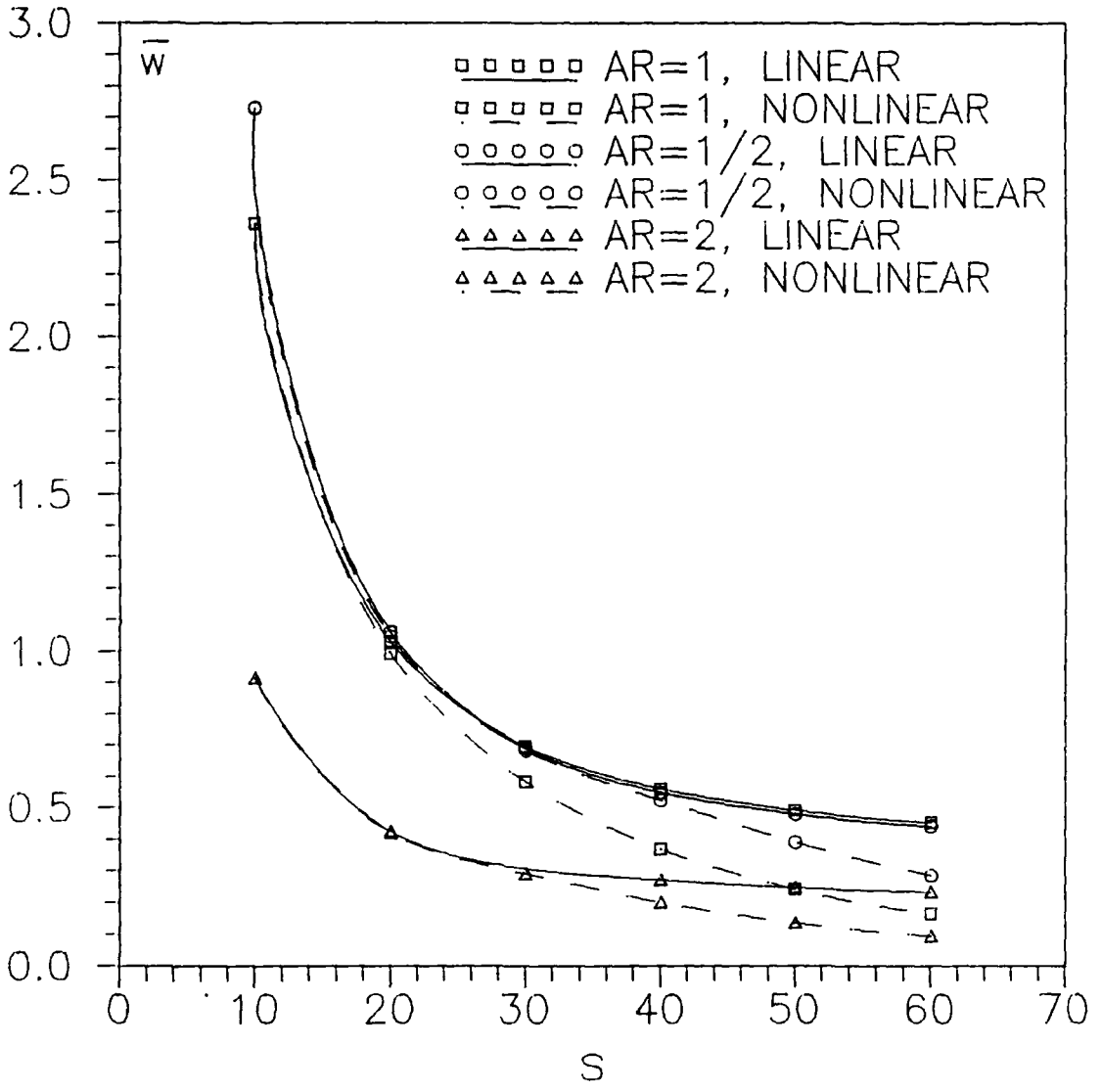

Figure C.7. $\bar{w}$ vs s for a clamped $[0_{12}/45_6/-45_6]_s$ plate made of material A

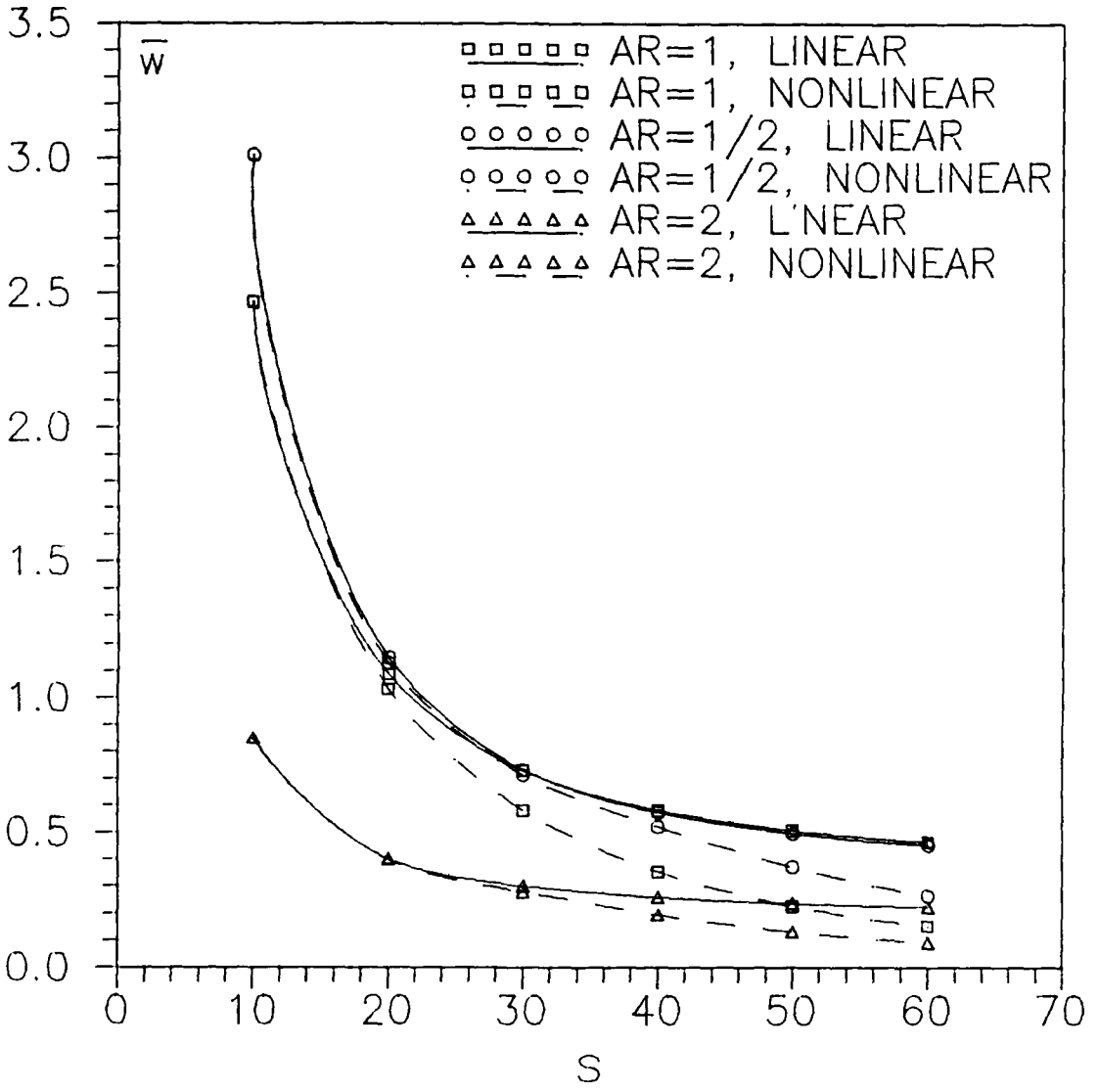

Figure C.8. $\bar{w}$ vs s for a clamped $[0_{12}/45_4/-45_4/90_4]_s$ plate made of material A

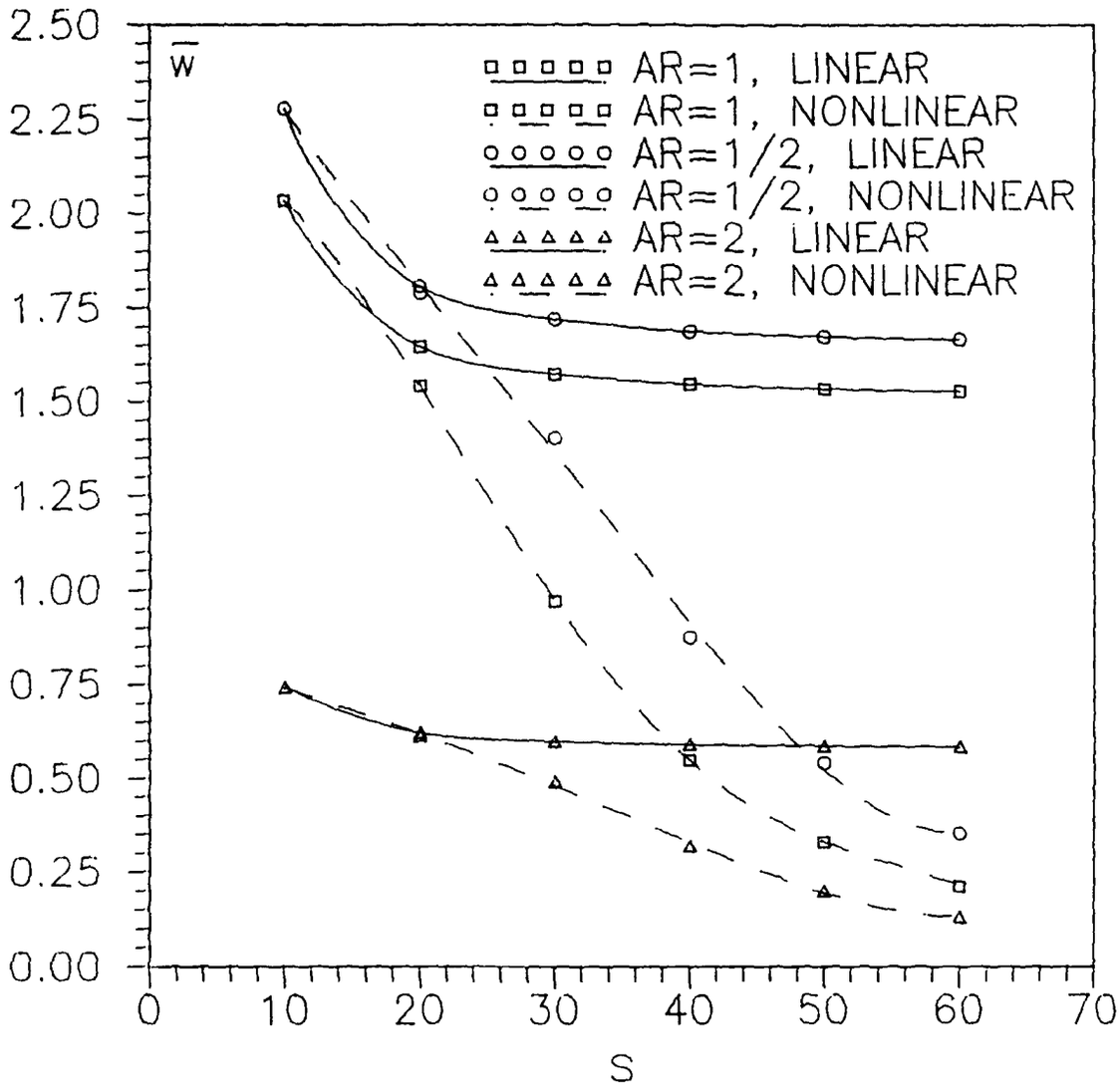

Figure C.9. $\bar{w}$ vs s for a simply supported $[0_{16}/90_8]_s$ plate made of material B

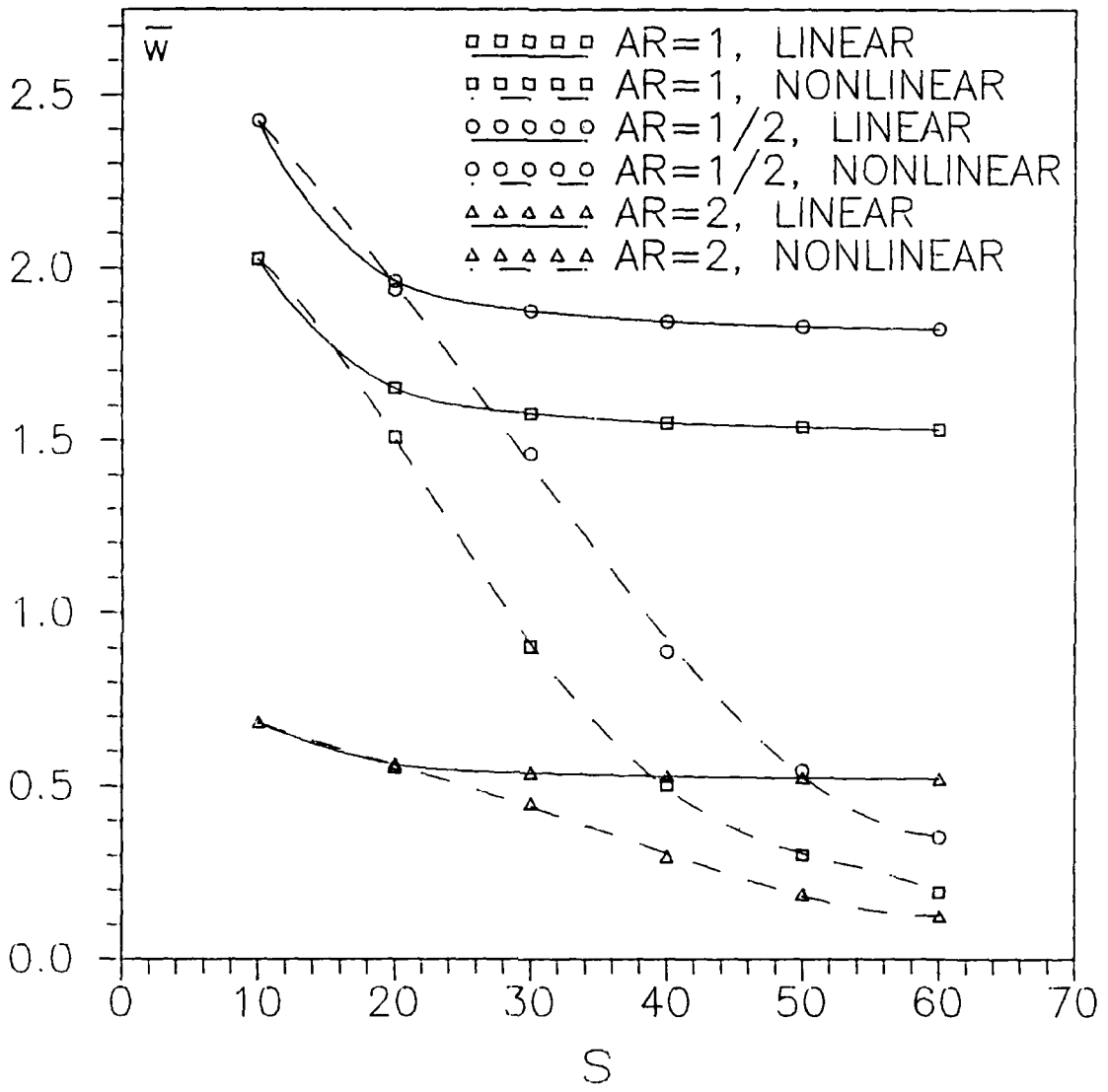

Figure C.10. $\bar{w}$ vs s for a simply supported $[0_{12}/60_6/-60_6]_s$ plate made of material B

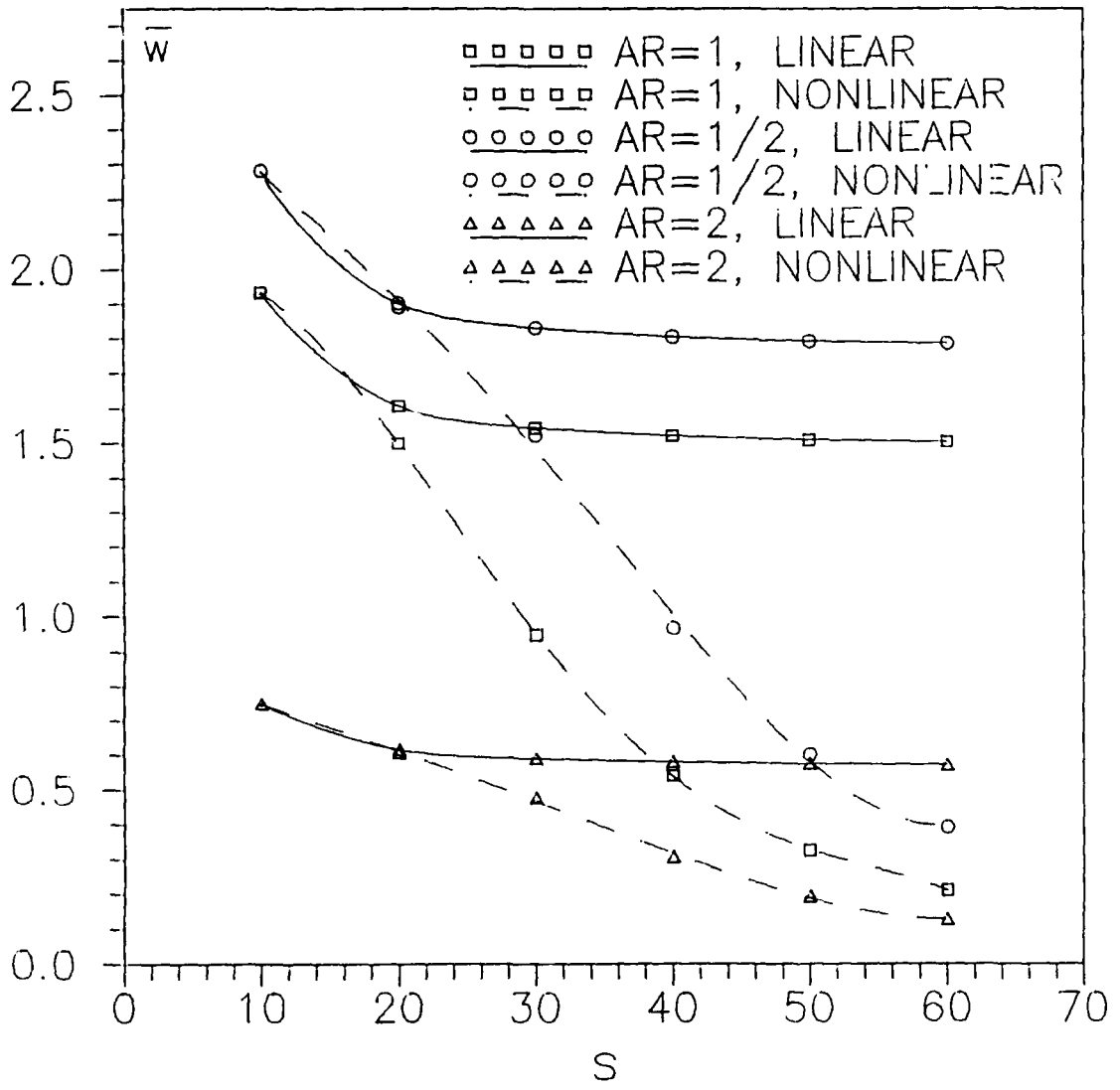

Figure C.11. $\bar{w}$ vs s for a simply supported $[0_{12}/45_6/-45_6]_s$ plate made of material B

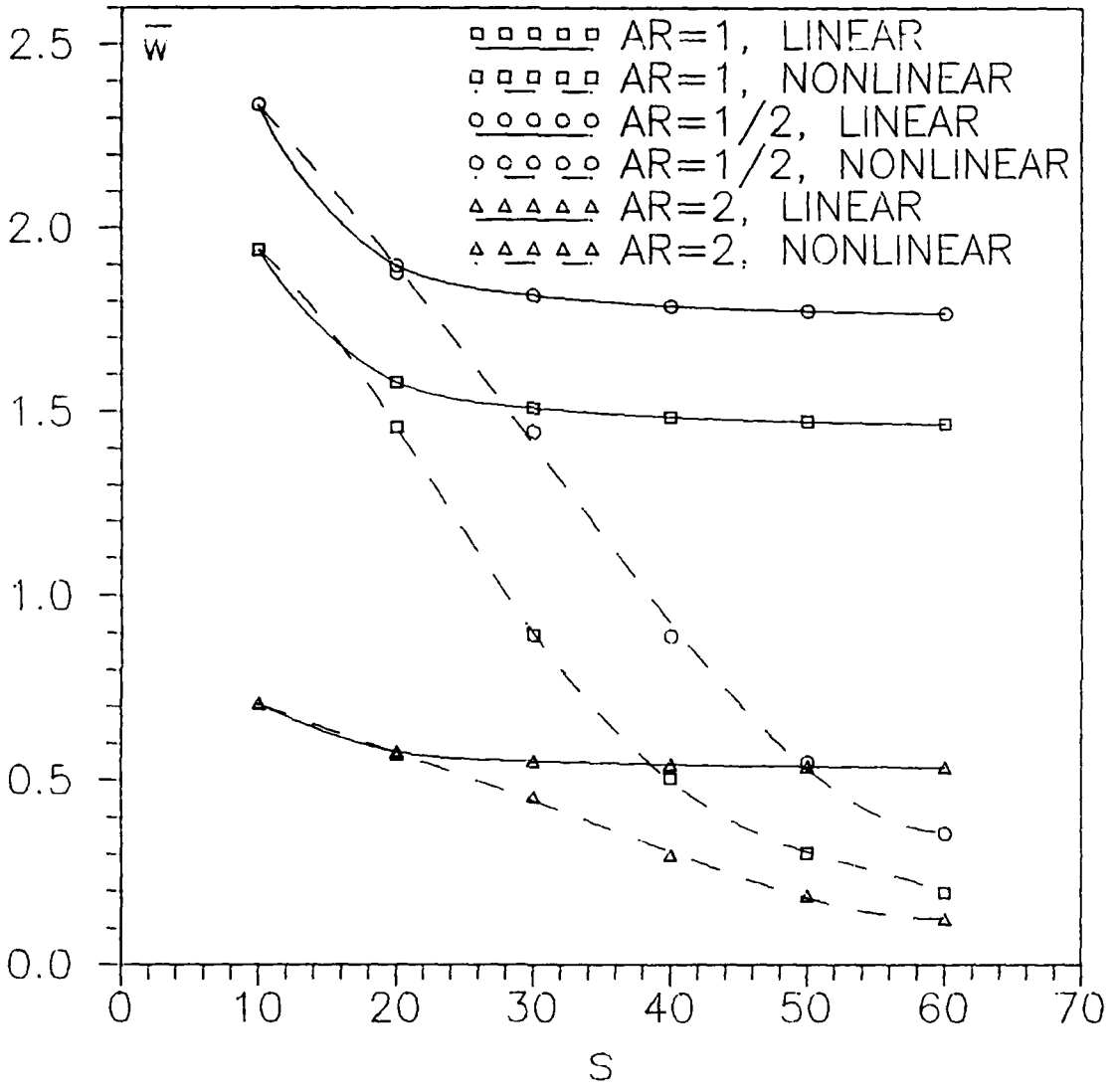

Figure C.12. $\bar{w}$ vs s for a simply supported $[0_{12}/45_4/-45_4/90_4]_s$ plate made of material B

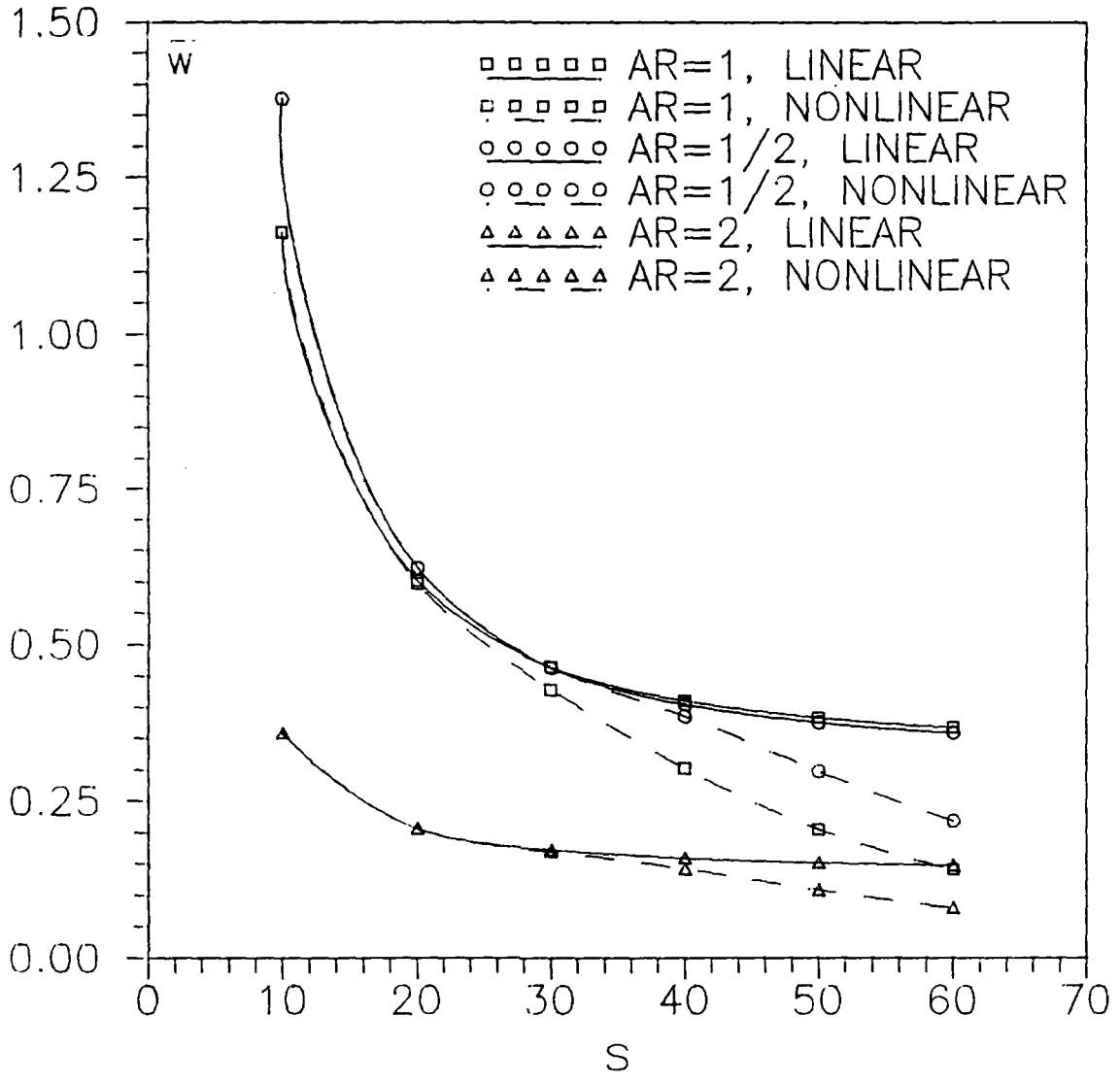

Figure C.13. $\bar{w}$ vs s for a clamped $[0_{16}/90_8]_s$ plate made of material B

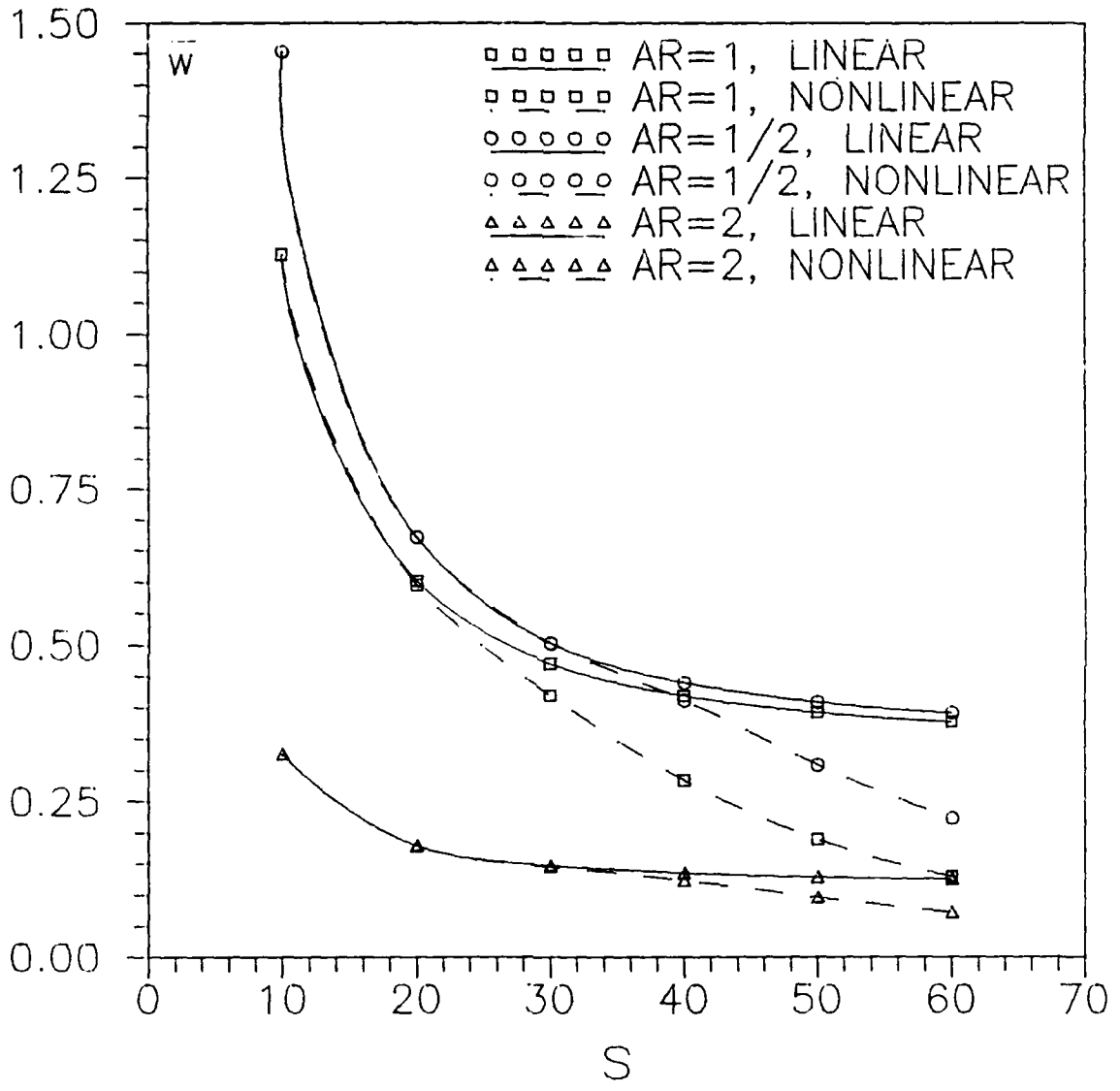

Figure C.14. $\bar{w}$ vs s for a clamped $[0_{12}/60_6/-60_6]_s$ plate made of material B

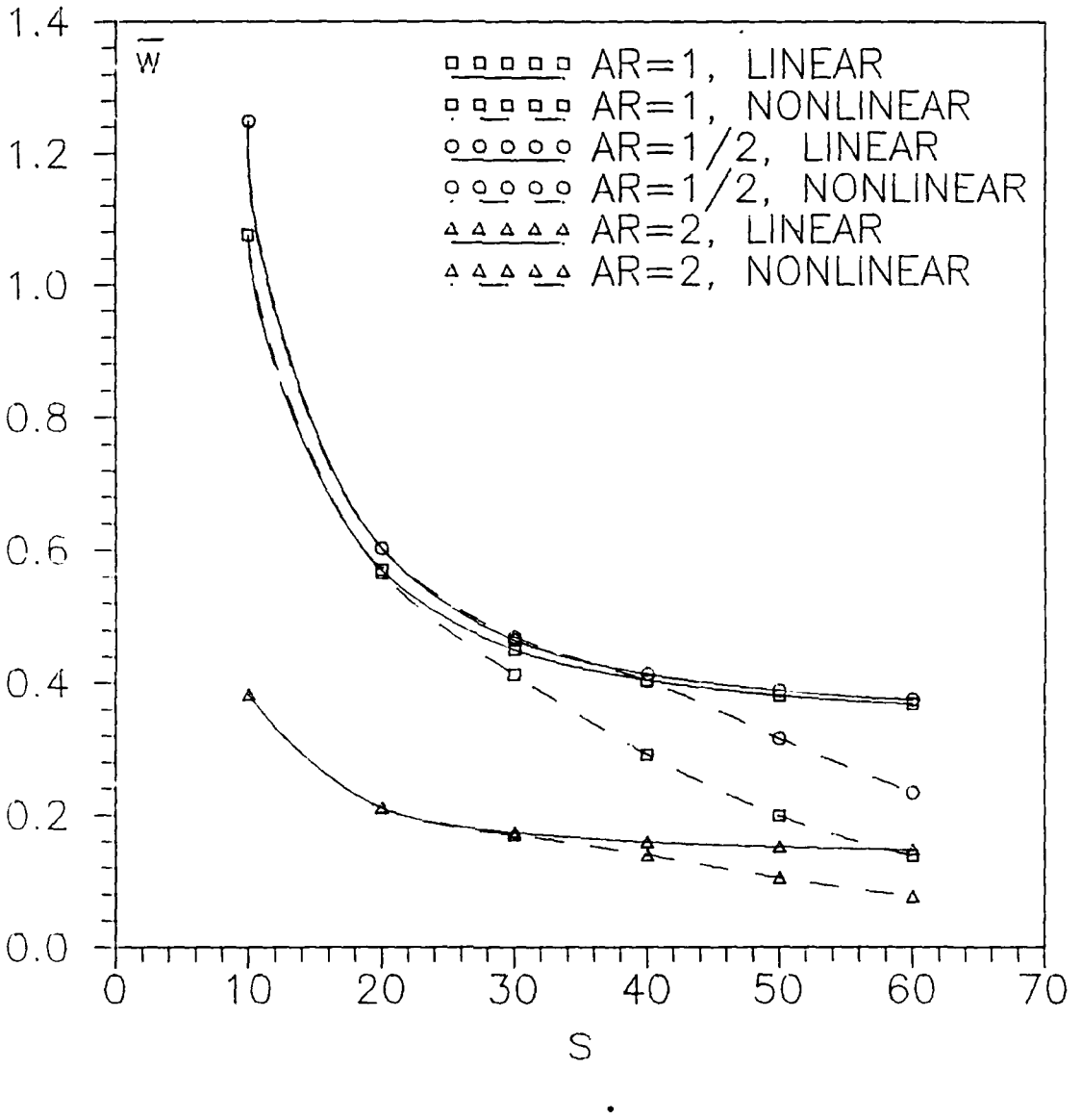

Figure C.15. $\bar{w}$ vs s for a clamped $[0_{12}/45_6/-45_6]_s$ plate made of material B

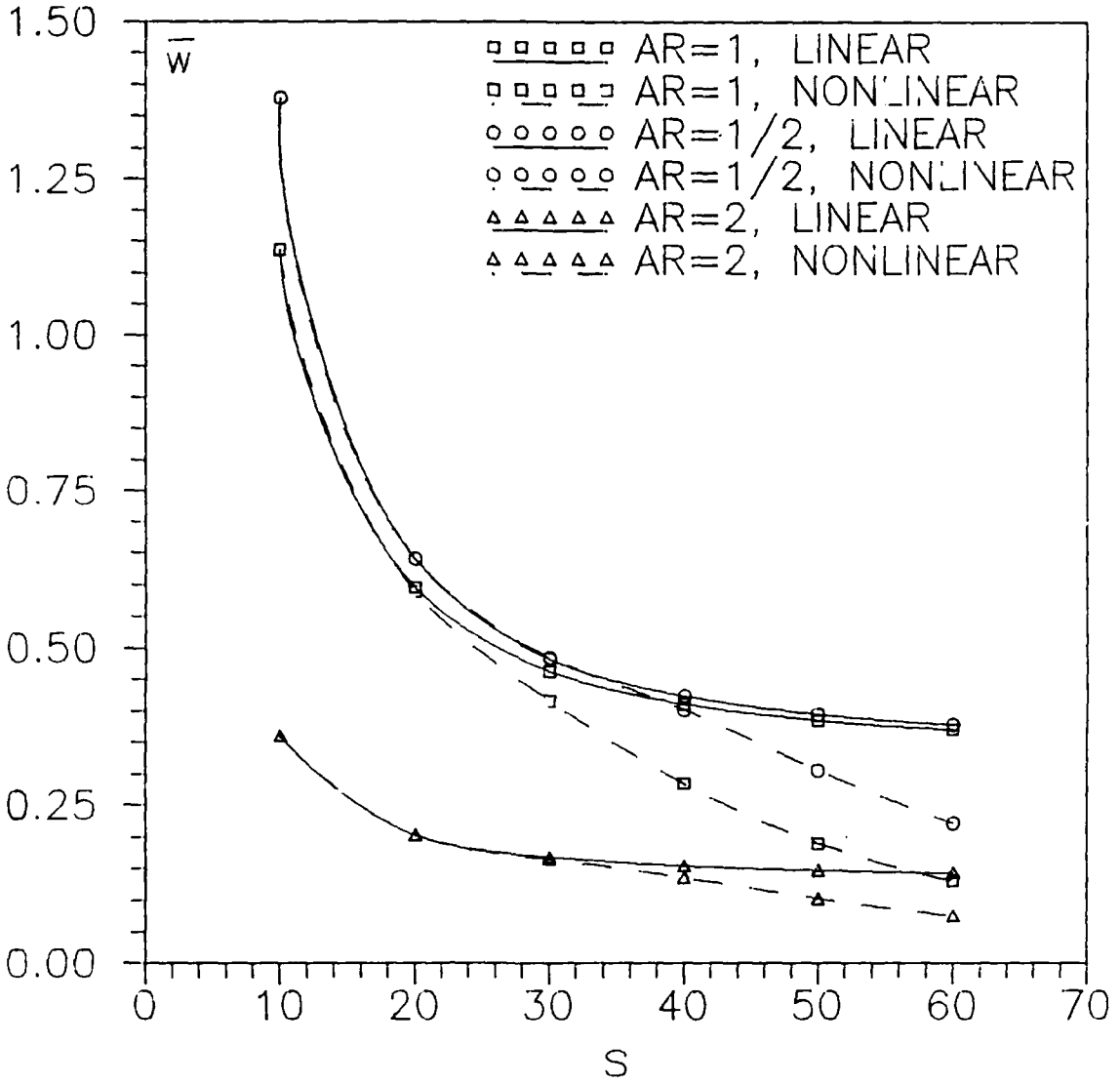

Figure C.16. $\bar{w}$ vs s for a clamped $[0_{12}/45_4/-45_4/90_4]_s$ plate made of material B

Bibliography

1. Ahmad, S., B. Irons, and O.C. Zienkiewicz. "Analysis of Thick and Thin Shell Structures by Curved Finite Elements," International Journal of Nonlinear Mathematics in Engineering, 2: 1970.

2. Ashton, J.E. and J.M. Whitney. Theory of Laminated Plates, Technomic, 1970.

3. Bathe, K.J. and A.P. Cimento. "Some Practical Procedures for the Solution of Nonlinear Finite Element Equations," Computer Methods in Applied Mechanics and Engineering, 22: 1980.

4. Bennett, J.A. "Nonlinear Vibration of Simply Supported Angle Ply Laminated Plates," AIAA Journal, 9: 1997-2003, 1971.

5. Bert, C.W. "Nonlinear Vibration of a Rectangular Plate Arbitrarily Laminated of Anisotropic Material," Journal of Applied Mechanics, 40: 452-458, 1973.

6. Cook, R.D. Concepts and Applications of Finite Element Analysis, New York: John Wiley and Sons, 1981.

7. Dennis, Capt Scott T. Large Displacement and Rotational Formulation for Laminated Cylindrical Shells Including Parabolic Transverse Shear. PhD dissertation. School of Engineering, Air Force Institute of Technology (AU), Wright-Patterson AFB OH, May 1988 DTIC NUMBER AD-194 871

8. Hildebrand, F.B., E. Reissner, and G.B. Thomas, Notes on the Foundations of the Theory of Small Displacements of Orthotropic Shells. NACA-TN-1833, 1949.

9. Hinrichsen, R.L. and A.N. Palazotto. "Nonlinear Finite Element Analysis of Thick Composite Plates Using a Cubic Spline Function," AIAA Journal, 24, 11: 1986.

10. John, F. "Estimates for the Derivatives of the Stresses in a Thin Shell and Interior Shell Equations," Communications on Pure and Applied Mechanics, 18: 1965.

11. Jones, R.J. Mechanics of Composite Materials, Cambridge: Hemisphere Publishing Co., 1975.

12. Koiter, W.T. "A Consistent First Approximation in the General Theory of Thin Elastic Shells," Proceedings of the Symposium on Theory of Thin Elasic Shells. Amsterdam, North Holland, 1960.

13. Koiter, W.T. "Foundations and Basic Equations of shell Theory-A Survey of Recent Progress," Theory of Thin Shells, ed by F.I. Niordson, IUTAM Symposium, Copenhagen, 1967.

14. Levinson, M. "An Accurate Simple Theory of the Statics and Dynamics of Elastic Plates," Mech Research Comm, 7: 1980.

15. Mindlin, R.D. "Influence of Rotatory Inertia and Shear on Flexural Motions of Isotropic Elastic Plates," Journal of Applied Mechanics, 18: 1951.

16. Murthy, M.V.V. An Improved Transverse Shear Deformation Theory for Laminated Anisotropic Plates, NASA-TP-1903, 1981.

17. Noor, A.K. and S.J. Hartley "Effect of Shear Deformation and Isotropy on the Nonlinear Response of Composite Plates," Developments in Composite Materials - 1. ed Holister, G., Barking, Essex, England: Applied Science Publishers, 55-65, 1977.

18. Noor, A.K., M.D. Mathers, and M.S. Anderson. "Exploiting Symmetries for Efficient Postbuckling Analysis of Composite Plates," AIAA Journal, 15, 1: 1977.

19. Owen, D.R.J. and E. Hinton Finite Elements in Plasticity Theory and Practice, Swansea UK: Pineridge Press, 1980.

20. Pagano, N.J. "Exact Solutions for Composite Laminates in Cylindrical Bending," Journal of Composite Materials, 3: 1969.

21. Pagano, N.J. "Influence of Shear Coupling in Cylindrical Bending of Anisotropic Laminates," Journal of Composite Materials, 4: 1970.

22. Pagano, N.J. "Exact Solutions for Rectangular Bidirectional Composites and Sandwich Plates," Journal of Composite Materials, 4: 1970.

23. Pagano, N.J. "Further Study of Composite Laminates Under Cylindrical Bending," Journal of Composite Materials, 5: 1971.

24. Palazotto, A.N. Class handout distributed in MECH 741, Advanced Topics in Composites. School of Engineering, Air Force Institute of Technology (AU), Wright-Patterson AFB OH, May 1988.

25. Palazotto, A.N. and W.P. Witt. "Formulation of a Nonlinear Compatible Finite Element or Analysis of Laminated Composites," Computers and Structures, 21, 6: 1985.

26. Phan, N.D. and J.N. Reddy. 'Analysis of Laminated Composite Plates Using a Higher Order Shear Deformation Theory,' International Journal for Nonlinear Methods in Engineering, 21: 1985.

27. Pryor, C.W. and R.M. Barker. 'A Finite Element Analysis Including Transverse Shear Effects for Applications to Laminated Plates,' AIAA Journal, 9,5: 1971.

28. Putcha, N.S. and J.N. Reddy. 'A Refined Mixed Shear Flexible Finite Element for the Nonlinear Analysis of Laminated Plates,' Computers and Structures, 22,4: 1986.

29. Rajasekaran, S. and D.W. Murray. 'Incremental Finite Element Matrices,' Journal of the Structural Division, ASCE: 1973.

30. Reddy, J.N. 'A Penalty Plate-Bending Element for the Analysis of Laminated Anisotropic Composite Plates,' International Journal of Numerical Methods in Engineering, 2: 1187-1206, 1980.

31. Reddy, J.N. 'Analysis of Layered Composite Plates Accounting for Large Deflections and Transverse Shear Strains,' in Recent Advances in Nonlinear Computational Mechanics, eds Hinton, Owen and Taylor, Swansea, UK: Pinridge Press, 1982.

32. Reddy, J.N. Energy and Variational Methods in Applied Mechanics. New York: John Wiley and Sons, 1984.

33. Reddy, J.N. 'A Simple Higher Order Theory for Laminated Composite Plates,' Journal of Applied Mechanics, 51: 1984.

34. Reddy, J.N. ' A Note on Symmetry Conditions in Transient Response of Unsymmetrically Laminated Anisotropic Plates,' International Journal of Nonlinear Mathematics in Engineering, 20, 1: 1984.

35. Reddy, J.N. and W.C. Chao. 'A Comparison of Closed Form and Finite Element Solution of Thick Laminated Anisotropic Rectangular Plates,' Nuclear Engineering and Design, 64: 1981.

36. Reddy, J.N. and W.C. Chao. 'Large Deflection and Large Amplitude Free Vibrations of Laminated Composite Material Plates,' Computed Structures, 13, 2: 341-347, 1981.

37. Reddy, J.N. and W.C. Chao. 'Nonlinear Bending of Thick Rectangular, Laminated Composite Plates,' International Journal of Nonlinear Mechanics: 1981.

38. Reddy, J.N. and N.D. Phan. 'Stability and Vibration of Isotropic, Orthotropic, and Laminated Plates According to a Higher Order Shear Deformation Theory,' Journal of Sound and Vibration, 98(2): 1985.

39. Reissner, E. 'The Effect of Transverse Shear Deformation on the Bending of Elastic Plates,' Journal of Applied Mechanics, 18: 1945.

40. Riks, E. 'Progress in Collapse Analysis,' Journal of Pressure Vessel Technology, 109: 1987.

41. Saada, Adel S. Elasticity Theory and Applications. Malabar, Florida: Krieger Publishing Company, 1983.

42. Srinivas, S. and A.K. Rao. 'Bending, Vibration,and Buckling of Simply Supported Thick Orthotropic Rectangular Plates and Laminates,' International Journal of Solids and Structures, 6: 1970.

43. Stricklin, J.A. and W.E. Haisler. 'Formulations and Solution Procedures for Nonlinear Structural Analysis,' Computers and Structures, 7: 1977.

44. Szilard, R. Theory and Analysis of Plates Classical and Numerical Methods Englewood Cliffs, NJ: Prentice-Hall, 1974.

45. Waszczyszyn, Z. 'Numerical Problems of Nonlinear Stability Analysis of Elastic Structures,' Computers and Structures, 17,1: 1983.

46. Whitney, J.M. and A.W. Leissa. 'Analysis of Heterogeeious Anisotropic Plates,' Journal of Applied Mechanics, 36: 261-266, 1969.

47. Whitney, J.M. and N.J. Pagano. 'Shear Deformation in Heterogeneous Plates,' Journal of Applied Mechanics, 1970.

48. Yang, P.C., C.H. Norris, and Y. Stavsky. 'Elastic Wave Propogation in Heterogenious Plates,' International Journal of Solids and Structures, 2: 1966.

49. Zaghloul, S.A. and J.B. Kennedy. 'Nonlinear Analysis of Unsymmetrically Laminated Plates,' Journal of the Engineering Mechanics Division, ASCE, 101,(EM3): 169-185, 1975.

50. Zienkiewicz, O.C., R.D. Taylor,and J.M. Too. 'Reduced Integration Technique in General Analysis of Plates and Shells,' International Journal of Nonlinear Mathematics in Engineering, 3: 1971.

Vita

Captain Marc E. Owens was born [redacted] He graduated from high school in [redacted] 1978 and attended Oregon State University, from which he recieved a Bachelor of Science in Mechanical Engineering in June of 1983. Upon graduation he recieved his commission in the USAF through the AFROTC program. He was called to active duty in October of 1983 and was assigned as a munitions test engineer with the 3246th Test Wing, Eglin AFB Florida until he entered the School of Engineering, Air Force Institute of Technology in June 1987.

[redacted]

UNCLASSIFIED
SECURITY CLASSIFICATION OF THIS PAGE

REPORT DOCUMENTATION PAGE

Form Approved
OMB No. 0704-0188

1a. REPORT SECURITY CLASSIFICATION UNCLASSIFIED	1b. RESTRICTIVE MARKINGS
2a. SECURITY CLASSIFICATION AUTHORITY	3. DISTRIBUTION/AVAILABILITY OF REPORT Approved for public release;
2b. DECLASSIFICATION/DOWNGRADING SCHEDULE	distribution unlimited
4. PERFORMING ORGANIZATION REPORT NUMBER(S) AFIT/GAE/AA/88D-29	5. MONITORING ORGANIZATION REPORT NUMBER(S)
6a. NAME OF PERFORMING ORGANIZATION School of Engineering 6b. OFFICE SYMBOL (If applicable) AFIT/ENY	7a. NAME OF MONITORING ORGANIZATION
6c. ADDRESS (City, State, and ZIP Code) Air Force Institute of Technology Wright-Patterson AFB OH 45433-6583	7b. ADDRESS (City, State, and ZIP Code)
8a. NAME OF FUNDING/SPONSORING ORGANIZATION Air Force Office of Scientific Research 8b. OFFICE SYMBOL (If applicable)	9. PROCUREMENT INSTRUMENT IDENTIFICATION NUMBER
8c. ADDRESS (City, State, and ZIP Code) AFOSR Bolling AFB, D.C. 20332-5000	10. SOURCE OF FUNDING NUMBERS PROGRAM ELEMENT NO. / PROJECT NO. / TASK NO / WORK UNIT ACCESSION NO.

11. TITLE (Include Security Classification)
FINITE ELEMENT ANALYSIS OF COMPOSITE PLATES INCLUDING SHEAR DEFORMATION

12. PERSONAL AUTHOR(S)
Marc E. Owens, B.S., Capt, USAF

13a. TYPE OF REPORT	13b. TIME COVERED	14. DATE OF REPORT (Year, Month, Day)	15. PAGE COUNT
MS Thesis	FROM _____ TO _____	1988 December	155

16. SUPPLEMENTARY NOTATION

17. COSATI CODES			18. SUBJECT TERMS (Continue on reverse if necessary and identify by block number)	
FIELD	GROUP	SUB-GROUP		
11	04		Composite Materials	Shear Strength
12	01		Finite Element Analysis	Nonlinear Systems
			Plates	Transverse Loads

19. ABSTRACT (Continue on reverse if necessary and identify by block number)

Thesis Advisor: Dr. Anthony N. Palazotto
Professor of Aeronautics and Astronautics
Department of Aeronautics and Astronautics

12 Jan 1989

20. DISTRIBUTION/AVAILABILITY OF ABSTRACT	21. ABSTRACT SECURITY CLASSIFICATION
☒ UNCLASSIFIED/UNLIMITED ☐ SAME AS RPT. ☐ DTIC USERS	UNCLASSIFIED

22a. NAME OF RESPONSIBLE INDIVIDUAL	22b. TELEPHONE (Include Area Code)	22c. OFFICE SYMBOL
Dr Anthony N. Palazotto, Professor	(513) 255-2040	AFIT/ENY

DD Form 1473, JUN 86 *Previous editions are obsolete.* SECURITY CLASSIFICATION OF THIS PAGE

UNCLASSIFIED

19. cont.

The purpose of this research is to study the effects of material properties, thickness ratio, aspect ratio, boundary conditions, and ply layup on the reactions of a transversely loaded rectangular composite plate. Geometric nonlinearities, i.e. the von Karman nonlinear plate equations, and through the thickness shear effects were included. Both geometrically linear and nonlinear solutions were done. This research was done using an existing finite element code with a four-noded, 28 DOF rectangular element.

All plates were 48 plies thick to be representative of a "real world" application. The ply layups were chosen to be a representative sampling of layups used in the field and had at least 50% of the plies in the 0° direction.

Material properties had the largest effect when the plate was thick. The linear solution approaches the classical laminated plate theory solution as the plate gets thin. The nonlinear solution deflects much less than the linear solution because the higher order terms significantly stiffen the plate. For a clamped plate the linear and nonliear solutions are comparible until the plate is quite thin.

Aspect ratio has a large effect on the plate for an isotropic material. However, in the ply layups investigated, aspect ratio had much less effect because half the fibers were oriented in the direction of the short dimension of the plate.

Ply layup did not have a great effect on the deflections of the plate. This occured because all the layups chosen had at least half the plies oriented in the same direction.